Article:
Wei, T., Batley, R., Liu, R. orcid.org/0000-0003-0627-3184 et al. (2 more authors) (2024) A method of time-varying demand distribution estimation for high-speed railway networks with user equilibrium model. Transportation Research Part E: Logistics and Transportation Review, 189. 103679. ISSN 1366-5545

https://doi.org/10.1016/j.tre.2024.103679

A Method of Time-varying Demand Distribution Estimation for HSR Networks with User Equilibrium Model

Tangjian Wei[a,b], Richard Batley[b], Ronghui Liu[b], Guangming Xu[c,*], Yili Tang[a,d]

a: Department of Civil and Environmental Engineering, Western University, London, Canada
b: Institute for Transport Studies, The University of Leeds, Leeds, UK
c: School of Traffic and Transportation Engineering, Central South University, Changsha, China
d: Department of Electrical and Computer Engineering, Western University, London, Canada
* Corresponding author. Email: xuguangming@csu.edu.cn (Guangming Xu)

Abstract: Time-varying demand distribution (TDD) is a critical input data for operation and management in HSR systems. This paper proposed a bi-level model to estimate the TDD with the ticket booking date and using the schedule-based User Equilibrium (UE) assignment. The up-level aims to determine the TDD with maximum entropy value and minimal error between the path flow (ticket booking volumes) and the corresponding equilibrium flows (determined from lower-level); the lower-level is a schedule-based UE assignment with rigid capacity constraints to reflect the interactions of ticket booking choices behaviors between different OD pairs in the HSR networks, and further, the advance booking cost is considered endogenously as a part of passenger choice equilibrium. The bi-level model is converted into a single-level model through equivalent complementary constraints. Then, based on linear relaxation, the single-level model is transformed into a mixed-integer quadratic program (MIQP). Furthermore, in order to improve the computational efficiency of the MIQP, the approach of reducing the calculation size of our problem is proposed. By solving the MIQP we get the information about the upper and lower bounds of our original problem, and then a global optimal solution algorithm with four piecewise interval strategies is proposed. The effectiveness and applicability of the proposed algorithm are illustrated with a simple case and three real-world cases.

Keywords: Time-varying demand estimation; Bi-level model; UE assignment; Linear relaxation; Global optimal solution

1. Introduction

In the past few decades, High-Speed Railway (HSR) has been very popular and has made great developments in densely populated countries and regions such as China, Japan and Europe. Especially in China, it has the world's largest HSR network with over 40,000 km of track in service as of 2021.[1] Whilst HSR has made a significant contribution to increasing passenger capacity with its high speed and high service frequency, many studies refer to operational challenges (Kaspi and Raviv, 2013; Niu et al., 2015; Xu et al., 2023a; Zhao et al., 2021) which are shifting the focus from meeting total demand volume to meeting the time-varying demand. That is to say, we seek not only to supply the capacity to meet total passenger demand for each OD pair, but also to improve the correspondence between the desired departure time distribution of passengers and the frequency and timing of train departures (as shown in Fig. 1). For a given HSR OD pair, each passenger will have a desired departure time[2], and the demand volumes at different desired departure time points may be different; this can be seen as the TDD for this

[1] Statista. High-speed railway in China – statistics & facts, 2023. https://www.statista.com/topics/7534/high-speed-rail-in-china/?kw=&crmtag=adwords&gclid=CjwKCAjw-vmkBhBMEiwAlrMeF4Up5jhzJEPx_ynUJneWiVECWYsRPk0_7BEz3_usZJxVDiybND2_hBoCiogQAvD_BwE#topicOverview. Accessed 30.06.2023

[2] Desired arrival time can be converted into desired departure time as the in-train time is fixed by the schedule and will not vary by the train flow.

OD pair (Xu et al., 2018b; Zhang et al., 2021). In the above studies about HSR operational problems for time-varying demand, the TDD is a key input – but no insight is given as to how to obtain it. Obviously, obtaining accurate TDD for the OD pair is very important to improve the service quality and HSR systems performance. Therefore, how to obtain TDD for the OD pair is a critical problem for the operation and management of the HSR systems, and this paper focuses on that problem.

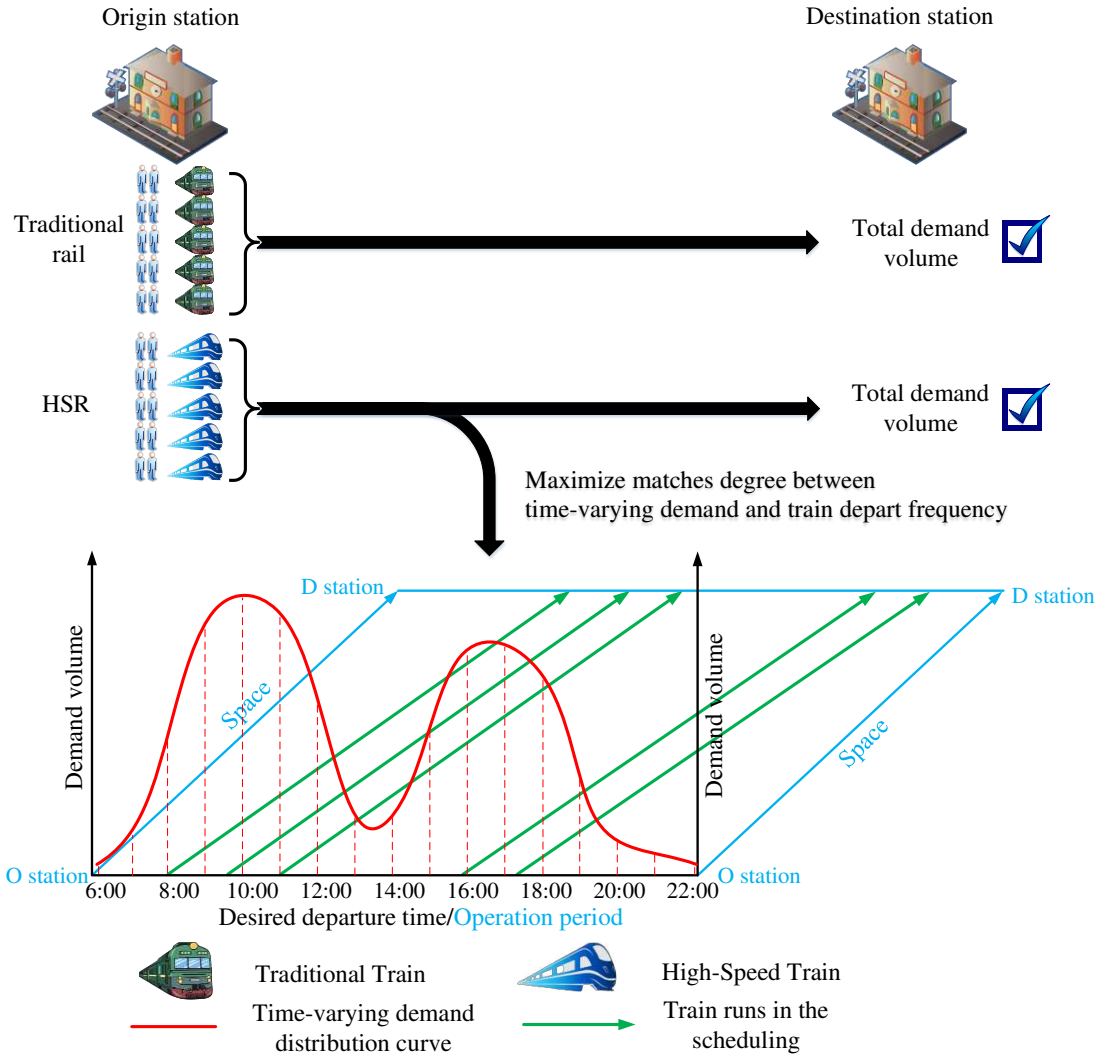

Fig. 1 Operational challenges in HSR

In recent years, demand estimation with time varying demand has been a hot topic in transport research, but the manifestation of this problem in HSR is somewhat different from other modes.

In traditional railway systems, demand forecasting traditionally relies on elasticity-based models where the core principle is that variations in fares or travel times will influence passenger rail demand (Börjesson and Eliasson, 2014; Liu et al., 2023; Qin et al., 2022; Wardman, 1997, 2006; Wardman et al., 2007; Wijeweera et al., 2014). In recent years, the emergence of the big data era has led to the gradual incorporation of machine learning technologies in railway demand forecasting. This includes the use of Neural Network (Tsai et al., 2009), Long Short Term Memory Network (Zhang et al., 2020) and the combined

forecasting models (Emami Javanmard et al., 2023; Qin et al., 2019; Wei et al., 2023; Wen et al., 2022). However, given the relatively slow speeds and lower transport capacities, the primary goal of conventional railway systems is to accommodate the total daily demand volumes between OD pairs. Consequently, the focus is on estimating or forecasting the overall daily demand volume rather than on the TDD within the day.

In road networks, this often called the dynamic demand estimation problem, whereby drivers are free to choose their departure times and routes, leading to variability in path time or cost varies on different arc/link flows at a given time of day, and on a given arc/link flow at different times of day. Researchers have used the likes of traffic count (Bierlaire and Crittin, 2004; Osorio, 2019), automatic vehicle identification counts (Tang et al., 2021; Zhou and Mahmassani, 2006) and license plate recognition information (Mo et al., 2020; Nakanishi and Western, 2005) to analyze and solve this problem. However, application of the same problem to HSR introduces some distinct issues: firstly, passengers' real departure times are governed by the schedule and discretized; secondly, the in-train time is constant and independent of changes in train flow (Wu et al., 2022; Zhao et al., 2021).

In urban transit networks, the departure times of passengers are also governed by the timetable but there is no need to book a ticket in advance to secure a seat under the First-Come-First-Served (FCFS) principle, and passengers' boarding time or smart transit card tap-on time can be approximated as the desired departure time (Shang et al., 2019; Shi et al., 2017; Wang et al., 2011; Zhao et al., 2022). However, HSR is typically subject to rigid seat capacity constraints under the First-Book-First-Served (FBFS) principle, and as a result the departure time of the chosen train can be significantly different from the desired departure time of the passenger.

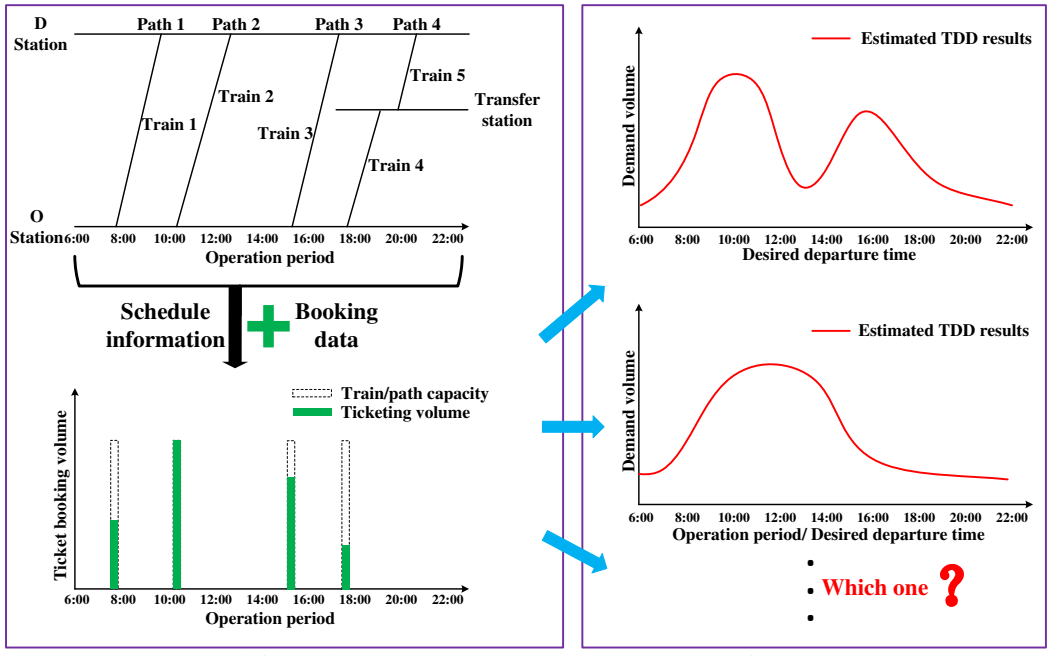

Fig. 2 HSR TDD estimation problem description

92

Table 1. A summary of studies on time-varying demand distribution estimation problems

Authors	Study topic	Transport mode	Input data	Arc/link/train capacity constraints	Governed by the schedule	Network level problem	Services principle	Modelling	Algorithm
Bierlaire and Crittin (2004)	Dynamic OD Estimation	Car traffic	Traffic counts, historical OD matrix	×	×	√	-	Least-square model	The least squares (LSQR) algorithm
Zhou and Mahmassani (2006)	Dynamic OD Estimation	Car traffic	Traffic count, AVI counts, historical OD matrix	×	×	√	-	Nonlinear ordinary least-squares estimation model	Iterative bilevel estimation procedure
Carrese et al. (2017).	Dynamic OD Estimation	Car traffic	Floating car data and traffic count	×	×	√	-	Extension of the Kalman Filter model	Simultaneous Perturbation Stochastic Approximation algorithm
Krishnakumari et al. (2020)	Dynamic OD Estimation	Car traffic	3D Supply pattern (link speeds, link flows), historical OD matrix	×	×	√	-	Production and attraction time series prediction model	Machine learning, weighted shortest path algorithm
Ros-Roca et al. (2022)	Dynamic OD Estimation	Car traffic	GPS data, traffic counts, historical OD matrix	×	×	√	-	Constrained non-linear optimization model	Quasi-Newton algorithm
Wong and Tong (1998)	Dynamic OD Estimation	Transit networks	Observed passenger counts	×	√	√	FCFS	Entropy-based model	Sparse algorithm
Yao et al. (2015)	Dynamic OD Estimation	Transit networks	AFC data, historical OD matrix	×	√	√	FCFS	Structural state-space model	Extended Kalman filtering algorithm
Cheng et al. (2022)	Dynamic OD Estimation	Metro networks	Smart cards data, historical OD matrix	×	√	√	FCFS	Low-rank high-order vector autoregression model	Tailored online update algorithm
Wei et al. (2019)	TDD Estimation	HSR	Ticket booking volume	×	√	×	FBFS	Rooftop model	SBPRA algorithm and MBPRA algorithm
This study	TDD Estimation	HSR	HSR schedule, ticket booking volume	√	√	√	FBFS	Bi-level model and Mixed-integer linear relaxation	SL-ETDDP Global Convergence Algorithm

93

Due to the above distinctions, the estimation methods or techniques used on the traditional speed railway network, road network and urban transit network cannot be readily applied to the HSR. In the case of HSR systems (e.g., Eurostar in EU, CRH in China), passengers must book the tickets in advance to get a seat reservation before travelling and this brings convenience to the TDD estimation problem. From the booking records and timetable information, the train/path flows for a given pair – i.e., the ticketing volumes at all departure times of the trains/paths which serve this OD pair – can be readily obtained (as shown in Fig. 2). To some extent, this train/path flow reflects the booking demand across all departure times, but it still has some challenges for our TDD estimation problem, as follows:

i) Governed by the timetable, train flows or path flows are discrete data within the operation period, and cannot reflect demand distribution during the periods when no trains depart;

ii) With FBFS and the train capacity constraint, a passenger's real departure time may deviate from his or her desired departure time, and this deviation will be exacerbated with more and more tickets sold out for the popular trains;

iii) Inferring demand distribution from the train/path flow may generate multiple solutions, or different TDDs may produce the same train/path flows, but we need to find a reasonable one (as shown in Fig. 2).

To date, a small number of studies have explored the estimation of TDD problems for HSR. Based on ticketing data of a single OD pair, Wei et al. (2019) studied the TDD estimation problem by simulating the ticket booking process. However, as a train will usually serve more than one OD pair, and each OD pair may carry several train services subject to rigid capacity constraints under the FBFS principle, the selling-out of any given train will affect the subsequent ticket booking behaviors of passengers of all OD pairs served by this train. Focusing on the context of a single OD pair may therefore be unduly restrictive, and it would be considerably more informative to solve the TDD estimation problem at the network level.

In Table 1, we present a summary of studies regarding the time-varying demand estimation problem and highlight the contribution of this paper against the existing literature. In particular, this study seeks to fill this gap in knowledge, by solving the estimation problem of TDD in the HSR network subject to rigid capacity constraints under the FBFS principle. Assuming a discrete representation of time, the space-time network is designed and a bi-level model is formulated. Then, we convert the bi-level model into a single-level model through equivalent constraints. In order to find the global optimal solution, our model is relaxed as a mixed-integer quadratic program (MIQP) and an optimal solution is obtained by iteratively solving the relaxed MIQP with the piecewise interval strategy. Our methods are tested on four cases and their advantages are illustrated by the results analysis. The methodology of the paper is summarized as Fig. 3 and the principal contributions are as follows.

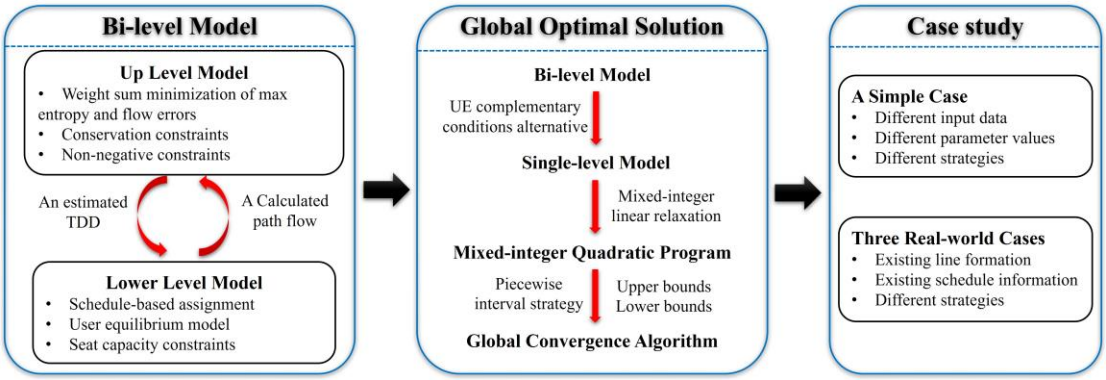

Fig. 3 Overall methodology

i) **This study proposes a bi-level model to estimate the TDD with the ticket booking volumes and using the schedule-based User Equilibrium (UE) assignment.** The upper-level aims to get the TDD with maximum entropy value and minimal error between the path flows (ticket booking volumes) and the corresponding space-time path flows or equilibrium flows (determined from lower-level); the lower-level is a schedule-based UE assignment with rigid capacity constraints to reflect the interactions of ticket booking choices behaviors between different OD pairs in the HSR networks, and furthermore, the advance booking cost is considered endogenously as a part of passenger choice equilibrium.

ii) **Based on model reformulation and linear relaxation, a global optimal solution algorithm with four piecewise interval strategies is designed.** We replace the lower-level problem with complement conditions and then convert the bi-level model into a single-level mode. Furthermore, using linear relaxation, we transform the single-level model into a MIQP. By solving the MIQP we can determine the information about the upper and lower bounds of our original problem, and then the global optimal solution algorithm with calculation size reduction approach and four piecewise interval strategies are proposed.

iii) **The effectiveness and applicability of the proposed algorithm are illustrated with a simple case and three real-world cases.** Specifically, the simple case shows the details of our algorithm result with different input data, different parameter values and different strategies. The second case illustrates the applicability and calculating efficiency of four strategies in a real-world network of Nanchang-Jiujiang Intercity Railway. And the third case study tests our algorithm in the real-world intersection network of Guangzhou-Zhuhai Intercity Railway with larger scale. In order to further analysis the application of our algorithm, we test it on a larger and more complex network in the Xi'an region HSR network.

The rest of this paper is organized as follows. Section 2 introduces the basic considerations of our problem, and Section 3 formulates our model. Section 4 uses linear relaxation to reformulate our model and propose the solution algorithm. Numerical studies are conducted in Section 5 and Section 6 concludes our paper.

2. Basic considerations

In this section, we first list the notation and then the assumptions of this paper are proposed.

2.1 Notations

Table 2. Parameters and variables

Symbol	Definition
Sets and indices	
(V, E)	HSR network, where V and E represent the Set of HSR stations and rail track sections
$(\mathbb{V}, \mathbb{A})$	Space-time network, where $\mathbb{V}$ and $\mathbb{A}$ represents set of space-time nodes and arcs
RS	Set of HSR OD pairs (with $(r, s) \in RS$)
K	Set of HSR trains (with $k \in K$)
V^k	Set of stop stations of train $k \in K$ (with $V^k = \left(v_1^k, v_2^k, \cdots, v_{n(k)}^k\right)$)
D^k	Set of departure time points of $k \in K$ (with $D^k = \left(d_1^k, d_2^k, \cdots, d_{n(k)-1}^k\right)$)
A^k	Set of arrival time points of $k \in K$ (with $A^k = \left(a_2^k, a_3^k, \cdots, a_{n(k)}^k\right)$)
A_{ac}	Set of access arcs (with $\left(r(t), d_i^k\right) \in A_{ac}$)
A_{in}	Set of in-train arcs (with $\left(d_i^k, a_{i+1}^k\right) \in A_{in}$)
A_{dw}	Set of dwell arcs (with $\left(a_i^k, d_i^k\right) \in A_{dw}$)
A_{tr}	Set of transfer arc (with $\left(a_i^k, d_i^{k'}\right) \in A_{tr}$)
A_{end}	Set of ending arc (with $\left(a_i^k, s^\infty\right) \in A_{end}$)
$P_{rs}(t)$	Set of feasible space-time paths for demand $q_{rs}(t)$ (with $p(t) \in P_{rs}(t)$)
$\bar{P}_{rs}(t)$	Set of feasible space-time paths with reduction in calculation size for demand $q_{rs}(t)$
P_{rs}	Set of paths for OD pair (r, s) (with $p \in P_{rs}$)
Q_{rs}^t	Set of breakpoints (with $q_{rs}^{t,n} \in Q_{rs}^t$)
$\Delta\tilde{Q}_{rs}^{t,h}$	Set of adding breakpoints at iteration h
Parameters	
$[T^1, T^2]$	Daily operation period (can be discretized as $[T^1, T^2] = [1,2, \cdots, T]$)
$\lvert k(i, i+1) \rvert$	Mileage of route train k from its stop station v_i^k to v_{i+1}^k
η', η''	The unit cost for the early and late departure
ω	The unit cost of travel time
δ	The minimum transfer time duration at the HSR station
$\gamma(k)$	The ticket fare rate of train $k \in K$
$\varphi(v)$	The transfer cost at station $v \in V$
u_k	The capacity of train $k \in K$
$\hat{f}_p$	The flow (ticket booking volume) of path p
$\delta_{p(t)}^a$	A binary variable, which equals one if arc a on path $p(t)$ and 0 otherwise.
U	An extremely small negative number
M	An extremely large positive number
N	The breakpoints number for piecewise interval by the demand of OD pair for linear relaxation
α_1, α_2	Weighting coefficient for objective function
ϑ	An extremely small positive number and close to 0
$\underline{q}_{rs}^t, \overline{q}_{rs}^t$	Lower and upper bounds of q_{rs}^t

ε	Convergence criterion
Variables	
q_{rs}^{t}	Demand with desired departure time at t of HSR OD pair $(r,s) \in RS$ (with $t = 1,2,\cdots,n$)
$f_{p(t)}$	The flow of feasible space-time path $p(t) \in P_{rs}(t)$
x_a	The flow on arc $a \in \mathbb{A}$
π_{rs}^{t}	Lagrange multipliers (can be seen as the minimal cost between OD pair $(r,s) \in RS$ for demand q_{rs}^{t})
π_a	Lagrange multipliers (can be seen as advance booking fee of space-time arc $a \in \mathbb{A}$)
$v_{p(t)}$	Lagrange multipliers (with $t = 1,2,\cdots T; p \in P_{rs}; (r,s) \in RS$)
l_a	Introduced 0-1 decision variables (with $a \in \mathbb{A}$)
$h_{p(t)}$	Introduced 0-1 decision variables (with $t = 1,2,\cdots T; p \in P_{rs}; (r,s) \in RS$)
$\lambda_{rs}^{t,n}$	Introduced 0-1 decision variables (with $n = 1,2,\cdots,N-1; t = 1,2,\cdots T; (r,s) \in RS$)
$\theta_{rs}^{t,n}$	Introduced decision variables (with $n = 1,2,\cdots,N; t = 1,2,\cdots T; (r,s) \in RS$)
$\mathcal{L}_{rs}^{t}$	Introduced decision variables (with $t = 1,2,\cdots T; (r,s) \in RS$)

2.2 Assumptions

In order to facilitate the presentation of our problem, the following assumptions are made:

A1: As high speed and high service frequency, the total transport capacity of each HSR OD pair can cover its total demand volumes. This assumption is consistent with reality most of the time where the tickets of some popular trains may be sold out, but the total demand volumes are still lower than supply capacity of HSR systems and some passengers may shift to less ideal trains at non-peak period (Niu et al., 2015; Xu et al., 2021). Compared with the traditional rail system, the transport capacity of the HSR system has greatly improved with its high speed and high service frequency. Additionally, the capacity of the HSR system can be further enhanced by flexible train formation (e.g., China's HSR train can expand from 8 coaches to 16 coaches). These means that the situation that the total transport capacity cannot cover its total demand volume is not common in the HSR systems, and only occurs on special holidays (such as the Chinese Spring Festival) or in special events (such as driver strikes or extreme weather). Since our research mainly focuses on the common conditions, we exclude the relatively unlikely situation through this assumption.

A2: The demand outside the operation period in a day is negligible and can be ignored. On the one hand, from technological considerations, HSR cannot provide 24-hour service. It needs a certain time period within a day for necessary rail inspection and equipment maintenance. Therefore, the demand outside the operation period cannot be met by the HSR systems, and there is no need to estimate this demand. On the other hand, from the demand perspective, the operation period of HSR is usually set during the daytime when the demand is high, while non-operation periods (maintenance periods) are usually set in the night (such as 0:00-5:59) when the demand is very low. Since the demand out of operation period is very low and be ignored, we only consider the time-varying demand distribution within the operation

period, which is similar to existing works (Wei et al., 2019; Wong and Tong, 1998).

A3: Passengers book their tickets (choose their train/path) to minimize their own travel cost. This assumption about rational consumers exists in almost all transportation studies using the UE theoretical framework (Huang et al., 2023; Wu et al., 2022). There may be some differences between it and the reality, but we want to use UE theory to provide a foundational framework for understanding and modeling the TDD estimation problem in the HSR networks. By utilizing this principle, we can develop models that more straightforwardly analyze and interpret passengers' choice behaviors. Further, we have relaxed the Assumption **A3** by extending our model from the UE framework to the Boundedly Rational User Equilibrium (BRUE) framework in the following Section 3.3, please refer to it for details.

3. Model formulation

In this section, we first propose the space-time network of the HSR systems, then a bi-level model and its corresponding single-level model are formulated for the TDD estimation problem.

3.1 Space-time network

Let (V, E) be the HSR track network, where V is the station set and E is the section set, and here the section is the rail track between two adjacent stations. For the HSR network (V, E), let RS be the OD pair set with $(r, s) \in RS$, and $[T^1, T^2]$ denotes the daily operation period of HSR systems. The continuous daily operation period $[T^1, T^2]$ can be discretized into T equal time intervals with $[T^1, T^2] = [1,2,\cdots,T]$ where the time length of each interval is $\frac{T^2-T^1}{T}$. Then given the timetable and based on the HSR network (V, E), we design the space-time network $(\mathbb{V}, \mathbb{A})$ as follows.

i) Space-time nodes

We denote the HSR train set as K in the timetable. For any train $k \in K$, define its stop stations set as $V^k = \left(v_1^k, v_2^k, \cdots, v_i^k, \cdots, v_{n(k)}^k\right)$, its departure time nodes set as $D^k = \left(d_1^k, d_2^k, \cdots, d_i^k, \cdots, d_{n(k)-1}^k\right)$, and its arrival time nodes set as $A^k = \left(a_2^k, a_3^k, \cdots, a_i^k, \cdots, a_{n(k)}^k\right)$, where $n(k)$ is the number of stop stations of train k. For train $k \in K$, the train segment from its stop station v_i^k to v_{i+1}^k is denoted as $k(i, i+1)$, and its corresponding mileage denoted as $|k(i, i+1)|$. Then in the space-time network, the departure node d_i^k and arrival point a_i^k means the departure and arrival events of train k at station v_i^k. For example, in Fig. 4 the departure and arrival nodes of train 1 are $d_1^1, a_2^1, d_2^1, a_3^1, d_3^1$ and d_4^1. The departure node of train 2 at station $v_1^2 = v_1$ is d_1^2, and its arrival node at station $v_2^2 = v_3$ is a_2^2, while station v_2 is skipped by this train.

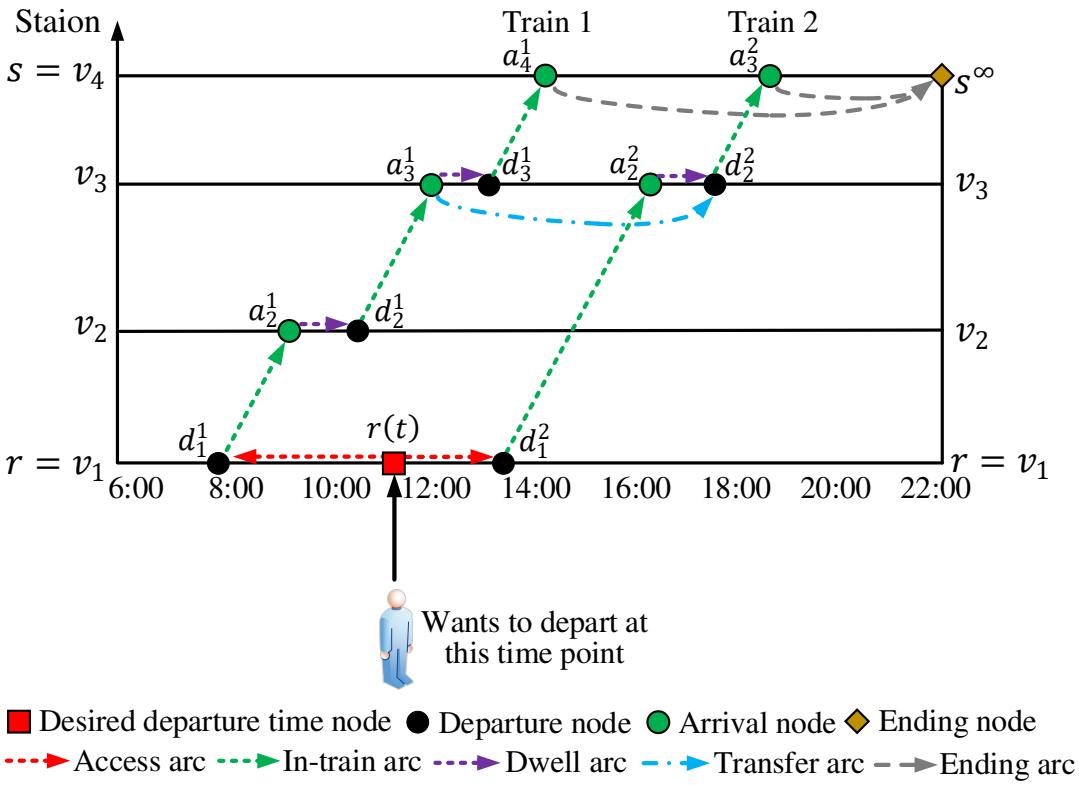

Fig. 4. Illustration space-time network

For the HSR OD pair $(r, s) \in RS$, let the virtual start node $r(t)$ represent the trip start for the passengers with desired departure time $t = 1,2,\cdots,n$ at original station r, and let the virtual end node s^∞ represent the end at the destination station s.

Then in the space-time network, the set of space-time nodes $\mathbb{V}$ consists of departure nodes, arrival nodes, virtual start nodes and virtual end nodes, which is expressed as Eq. (1).

$$\mathbb{V} = \{d_i^k \in D^k\} \cup \{a_i^k \in A^k\} \cup \{r(t) | (r,s) \in RS; t = 1,2,\cdots,T\} \cup \{s^\infty | s \in V\} \quad (1)$$

ii) Space-time arcs

Access arc $\left(r(t), d_i^k\right)$, from the desired departure node $r(t)$ of the passenger to the real departure node d_i^k of the chosen train at the original station r ($v_i^k = r$), which means for the HSR OD pair $(r, s) \in RS$, passengers whose desired departure time is t, book the tickets of train $k \in K$ with the departure time d_i^k to start their trips. And the set of access arcs is denoted A_{ac}.

In-train arc $\left(d_i^k, a_{i+1}^k\right)$, from the departure node d_i^k at station v_i^k of train $k \in K$ to its next arrival node a_{i+1}^k at station v_{i+1}^k, reflects passengers' journeys from station v_i^k to v_{i+1}^k with train $k \in K$. The set of in-train arcs can be denoted as A_{in}.

Dwell arc $\left(a_i^k, d_i^k\right)$, from the arrival node a_i^k at station v_i^k of train $k \in K$ to its next departure node d_i^k, shows that passengers wait for a dwell time at station v_i^k on train $k \in K$. The set of dwell arcs is denoted A_{dw}.

Transfer arc $\left(a_i^k, d_{i'}^{k'}\right)$, from the arrival node a_i^k of train $k \in K$ at station v_i^k to the departure node $d_{i'}^{k'}$ of the first subsequent train $k' \in K$ at this station ($v_{i'}^{k'} = v_i^k$) whose

departure time is greater than the minimum transfer time duration δ, such as $\delta = 10$ minutes. It reflects passengers making a transfer from train k to k' at station $v_i^k = v_{i'}^{k'}$. The set of transfer arcs is denoted as A_{tr}.

Ending arc $\left(a_i^k, s^\infty\right)$, from the arrival node a_i^k at station $v_i^k = s \in V$ to its corresponding ending node s^∞, shows the ending of passengers' journeys. The set of ending arc is denoted A_{end}.

Thus, in the space-time network, the set of space-time arcs $\mathbb{V}$ consists of access arcs, in-train arcs, dwell arcs, transfer arcs and ending arcs, which is represented as Eq. (2).

$$\mathbb{A} = A_{ac} \cup A_{in} \cup A_{dw} \cup A_{tr} \cup A_{end} \tag{2}$$

iii) Space-time arc cost

The total travel cost for a HSR passenger consists of adjusted departure time cost, travel time cost, ticket fare and transfer cost. Then the arc cost can be expressed as Eq. (3).

$$c_a = \begin{cases} \eta' \cdot \max\{0, t - d_i^k\} + \eta'' \cdot \max\{0, d_i^k - t\}, & a = \left(r(t), d_i^k\right) \in A_{ac} \\ \omega \cdot \left(a_{i+1}^k - d_i^k\right) + \gamma(k) \cdot |k(i, i+1)|, & a = \left(d_i^k, a_{i+1}^k\right) \in A_{in} \\ \omega \cdot \left(d_i^k - a_i^k\right), & a = \left(a_i^k, d_i^k\right) \in A_{dw} \\ \omega \cdot \left(d_{i'}^{k'} - a_i^k\right) + \varphi\left(v_i^k\right), & a = \left(a_i^k, d_{i'}^{k'}\right) \in A_{tr} \\ 0, & a = \left(a_i^k, s^\infty\right) \in A_{end} \end{cases} \tag{3}$$

where, η' and η'' are the unit costs for early and late departures, and we assume the cost of the adjusted departure time penalty to be linear with the adjustment time, which is similar to many previous studies (Abegaz et al., 2017; Hamdouch et al., 2011; Liang et al., 2024; Tang et al., 2019, 2020b; Yang and Tang, 2018); ω is the unit cost of travel time; $\gamma(k)$ is the ticket fare rate of train $k \in K$, and $\varphi(v)$ is the transfer cost at station $v \in V$.

iv) Space-time arc capacity

In HSR space-time network $(\mathbb{V}, \mathbb{A})$, let u_a be the capacity of space-time arc $a \in \mathbb{A}$. The capacity of in-train arc is equal to its corresponding train capacity, and the capacity of other space-time arcs can be set as infinite. Then the capacity can be represented as Eq. (4).

$$u_a = \begin{cases} \infty, & a = \left(r(t), d_i^k\right) \in A_{ac} \\ u_k, & a = \left(d_i^k, a_{i+1}^k\right) \in A_{in} \\ \infty, & a = \left(a_i^k, d_i^k\right) \in A_{dw} \\ \infty, & a = \left(a_i^k, d_i^{k'}\right) \in A_{tr} \\ \infty, & a = \left(a_i^k, s^\infty\right) \in A_{end} \end{cases} \tag{4}$$

Where u_k is the capacity of train $k \in K$.

v) Path and feasible space-time path

For any HSR OD pair $(r, s) \in RS$, denote all paths from the departure node at station r to the arrival node at station s as the set P_{rs}. For any path $p \in P_{rs}$, its flow is denoted as $\hat{f}_p$, which represents the ticket booking volume of p and can be obtained from the ticket booking system. Taking Fig. 4 as an example, the three paths p^1, p^2 and p^3 for OD pair (v_1, v_4) are shown as below, and their corresponding path flows $\hat{f}_{p^1}, \hat{f}_{p^2}$ and $\hat{f}_{p^3}$ can be obtained from the ticket

booking system.

$$p^1 = \{(d_1^1, a_2^1), (a_2^1, d_2^1), (d_2^1, a_3^1), (a_3^1, d_3^1), (d_3^1, a_4^1)\}$$
$$p^2 = \{(d_1^2, a_2^2), (a_2^2, d_2^2), (d_2^2, a_3^2)\}$$
$$p^3 = \{(d_1^1, a_2^1), (a_2^1, d_2^1), (d_2^1, a_3^1), (a_3^1, d_2^2), (d_2^2, a_3^2)\}$$

where, paths p^1 and p^2 use Train 1 and Train 2 respectively to get to the destination, and p^3 first uses Train 1 and then transfers to Train 2 at station v_3 to get to the destination.

For demand q_{rs}^t, let $p(t)$ be the feasible space-time path from the desired departure time node $r(t)$ connected to the path p by access arc, and then ending up at destination node s^∞ with ending arc, and this $p(t)$ means the passengers with desired departure time t choose path p to destination to form the space-time path. And the feasible space-time path set for demand q_{rs}^t is denoted $P_{rs}(t)$. Take demand q_{14}^t in Fig. 4 as an example. For the passengers with desired departure time t, their feasible space-time paths are the follows.

$$p^1(t) = \{(r(t), d_1^1), (d_1^1, a_2^1), (a_2^1, d_2^1), (d_2^1, a_3^1), (a_3^1, d_3^1), (d_3^1, a_4^1), (a_4^1, s^\infty)\}$$
$$p^2(t) = \{(r(t), d_1^2), (d_1^2, a_2^2), (a_2^2, d_2^2), (d_2^2, a_3^2), (a_3^2, s^\infty)\}$$
$$p^3(t) = \{(r(t), d_1^1), (d_1^1, a_2^1), (a_2^1, d_2^1), (d_2^1, a_3^1), (a_3^1, d_2^2), (d_2^2, a_3^2), (a_3^2, s^\infty)\}$$

Denote the flow and cost of feasible space-time path $p(t)$ as $f_{p(t)}$ and $c_{p(t)}$ respectively. For demand q_{rs}^t, the feasible space-time path cost of $p(t) \in P_{rs}(t)$ is the sum of the costs for all space-time arcs along this path. In the HSR systems, the transport capacity is significantly improved due to the high speed and high departure frequency of train services. Consequently, passengers are more willing to depart at their desired departure times (choose the train closest to their desired departure times) and more sensitive to the adjusted desired departure time penalty. Thus, the cost $c_{p(t)}$ is formulated as a generalized cost which combinate the adjusted departure time cost, travel time cost, tickets fare and transfer cost. And it can be represented as Eq. (5).

$$c_{p(t)} = \sum_{a \in p(t)} c_a, \qquad p(t) \in P_{rs}(t); t = 1,2,\cdots,T; (r,s) \in RS \quad (5)$$

From the above description, our problem can be stated more formally as: given the HSR schedule we can use the above space-time network to determine the capacity u_a and cost c_a of each space-time arc $a \in \mathbb{A}$, and together with the ticket booking volume $\hat{f}_p$ of each path $p \in P_{rs}, (r,s) \in RS$ from ticket booking system, then we need to estimate the TDD $q_{rs}^t, t \in [T^1, T^2]$ for each HSR OD pair $(r,s) \in RS$.

3.2 Bi-level model for estimating the TDD problem (BL-ETDDP)

Based on the above analysis, we formulate the following Bi-Level model (M1) for Estimating the TDD problem (abbreviated by BL-ETDDP) as shown in Fig. 5.

Upper level:

$$\min Z(\boldsymbol{q}) = \alpha_1 \sum_{(r,s) \in RS} \sum_{t=1}^{T} (q_{rs}^t \ln q_{rs}^t - q_{rs}^t) + \alpha_2 \sum_{(r,s) \in RS} \sum_{p \in P_{rs}} \left(\sum_{t=1}^{T} f_{p(t)} - \hat{f}_p \right)^2 \quad (6)$$

subject to

$$q_{rs}^t \geq 0, \qquad t = 1,2,\ldots,T; (r,s) \in RS \quad (7)$$

$$\sum_{p\in P_{rs}} \hat{f}_p = \sum_{t=1}^{T} q_{rs}^t, \qquad (r,s) \in RS \quad (8)$$

Lower level:

$$\min Z(\mathbf{f}) = \sum_{a\in\mathbb{A}} c_a \cdot x_a \quad (9)$$

subject to

$$q_{rs}^t = \sum_{p\in P_{rs}} f_{p(t)}, \qquad t = 1,2,\cdots,T; (r,s) \in RS \quad (10)$$

$$x_a \le u_a, \qquad a \in \mathbb{A} \quad (11)$$

$$f_{p(t)} \ge 0, \qquad t = 1,2,\cdots,T; p \in P_{rs}; (r,s) \in RS \quad (12)$$

$$x_a = \sum_{(r,s)\in RS} \sum_{p\in P_{rs}} \sum_{t=1}^{T} f_{p(t)} \cdot \delta_{p(t)}^a, \qquad a \in \mathbb{A} \quad (13)$$

where $\delta_{p(t)}^a$ is the path-arc parameter, and its value can be determined by Eq. (14).

$$\delta_{p(t)}^a = \begin{cases} 1, \text{if arc } a \text{ is on path } f_{p(t)} \\ 0, \text{otherwise} \end{cases}, \qquad a \in \mathbb{A}; t = 1,2,\cdots,T; p \in P_{rs}; (r,s) \in RS \quad (14)$$

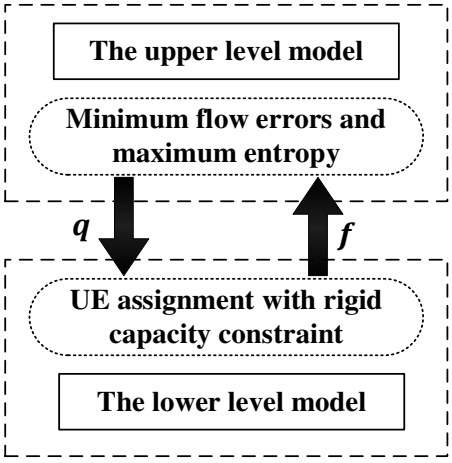

Fig. 5. Illustration of the Bi-level model

In the upper-level, Eq. (6) is the weighted sum minimization of the least squares term and maximum entropy term. The least squares term seeks to obtain a TDD with a minimal error between the booking volumes $\hat{f}_p$ of p and its corresponding feasible space-time path flow $f_{p(t)}$, where $f_{p(t)}$ is the equilibrium flow obtained by solving the lower-level model. As there may be more than one TDD that meets the requirements, we choose the one with maximal entropy value. The maximum entropy framework considers that all possible states of the variables have equal probability to occur and selects the most likely state consistent with the evidence available (Shannon, 1948; Teye et al., 2017). Following this principle, López-Ospina et al. (2022); Van Zuylen and Willumsen (1980); Xie et al. (2011) proposed their maximum entropy models to predict a most likely OD flow pattern for the road network with the observed link traffic counts. Wong and Tong (1998) use the maximum entropy approach to estimate the time-dependent OD matrices based on the measured link flow rates at each time interval for public transit network. This principle is particularly useful in situations where we have limited or incomplete information about a system, e.g., no demand information during the period with no train

departing. Following these papers, given the constraints and data available we develop a maximum entropy-based model to estimate an unbiased and most likely TDD pattern (over desired departure time).

Eq. (7) are the non-negative constraints of the decision variable q_{rs}^t. And Eq. (8) means that the demand from all desired departure times for an OD pair will be served by all paths of this OD pair.

In the lower-level, Eq. (9) minimizes the total cost in the HSR networks, where x_a is the flow on arc $a \in \mathbb{A}$. Eq. (10) are the conservation constraints which means demand q_{rs}^t must be serviced by all paths in P_{rs} between OD pair $(r,s) \in RS$. Eqs. (11) are capacity constraining for space-time arcs[3], and the non-negative constraints of feasible space-time path flows are shown in Eqs. (12). Eqs. (13) and (14) are the calculations of space-time arc flow x_a from the feasible space-time path flow $f_{p(t)}$. Therefore, for a given TDD q_{rs}^t from the upper-level, the feasible space-time path flow $f_{p(t)}$ can be determined by solving the lower-level model.

There are many previous studies on the bi-level model (Szeto and Jiang, 2014; Tang et al., 2020a; Xi et al., 2023; Yang and Bell, 2001), and in this paper, we will use complementary constraints to replace the lower-level program and convert the bi-level model into a single-level model, and then use linear relaxation to design the global optimal algorithm.

Before we analyze the above model, we first introduce the definition of User Equilibrium (UE) as applicable to HSR systems.

Definition 1 (UE): In HSR systems, with the principle of passengers booking their tickets to minimize their travel cost, the UE will be achieved when, for all passengers with the same desire departure time for the same OD pair, all used paths have equal and minimal cost, and all other unused paths have higher costs.

Proposition 1. In the HSR systems, with rigid seat capacity constraints and flow-independent cost components, the linear programming (LP) of the lower-level model is equivalent to UE.

Proof. We get the Lagrange function for the LP as the following:

$$L = \sum_{a\in\mathbb{A}} c_a \cdot x_a - \sum_{(r,s)\in RS} \sum_{t=1}^{T} \pi_{rs}^t \cdot \left(\sum_{p\in P_{rs}} f_{p(t)} - q_{rs}^t \right) - \sum_{a\in\mathbb{A}} \pi_a \cdot (u_a - x_a)$$

$$- \sum_{(r,s)\in RS} \sum_{p\in P_{rs}} \sum_{t=1}^{T} v_{p(t)} \cdot f_{p(t)} \tag{15}$$

where π_{rs}^t, π_a and $v_{p(t)}$ are the corresponding Lagrange multipliers for constraints (10), (11) and (12) respectively. Then the Kuhn-Tucker (KT) conditions of the above lower-level LP problem can be derived as follows:

$$\sum_{a\in\mathbb{A}} c_a \cdot \delta_{p(t)}^a - \pi_{rs}^t + \sum_{a\in\mathbb{A}} \pi_a \cdot \delta_{p(t)}^a - v_{p(t)} = 0, t = 1,2,\cdots,T; p \in P_{rs}; (r,s) \in RS \tag{16}$$

$$\begin{cases} u_a \geq x_a \\ \pi_a \geq 0 \\ \pi_a \cdot (u_a - x_a) = 0 \end{cases}, \quad a \in \mathbb{A} \tag{17}$$

[3] This arc-based capacity constraints can be extended to the space-time path-based capacity constraints by considering the seat allocation scheme. Since the rest of the subsequent technical processes are the same and we can only choose one of the two (arc-based and space-time path-based), we retain the current model to maintain scalability.

$$\begin{cases} f_{p(t)} \geq 0 \\ v_{p(t)} \geq 0 \\ f_{p(t)} \cdot v_{p(t)} = 0 \end{cases}, \quad t = 1,2,\cdots T; p \in P_{rs}; (r,s) \in RS \quad (18)$$

In the railway system, passengers need to select the train service and book the tickets in advance, using either the on-site or online ticketing system. Due to rigid train capacity constraints, individual passengers may not be able to obtain their preferred train service, depending on how many passengers are competing and how early they make their ticket booking. This "early booking" to ensure ticket availability indeed can yield non-negligible cost to passengers, which is defined as the advance booking cost. By analyzing passenger choice equilibrium, it can be better understood how much individuals are willing to pay for securing tickets on their preferred trains with ideal departure and arrival times, as well as shorter journey times. In situations where the passenger demand is low and trains have residual capacity, there is no need for passengers to book tickets in advance. However, during peak periods popular trains are expected to be fully occupied. As a result, passengers must book tickets much further in advance. This reflects their willingness to pay a higher cost to secure their desired train tickets. Eq. (17) above is equivalent to Eq. (19) which follows. And the Lagrange multiplier π_a can be seen as the advance booking cost of arc $a \in \mathbb{A}$ to secure a seat. Then Eq. (19) means that if the flow of arc $a \in \mathbb{A}$ equals its capacity, i.e., $x_a = u_a$, then the advance booking fee of arc $a \in \mathbb{A}$ is larger than or equal to zero, i.e., $\pi_a \geq 0$, and passengers need to book early enough to secure a ticket; and if the flow of arc $a \in \mathbb{A}$ less than its capacity, i.e., $x_a < u_a$, then there is no advance booking fee of arc $a \in \mathbb{A}$, i.e., $\pi_a = 0$, and passengers can book the tickets just before boarding as there are always available tickets.

$$\begin{cases} \pi_a \geq 0, & \text{if } x_a = u_a \\ \pi_a = 0, & \text{if } x_a < u_a \end{cases}, \quad a \in \mathbb{A} \quad (19)$$

Then the total travel cost for passengers choosing feasible space-time path $p(t)$ is the sum of arc costs and advance booking cost of all arcs along the path, i.e., $\sum_{a \in p(t)}(c_a + \pi_a) = c_{p(t)} + \sum_{a \in p(t)} \pi_a$. And from Eqs. (5), (16) and (18), we can obtain:

$$\begin{cases} f_{p(t)} \geq 0 \\ c_{p(t)} + \sum_{a \in \mathbb{A}} \pi_a \cdot \delta_{p(t)}^a - \pi_{rs}^t \geq 0 \\ f_{p(t)} \cdot \left(c_{p(t)} + \sum_{a \in \mathbb{A}} \pi_a \cdot \delta_{p(t)}^a - \pi_{rs}^t \right) = 0 \end{cases}, \quad t = 1,2,\cdots T; p \in P_{rs}; (r,s) \in RS \quad (20)$$

$$\begin{cases} c_{p(t)} + \sum_{a \in \mathbb{A}} \pi_a \cdot \delta_{p(t)}^a = \pi_{rs}^t, \text{if } f_{p(t)} > 0 \\ c_{p(t)} + \sum_{a \in \mathbb{A}} \pi_a \cdot \delta_{p(t)}^a \geq \pi_{rs}^t, \text{if } f_{p(t)} = 0 \end{cases}, \quad t = 1,2,\cdots T; p \in P_{rs}; (r,s) \in RS \quad (21)$$

For the Lagrange multiplier π_{rs}^t, it can be seen as the minimal cost between OD pair $(r,s) \in RS$ for demand q_{rs}^t. And Eq. (20) is equivalent to the subsequent Eq. (21). From Eq. (21) we can establish that if any passengers associated with demand q_{rs}^t choose the feasible space-time path $p(t) \in P_{rs}(t)$, i.e., $f_{p(t)} > 0$, then the actual cost of path $p(t)$ (path cost $c_{p(t)}$ and the advance ticket booking cost $\sum_{a \in \mathbb{A}} \pi_a \cdot \delta_{p(t)}^a$) equals the minimal cost between OD pair (r,s) for demand $q_{rs}(t)$, i.e., $c_{p(t)} + \sum_{a \in \mathbb{A}} \pi_a \cdot \delta_{p(t)}^a = \pi_{rs}^t$; and if no passenger uses the feasible space-time path $p(t) \in P_{rs}(t)$, i.e., $f_{p(t)} = 0$, then the actual cost of path $p(t)$ is larger than or equal to the minimal cost between OD pair (r,s) for demand $q_{rs}(t)$, i.e., $c_{p(t)} +$

$\sum_{a\in\mathbb{A}} \pi_a \cdot \delta^a_{p(t)} \geq \pi^t_{rs}$. This means that Eq. (21) meets Definition 1 and the lower-level model of M1 is the UE. □

3.3 Single-level model for estimating TDD problem (SL-ETDDP)

From the above analysis, we know that the lower-level of M1 is the UE, and the UE is equivalent with its complementary conditions Eqs. (10), (16) and (19). Then, by replacing the lower-level problem with complementary conditions, the BL-ETDDP model M1 can be convert into single level model M2 for estimating TDD problem (SL-ETDDP), which is shown as below.

M2:

$$\min Z(\boldsymbol{q}) = \alpha_1 \sum_{(r,s)\in RS} \sum_{t=1}^{T} (q^t_{rs} \ln q^t_{rs} - q^t_{rs}) + \alpha_2 \sum_{(r,s)\in RS} \sum_{p\in P_{rs}} \left(\sum_{t=1}^{T} f_{p(t)} - \hat{f}_p \right)^2 \quad (6)$$

subject to

Eqs. (7)-(8), (10), (13), (17) and (20).

In addition, the above model estimates the TDD involving the UE passenger assignment method, and it can be extended to adopting the Boundedly Rational User Equilibrium (BRUE) passenger assignment modeling, please see the Appendix A for more details.

4. Solution algorithm

In this section, we first relax the SL-ETDDP model M2 to the MIQP by mixed-integer linear relaxation. And based on the global solution of MIQP, we will discuss how to reduce the calculation size of our problem and the idea of obtaining the optimal solution to our original problem. Then, four strategies will be proposed to obtain the global optimal solution. And the algorithm of our problem will be designed in the last subsection.

The piece-wise linear approximation method has been utilized to reformulate problems and along with the development of global optimization algorithms, has garnered significant interest among researchers focusing on transportation optimization issues. Examples include transportation network design challenges within the frameworks of UE or Stochastic User Equilibrium (SUE) constraints by the studies from Liu and Wang (2015); Luathep et al. (2011); Wang and Lo (2010). Furthermore, it has been explored in addressing toll design issues by Ekström et al. (2012); Zhang and van Wee (2012). More recent contributions, such as those from Froger et al. (2019); Montoya et al. (2017); Zhou et al. (2022), have applied the piece-wise linear approximation method to approximate nonlinear charging functions for Electric Vehicle charging scheduling problems, as well as Caicedo et al. (2023); Liu et al. (2019) applied it in bike network design problems. In this paper, the piece-wise linear approximation method is introduced into the estimation of TDD problems for HSR systems. Drawing inspiration from Liu and Wang (2015); Xu et al. (2022), we have developed a custom range reduction technique to tighten the feasible region of the TDD estimation problem. This is prior to applying the global optimal solution algorithm detailed herein, and it significantly reduces the computational time required to achieve results.

4.1 Mixed-integer linear relaxation

i) Linear relaxation of constraints

In the above SL-ETDDP model M2, nonlinear constraints Eq. (17) and Eq. (20) can be replaced by the following linear constraints Eq. (22) and Eq. (23) respectively.

$$\begin{cases} U \cdot l_a + \varepsilon \le \pi_a \le M \cdot (1 - l_a) \\ U \cdot l_a \le u_a - x_a \le M \cdot l_a \\ u_a - x_a \ge 0 \\ \pi_a \ge 0 \\ l_a \in \{0,1\} \end{cases}, \quad a \in \mathbb{A} \tag{22}$$

$$\begin{cases} U \cdot h_{p(t)} + \vartheta \le f_{p(t)} \le M \cdot (1 - h_{p(t)}) \\ U \cdot h_{p(t)} \le c_{p(t)} + \sum_{a \in \mathbb{A}} \pi_a \cdot \delta_{p(t)}^a - \pi_{rs}^t \le M \cdot h_{p(t)} \\ c_{p(t)} + \sum_{a \in \mathbb{A}} \pi_a \cdot \delta_{p(t)}^a - \pi_{rs}^t \ge 0 \\ f_{p(t)} \ge 0 \\ h_{p(t)} \in \{0,1\} \end{cases}, t = 1,2,\cdots T; p \in P_{rs}; (r,s) \in RS \tag{23}$$

where U is an extremely small negative number; M is an extremely large positive number; ϑ is an extremely small positive number and close to 0; and l_a, $h_{p(t)}$ are 0-1 decision variables.

Then, all the constraints in the SL-ETDDP model M2 are linear, by replacing Eq. (17) and Eq. (20) with Eq. (22) and Eq. (23) respectively.

ii) Linear relaxation of objective function

For the above model M2, the objective function is nonlinear with the logarithmic term (maximum entropy) and quadratic term (least square). Similar to existing studies (Liu et al., 2019; Liu and Wang, 2015; Vielma et al., 2010), the logarithmic term can be linearized in piecewise manner by the linear approximate method. The objective function Eq. (6) can be represented as:

$$\min Z_2 = \alpha_1 \sum_{(r,s) \in RS} \sum_{t=1}^{T} \mathcal{L}_{rs}^t + \alpha_2 \sum_{(r,s) \in RS} \sum_{p \in P_{rs}} \left(\sum_{t=1}^{T} f_{p(t)} - \hat{f}_p \right)^2 \tag{24}$$

$$\mathcal{L}_{rs}^t = q_{rs}^t \ln q_{rs}^t - q_{rs}^t, \quad t = 1,2,\dots,T; (r,s) \in RS \tag{25}$$

Obviously, the second partial derivative of Eq. (25) with respect to its decision variable (q_{rs}^t) is larger than 0, then Eq. (25) is a convex function on its closed interval.

For Eq. (25), denote the lower and upper bounds of q_{rs}^t as $\underline{q}_{rs}^t$ and $\overline{q}_{rs}^t$ respectively (their values will be discussed in the next subsection). The interval $\left[\underline{q}_{rs}^t, \overline{q}_{rs}^t\right], t = 1,2,\dots,T; (r,s) \in RS$ can be divided uniformly into $N-1$ intervals by the set of breakpoints $q_{rs}^{t,n} \in Q_{rs}^t$ which is calculated by Eq. (26).

$$Q_{rs}^t = \left\{ q_{rs}^{t,n} \middle| q_{rs}^{t,n} = \underline{q}_{rs}^t + \frac{\overline{q}_{rs}^t - \underline{q}_{rs}^t}{N-1} \cdot (n-1), n = 1,2,\cdots,N \right\}, \quad t = 1,2,\dots,T; (r,s) \in RS \tag{26}$$

As shown in Fig. 6, linear relaxation of Eq. (25) is set to be the region above all tangent lines and below all curve chords. The tangential support is constructed at each $q_{rs}^{t,n} \in Q_{rs}^{t}$ and the curve chords are formed by connecting two adjacent points $q_{rs}^{t,n}$ and $q_{rs}^{t,n+1}$ for $n = 1,2,\cdots,N-1$.

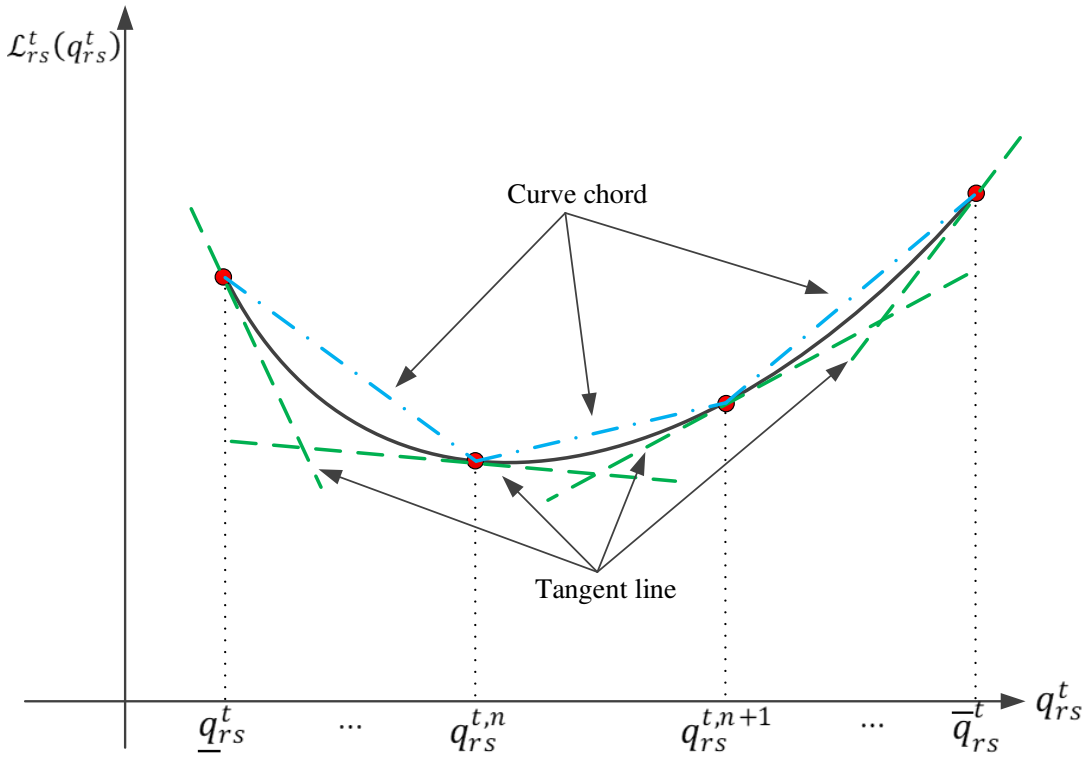

Fig 6. Linear relaxation

Then the relaxation of $\mathcal{L}_{rs}^{t}(q_{rs}^{t})$ with breakpoints $q_{rs}^{t,n} \in Q_{rs}^{t}, n = 1,2,\cdots,N$ can be constructed as follows:

$$\mathcal{L}_{rs}^{t} \geq -q_{rs}^{t,n} + q_{rs}^{t} \cdot \ln q_{rs}^{t,n}, \quad \forall q_{rs}^{t,n} = \underline{q}_{rs}^{t} + \frac{\overline{q}_{rs}^{t} - \underline{q}_{rs}^{t}}{N-1} \cdot (n-1), n = 1,2,\cdots,N \tag{27}$$

$$\sum_{n=1}^{N} \theta_{rs}^{t,n} \cdot q_{rs}^{t,n} = q_{rs}^{t} \tag{28}$$

$$\sum_{n=1}^{N} \theta_{rs}^{t,n} \cdot \mathcal{L}_{rs}^{t}\left(q_{rs}^{t,n}\right) \geq \mathcal{L}_{rs}^{t}(q_{rs}^{t}) \tag{29}$$

$$\sum_{n=1}^{N} \theta_{rs}^{t,n} = 1 \tag{30}$$

$$\theta_{rs}^{t,n} \geq 0, \qquad n = 1,2,\cdots,N \tag{31}$$

$$\theta_{rs}^{t,n} \leq \lambda_{rs}^{t,n-1} + \lambda_{rs}^{t,n}, \qquad n = 2,3,\cdots,N-1; \theta_{rs}^{t,1} \leq \lambda_{w}^{t,1}; \theta_{w}^{t,N} \leq \lambda_{w}^{t,N-1} \tag{32}$$

$$\sum_{n=1}^{N-1} \lambda_{rs}^{t,n} = 1 \tag{33}$$

$$\lambda_{rs}^{t,n} = \{0,1\}, \qquad n = 1,2,\cdots,N-1 \tag{34}$$

Since the right-hand side of Eq. (27) denotes all the tangent lines, then this equation ensures that $\mathcal{L}_{rs}^{t}$ are above the tangent lines. If q_{rs}^{t} is within the interval $\left[q_{rs}^{t,n^*}, q_{rs}^{t,n^*+1}\right]$, i.e., $\lambda_{rs}^{t,n^*} = 1$ from Eq. (34), then we can get $0 \le \theta_{rs}^{t,n^*} \le 1$, $0 \le \theta_{rs}^{t,n^*+1} \le 1$ and $\theta_{rs}^{t,n} = 0,\ n = 1,2,\cdots,N; n \ne n^*, n^*+1$ from Eqs. (30)-(33). Next, we can obtain $\theta_{w}^{t,n^*} + \theta_{w}^{t,n^*+1} = 1$ by Eq. (30), and from Eqs. (29)-(30) we can get $\theta_{w}^{t,n^*} \cdot \mathcal{L}_{w}^{t,n^*} + \theta_{w}^{t,n^*+1} \cdot \mathcal{L}_{w}^{t,n^*+1} \ge \mathcal{L}_{w}^{t}$, where the left-hand side means the curve chord from $\left(q_{w}^{t,n^*}, \mathcal{L}_{w}^{t,n^*}\right)$ to $\left(q_{w}^{t,n^*+1}, \mathcal{L}_{w}^{t,n^*+1}\right)$. And Eqs. (28)-(34) together constrain $\mathcal{L}_{w}^{t}$ to be smaller than those defined by all curve chords. Thus, the logarithm constraint Eq. (25) can be linearized by the linear constraints Eqs. (27)-(34).

With the above linear relaxation, SL-ETDDP model M2 can be relaxed into the following model M3.

M3:

$$\min Z_3 = \alpha_1 \sum_{(r,s)\in RS} \sum_{t=1}^{T} \mathcal{L}_{rs}^{t} + \alpha_2 \sum_{(r,s)\in RS} \sum_{p\in P_{rs}} \left(\sum_{t=1}^{T} f_{p(t)} - \hat{f}_p \right)^2 \tag{24}$$

subject to

Eqs. (7)-(8), (10), (13), (22)-(23)

Constraints in Eqs. (27)-(34), $t = 1,2,\ldots,T; (r,s) \in RS$

For the above model M3, as the quadratic term (least square) in the objective function and all constraints are linear with integer or continuous variables, this model is the MIQP[4]. Furthermore, as the objective function of model M3 is the convex quadratic[5], we can obtain its global optimal solutions by some commercial solvers such as GUROBI and CPLEX. In this paper, we use GUROBI to calculate the model M3.

Next, we will discuss how to reduce the calculation size of our problem to help us improve the computational efficiency.

4.2 Reducing the calculation size

In the above model M3, for any HSR OD pair $(r,s) \in RS$, we can obtain all path flows from the ticketing system, and those paths form the set P_{rs} of paths for OD pair (r,s), i.e., the $\hat{f}_p$ of path $p \in P_{rs}$ and the path set P_{rs} can be obtained from the ticketing system. As the HSR operation period $[T^1, T^2]$ is discretized into T equal time intervals, for any HSR OD pair $(r,s) \in RS$, it will generate $T \cdot |P_{rs}|$ access arcs and $T \cdot |P_{rs}|$ feasible space-time paths for this OD pair, where $|P_{rs}|$ is the path number of P_{rs}. Denote $|\mathbb{A}|$ and $|W|$ as the total number of the arcs and OD pairs of the HSR space-time network respectively. Then the calculation size of the above model M3 is shown as Table 3 (Original size column).

Table 3. The comparison of the calculation sizes of model M3 before and after the calculation size reduction approach

Calculation size	Original size	Updated scale after reducing calculation size

[4] ILOG CPLEX Optimization Studio, 'MIQCP: mixed integer programs with quadratic terms in the constraints'. https://www.ibm.com/docs/en/icos/20.1.0?topic=smippqt-miqcp-mixed-integer-programs-quadratic-terms-in-constraints

[5] ILOG CPLEX Optimization Studio, 'Distinguishing between convex and nonconvex QPs'. https://www.ibm.com/docs/en/icos/20.1.0?topic=qp-distinguishing-between-convex-nonconvex-qps

Constraints number	$(3N+6)T\lvert W\rvert+\lvert W\rvert+7\lvert\mathbb{A}\rvert+\sum_{(r,s)\in RS}\lvert P_{rs}\rvert+7\sum_{(r,s)\in RS}T\lvert P_{rs}\rvert$	$(3N+6)T\lvert W\rvert+\lvert W\rvert+7\lvert\bar{\mathbb{A}}\rvert+\sum_{(r,s)\in RS}\lvert P_{rs}\rvert+7\sum_{(r,s)\in RS}\sum_{t=1}^{T}\lvert\bar{P}_{rs}(t)\rvert$
Variables number	$(2N+2)T\lvert W\rvert+3\lvert\mathbb{A}\rvert+\sum_{(r,s)\in RS}\lvert P_{rs}\rvert+3\sum_{(r,s)\in RS}T\lvert P_{rs}\rvert$	$(2N+2)T\lvert W\rvert+3\lvert\bar{\mathbb{A}}\rvert+\sum_{(r,s)\in RS}\lvert P_{rs}\rvert+3\sum_{(r,s)\in RS}\sum_{t=1}^{T}\lvert\bar{P}_{rs}(t)\rvert$
Continuous variable	$(N+3)T\lvert W\rvert+2\lvert\mathbb{A}\rvert+\sum_{(r,s)\in RS}\lvert P_{rs}\rvert+2\sum_{(r,s)\in RS}T\lvert P_{rs}\rvert$	$(N+3)T\lvert W\rvert+2\lvert\bar{\mathbb{A}}\rvert+\sum_{(r,s)\in RS}\lvert P_{rs}\rvert+2\sum_{(r,s)\in RS}\sum_{t=1}^{T}\lvert\bar{P}_{rs}(t)\rvert$
Binaries	$(N-1)T\lvert W\rvert+\lvert\mathbb{A}\rvert+\sum_{(r,s)\in RS}T\lvert P_{rs}\rvert$	$(N-1)T\lvert W\rvert+\lvert\bar{\mathbb{A}}\rvert+\sum_{(r,s)\in RS}\sum_{t=1}^{T}\lvert\bar{P}_{rs}(t)\rvert$

From the above table we know that the calculation size of the model M3 will increase rapidly with the expansion of network scale (associated with feasible space-time path number $\sum_{(r,s)\in RS}T|P_{rs}|$ and arc number $|\mathbb{A}|$ of the network) and the increase of piecewise interval number (associate with N). In this section, we will discuss how to reduce the calculation size to improve the solution speed.

For the OD pair $(r,s)\in RS$, if no measures are taken to reduce the computing size, the desired departure time node $r(t), t=1,2,\cdots,T$ will generate the access arc with any path $p\in P_{rs}$, and then it will have $|P_{rs}(t)|=|P_{rs}|$ feasible space-time paths for this node (as shown in Fig. 7), where $|P_{rs}(t)|$ denotes the number of feasible space-time paths in $P_{rs}(t)$.

For feasible space-time paths set $P_{rs}(t)$, its corresponding set by reduction in calculation size is denoted as $\bar{P}_{rs}(t)$, and the number of feasible space-time paths in $\bar{P}_{rs}(t)$ is represented as $|\bar{P}_{rs}(t)|$. The arc set and access arc set after the reduction in calculation size are denoted as $\bar{\mathbb{A}}$ and $\bar{A}_{ac}$, and its corresponding arc numbers are denoted as $|\bar{\mathbb{A}}|$ and $|\bar{A}_{ac}|$ respectively. For the desired departure time t of OD pair $(r,s)\in RS$, we undertake the following steps to obtain the $\bar{P}_{rs}(t)$ and $\bar{A}_{ac}$ (as shown in Fig. 7).

First, we use the Eq. (5) to calculate the cost for all feasible space-time paths in $P_{rs}(t)$, and then sort them in order of cost from smallest to largest. After this the set of all these ordered feasible space-time paths are still denoted as set $P_{rs}(t)=\{\tilde{p}^1(t),\tilde{p}^2(t),\cdots,\tilde{p}^{|P_{rs}(t)|}(t)\}$.

Second, for $\tilde{p}^j(t)$ from $j=1$ to $|P_{rs}(t)|$, we check the flow of each arc passed by $\tilde{p}^j(t)$ whether it reaches its capacity or not. If at least one arc traversed by $\tilde{p}^j(t)$ has reached its capacity, i.e., $\exists a\in\tilde{p}^j(t), x_a=u_a$, put this $\tilde{p}^j(t)$ into set $\bar{P}_{rs}(t)$ and continue the process. This suggests that the capacity of $\tilde{p}^j(t)$ may be insufficient to meet the demand from the desired departure time t (i.e., demand q_{rs}^t). Consequently, it is possible for the demand q_{rs}^t to utilize other feasible space-time paths, $\tilde{p}^{j'}(t), j'=j+1,j+2,\cdots,|P_{rs}(t)|$. If all the flow of each arc passed by $\tilde{p}^j(t)$ has not reached its capacity, i.e., $x_a<u_a, a\in\tilde{p}^j(t)$, put it into set $\bar{P}_{rs}(t)$, i.e., $\bar{P}_{rs}(t)=\bar{P}_{rs}(t)\cup\{\tilde{p}^j(t)\}$ and break the process. This indicates that the capacity of $\tilde{p}^j(t)$ is sufficient to meet the demand q_{rs}^t. Based on Assumption **A3**, it is understood that the demand q_{rs}^t will not choose other feasible space-time paths, i.e., $\tilde{p}^{j'}(t), j'=j+1,j+2,\cdots,|P_{rs}(t)|$, because these paths are the worse options than $\tilde{p}^j(t)$.

Third, after the above process, we can get the path set $\bar{P}_{rs}(t)$, in which the feasible space-

time paths have the possibilities to be chosen by the demand q_{rs}^t. It is known that $\bar{P}_{rs}(t) \subseteq P_{rs}(t)$, and $|\bar{P}_{rs}(t)| \leq |P_{rs}(t)|$. And the access arcs associated with feasible space-time paths in $\bar{P}_{rs}(t)$ can form the set $\bar{A}_{ac}$.

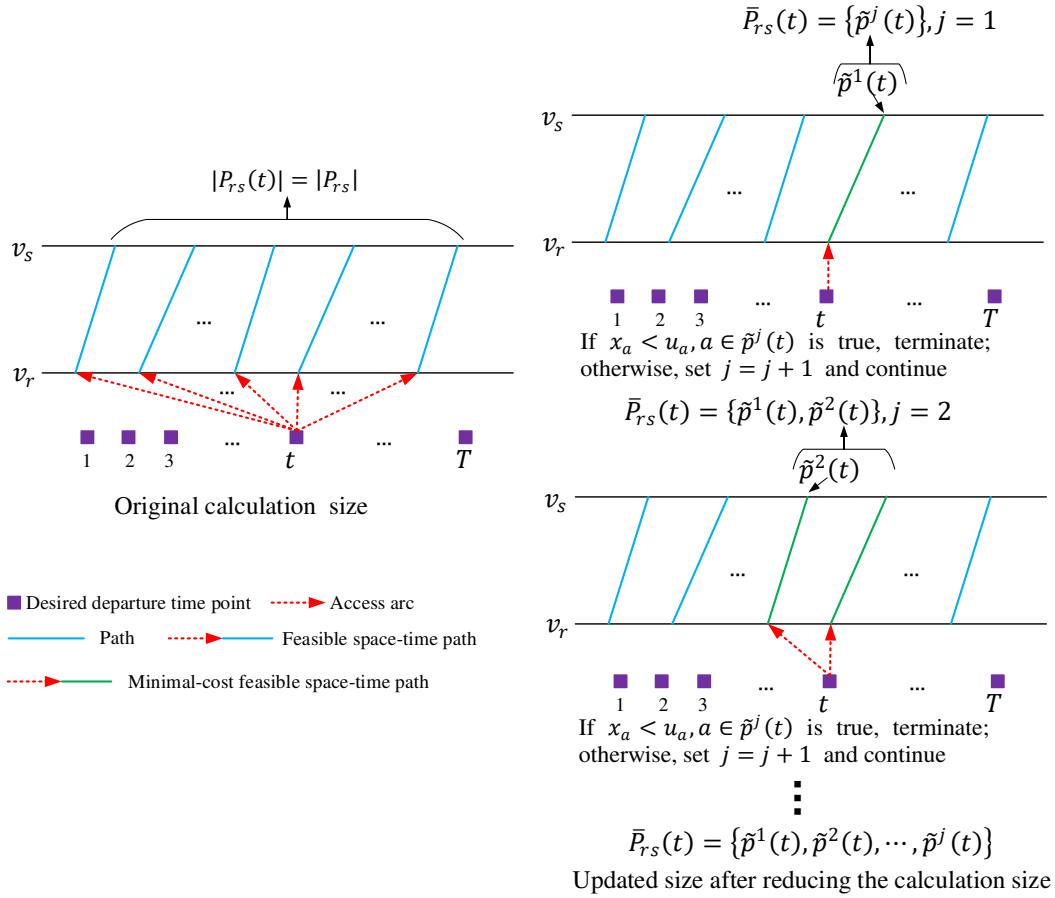

Fig 7. The comparison between original calculation size and after reduction size

From the above steps, the number of feasible space-time paths from node $r(t)$ can be reduced from $|P_{rs}(t)| = |P_{rs}|$ to $|\bar{P}_{rs}(t)|$, and the number of access arc can also be reduced from $|P_{rs}(t)| = |P_{rs}|$ to $|\bar{P}_{rs}(t)|$. Further, the number of feasible space-time paths for the model M3 can be reduced from $\sum_{(r,s)\in RS} T|P_{rs}|$ to $\sum_{(r,s)\in RS} \sum_{t=1}^{T} |\bar{P}_{rs}(t)|$, and similarly, the access arc number is decreased from $\sum_{(r,s)\in RS} |P_{rs}| \cdot |T|$ to $\sum_{(r,s)\in RS} \sum_{t=1}^{T} |\bar{P}_{rs}(t)|$. As the proportion of arcs that have reached the capacity is usually not large, the number of constraints and variables of model M3 can be greatly reduced. And the comparison of the calculation sizes of model *M3* before and after this calculation reduction approach are shown in *Table 2*.

Meanwhile, we can also reduce the calculation size by reducing the piecewise interval number N and this can be done by the following steps. In the original size situation, as the desired departure time node $r(t)$ connects with all paths in P_{rs}, i.e., all paths in P_{rs} have the possibility to be chosen by the demand q_{rs}^t, the upper bound of demand q_{rs}^t needs to be set as the sum flows of all paths for this OD pair, i.e., $\overline{q}_{rs}^t = \sum_{p\in P_{rs}} \hat{f}_p$. The lower bound of its demand q_{rs}^t can be set as 0, i.e., $\underline{q}_{rs}^t = 0$. While, after reducing the number of space-time paths and get the set $\bar{P}_{rs}(t)$, the upper bound of demand q_{rs}^t can be set as $\overline{q}_{rs}^t = \sum_{p(t)\in \bar{P}_{rs}(t)} \hat{f}_p \leq \sum_{p\in P_{rs}} \hat{f}_p$. The updated information about the upper and lower bound of demand q_{rs}^t are shown in Table

4.

Table 4. The information of upper and lower bound of the variable q_{rs}^t

Demand q_{rs}^t	Original size	Updated one after reducing calculation size
Upper bound	$\sum_{p\in P_{rs}} \hat{f}_p$	$\sum_{p(t)\in \bar{P}_{rs}(t)} \hat{f}_p$
Lower bound	0	0

With the above tightening of the feasible region for the demand q_{rs}^t, we can reduce the piecewise interval number N, and together with the reducing numbers of space-time paths and access arcs for the desired departure time node, we can reduce the calculation size of model M3. Based on the above analysis, we proposed the Reduce Calculation Size Algorithm as follows.

Algorithm 1: Reduce Calculation Size Algorithm.

Step 0: Initialization.

Partition the daily operation period into T equal time intervals with $[T^1, T^2] = [1,2,\cdots,T]$;

Obtain the capacity u_a and cost c_a of each space-time arc $a \in \mathbb{A}$;

Obtain path set P_{rs} and the flow $\hat{f}_p$ of each path $p \in P_{rs}, (r,s) \in RS$ from ticketing system;

Obtain the original size of feasible space-time path set $P_{rs}(t)$ and the cost $c_{p(t)}$ of each feasible space-time path $p(t) \in P_{rs}(t)$ for $(r,s) \in RS, t = 1,2,\dots,T$;

Set $\bar{P}_{rs}^t = \emptyset$ and $\bar{P}_{rs}(t) = \emptyset$ for all $t = 1,2,\dots,T$; $(r,s) \in RS$;

Set $\bar{\mathbb{A}} = \emptyset$ and $\bar{A}_{ac} = \emptyset$;

Step 1: Reduce the numbers of feasible space-time paths and number of access arcs

For each OD pair $(r,s) \in RS$ and each desired departure time $t = 1,2,\cdots,T$

Using Eq. (5) to calculate the cost for all feasible space-time paths in $P_{rs}(t)$, and sort them in increasing order of cost, i.e., $\{\tilde{p}^1(t), \tilde{p}^2(t), \cdots, \tilde{p}^{|P_{rs}(t)|}(t)\}$;

For $j = 1$ to $|P_{rs}(t)|$

$\bar{P}_{rs}(t) = \bar{P}_{rs}(t) \cup \{\tilde{p}^j(t)\}$;

If $x_a < u_a, a \in \tilde{p}^j(t)$ or $j = |\tilde{P}_{rs}(t)|$

break;

else

$j = j + 1$;

The access arcs associated with feasible space-time paths in $\bar{P}_{rs}(t)$ are added to set $\bar{A}_{ac}$.

Step 2: Tighten the feasible region of demand q_{rs}^t

For each OD pair $(r,s) \in RS$ and each desired departure time $t = 1,2,\cdots,T$

Update the upper bound and lower bound of demand q_{rs}^t as $\overline{q}_{rs}^t = \sum_{p(t)\in\bar{P}_{rs}(t)} \hat{f}_p$ and $\underline{q}_{rs}^t = 0$ respectively.

Step 3: Output

Output the set $\bar{P}_{rs}(t)$, the upper bound $\overline{q}_{rs}^t$ and lower bound $\underline{q}_{rs}^t$ of demand q_{rs}^t for all $t = 1,2,\cdots,T$, $(r,s) \in RS$;

Output the access set $\bar{\mathbb{A}} \leftarrow \bar{A}_{ac} \cup (\mathbb{A}/A_{ac})$.

Next, based on the global solution of model M3, we will discuss the idea to obtain the optimal solution of our original problem.

4.3 Lower and upper bounds

With the intention to simplify, we define $\boldsymbol{q} = \{q_{rs}^t | t = 1,2,\cdots T; (r,s) \in RS\}$ and $\boldsymbol{f} = \{f_{p(t)} | t = 1,2,\cdots,T; p \in P_{rs}; (r,s) \in RS\}$, then the SL-ETDDP model M2 can be abbreviated as:

$$(\mathbf{M2}): \min Z_2 = F_2(\boldsymbol{q}, \boldsymbol{f})$$

subject to

$$G(\boldsymbol{q}, \boldsymbol{f}) \leq 0$$

Define $\boldsymbol{\mathcal{L}} = \{\mathcal{L}_{rs}^t | t = 1,2,\cdots T; (r,s) \in RS\}$, then model M3 can be abbreviated as:

$$(\mathbf{M3}): \min Z_3 = F_3(\boldsymbol{q}, \boldsymbol{f}, \boldsymbol{\mathcal{L}})$$

subject to

$$G(\boldsymbol{q}, \boldsymbol{f}, \boldsymbol{\mathcal{L}}) \leq 0$$

i) lower bound

For model M3, it is a relaxed programing from model M2. Then the lower bound of model M2 can be determined by solving the M3 and obtaining its global optimal solution $(\boldsymbol{q}, \boldsymbol{f}, \boldsymbol{\mathcal{L}})$, i.e.,

$$F_3(\boldsymbol{q}, \boldsymbol{f}, \boldsymbol{\mathcal{L}}) \leq F_2(\boldsymbol{q}^*, \boldsymbol{f}^*) \tag{35}$$

where $(\boldsymbol{q}^*, \boldsymbol{f}^*)$ represents the global optimal solution of M2.

ii) upper bound

As all the constraints in model M2 are also in M3, the global optimal solution $(\boldsymbol{q}, \boldsymbol{f}, \boldsymbol{\mathcal{L}})$ of M3 is also the feasible solution of M2. Then, the upper bound of model M2 can be determined from its objective function Eq. (6) by using $(\boldsymbol{q}, \boldsymbol{f})$, i.e.,

$$F_2(\boldsymbol{q}^*, \boldsymbol{f}^*) \leq F_2(\boldsymbol{q}, \boldsymbol{f}) \tag{36}$$

iii) global optimal solution

Therefore, based on Eqs. (35)-(36), the global optimal solution $(\boldsymbol{q}^*, \boldsymbol{f}^*)$ of model M2 satisfies the following Eq. (37).

$$F_3(\boldsymbol{q}, \boldsymbol{f}, \boldsymbol{\mathcal{L}}) \leq F_2(\boldsymbol{q}^*, \boldsymbol{f}^*) \leq F_2(\boldsymbol{q}, \boldsymbol{f}) \tag{37}$$

As was shown in section 3.3, our original BL-ETDDP model M1 is equivalent to the SL-ETDDP model M2. Then, the global optimal solution $(\boldsymbol{q}^*, \boldsymbol{f}^*)$ of model M2 is just the global optimal solution of our original problem.

Thus, we can use the idea of successive linear approximations to obtain the global solution of our original problem. Firstly, we begin with an initial breakpoint number N to divide the domain $\left[\underline{q}_{rs}^t, \overline{q}_{rs}^t\right]$ into $N-1$ uniformly intervals by Eq. (26). Secondly, we use GUROBI to calculate model M3 and determine its global optimal solution $(\boldsymbol{q}, \boldsymbol{f}, \boldsymbol{\mathcal{L}})$. Thirdly, we can use Eq.

(37) to obtain the lower and upper bounds of model M2. Fourthly, we calculate the difference between the upper and lower bounds of model M2 and test convergence: if the difference is smaller than the convergence criterion, then solution $(\boldsymbol{q}, \boldsymbol{f})$ can be seen as the global solution of model M2 for output; otherwise more breakpoints need to be added to increase the number of piecewise intervals of domain $\left[\underline{q}_{rs}^{t}, \overline{q}_{rs}^{t}\right]$ for the purpose of making the region constrained by Eqs. (27)-(34) closer to the logarithmic function Eq. (25), and then we return to the second stage.

The key element of the above successive linear approximations is replacing the logarithmic function with more piecewise intervals step-by-step. As the piecewise interval number approaches infinity, the region constrained by Eqs. (27)-(34) becomes the same as the logarithmic function Eq. (25). In practice, we can get a satisfactory result without the need for an infinite number of piecewise intervals. In the following section 4.4, we will discuss the strategy design for adding the breakpoints to divide the domain $\left[\underline{q}_{rs}^{t}, \overline{q}_{rs}^{t}\right]$ into more piecewise intervals.

4.4 Piecewise interval strategy

Denote $Q_{rs}^{t,h}$ as the breakpoints set in $\left[\underline{q}_{rs}^{t}, \overline{q}_{rs}^{t}\right], t = 1,2,\cdots T; (r,s) \in RS$ at iteration number h, and its corresponding breakpoint number is denoted as $N(h)$, then the piecewise intervals number at iteration number h can be expressed as $N(h) - 1$. Let $\Delta\tilde{Q}_{rs}^{t,h}$ be the set of breakpoints which need to be added to increase the number of piecewise intervals at iteration number h, and denote $q_{rs}^{t}(h)$ to be the solution of M3 at iteration number h. Next, we will introduce four strategies (as shown in Fig. 8) of adding the breakpoints set $\Delta\tilde{Q}_{rs}^{t,h}$ to increase the number of piecewise intervals within a certain range of the domain after each iteration.

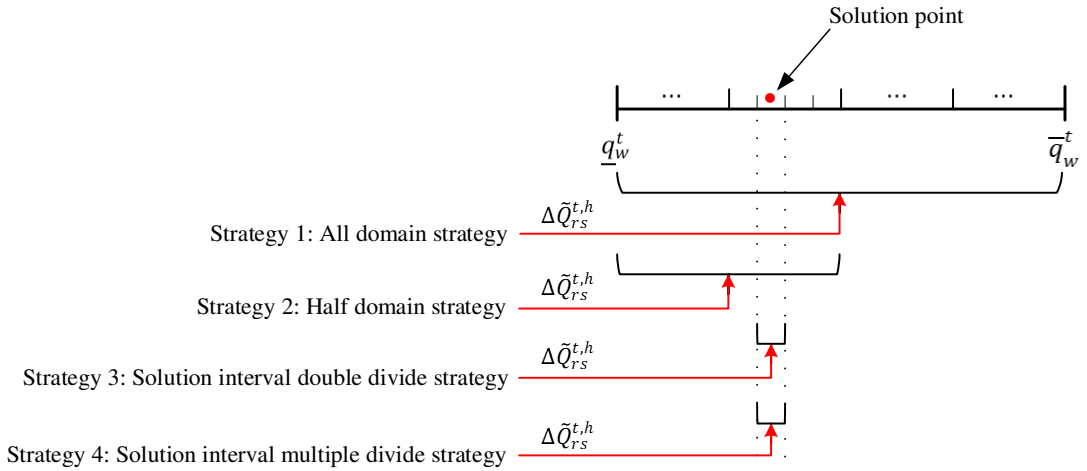

Fig. 8. Strategy for adding the breakpoints.

i) All domain strategy

This strategy means that we double the number of piecewise intervals in the whole domain $\left[\underline{q}_{rs}^{t}, \overline{q}_{rs}^{t}\right], (r,s) \in RS$ and the whole domain will still be redivided uniformly. The set of additional breakpoints set $\Delta\tilde{Q}_{rs}^{t,h}$ can be calculated by Eq. (38).

$$\Delta\tilde{Q}_{rs}^{t,h}=\left\{\tilde{q}_{rs}^{t,n}=\frac{q_{rs}^{t,n}+q_{rs}^{t,n+1}}{2}\middle|q_{rs}^{t,n},q_{rs}^{t,n+1}\in Q_{rs}^{t,h};n=1,2,\cdots,N(h)-1\right\},$$
$$t=1,2,\ldots,T;(r,s)\in RS \quad (38)$$

ii) Half domain strategy

In this strategy, we double the number of piecewise intervals in the half domain $\left[\underline{q}_{rs}^{t},\overline{q}_{rs}^{t}\right],(r,s)\in RS$ where the solution $q_{rs}^{t}(h)$ is located in, and this half domain will still be redivided uniformly. Denote the breakpoint that divides the domain $\left[\underline{q}_{rs}^{t},\overline{q}_{rs}^{t}\right],(r,s)\in RS$ into two half parts as q_{rs}^{t,n^*}, i.e., $q_{rs}^{t,n^*}=\frac{\overline{q}_{rs}^{t}+\underline{q}_{rs}^{t}}{2}$. Then the set of additional breakpoints set $\Delta\tilde{Q}_{rs}^{t,h}$ can be calculated by Eq. (39).

$$\Delta\tilde{Q}_{rs}^{t,h}=\begin{cases}\left\{\tilde{q}_{rs}^{t,n}=\frac{q_{rs}^{t,n}+q_{rs}^{t,n+1}}{2}\middle|q_{rs}^{t,n},q_{rs}^{t,n+1}\in Q_{rs}^{t,h};n=1,2,\cdots,n^*-1\right\}, & \text{if } q_{rs}^{t}(h)\le q_{rs}^{t,n^*}\\ \left\{\tilde{q}_{rs}^{t,n}=\frac{q_{rs}^{t,n}+q_{rs}^{t,n+1}}{2}\middle|q_{rs}^{t,n},q_{rs}^{t,n+1}\in Q_{rs}^{t,h};n=n^*,n^*+1,\cdots,N(h)-1\right\}, & \text{if } q_{rs}^{t}(h)>q_{rs}^{t,n^*}\end{cases},$$
$$t=1,2,\ldots,T;(r,s)\in RS \quad (39)$$

iii) Solution interval double divide strategy

In this strategy, a breakpoint will be added to the interval where the solution located in, and this interval will be redivided uniformly. The interval where the solution $q_{rs}^{t}(h)$ located in is denoted as $\left[q_{rs}^{t,\bar{n}},q_{rs}^{t,\bar{n}+1}\right]$, i.e., $q_{rs}^{t,\bar{n}}\le q_{rs}^{t}(h)<q_{rs}^{t,\bar{n}+1}$. Then $\Delta\tilde{Q}_{rs}^{t,h}$ can be calculated by Eq. (40).

$$\Delta\tilde{Q}_{rs}^{t,h}=\left\{\tilde{q}_{rs}^{t,n}=\frac{q_{rs}^{t,\bar{n}}+q_{rs}^{t,\bar{n}+1}}{2}\middle|q_{rs}^{t,\bar{n}},q_{rs}^{t,\bar{n}+1}\in Q_{rs}^{t,h}\right\},t=1,2,\ldots,T;(r,s)\in RS \quad (40)$$

iv) Solution interval multiple divide strategy

In this strategy, a fixed number N_0 of breakpoints will be added to the interval $\left[q_{rs}^{t,\bar{n}},q_{rs}^{t,\bar{n}+1}\right]$ where the solution $q_{rs}^{t}(h)$ is located, and this interval will be redivided uniformly. Then $\Delta\tilde{Q}_{rs}^{t,h}$ can be calculated by Eq. (41).

$$\Delta\tilde{Q}_{rs}^{t,h}=\left\{\tilde{q}_{rs}^{t,n}=q_{rs}^{t,\bar{n}}+\frac{\left(q_{rs}^{t,\bar{n}+1}-q_{rs}^{t,\bar{n}}\right)\cdot n}{N_0+1}\middle|q_{rs}^{t,\bar{n}},q_{rs}^{t,\bar{n}+1}\in Q_{rs}^{t,h};n=1,2,\cdots,N_0-1\right\},$$
$$t=1,2,\ldots,T;(r,s)\in RS \quad (41)$$

With the above strategies, we can obtain the set of additional breakpoints $\Delta\tilde{Q}_{rs}^{t,h}$, update the breakpoints set by Eq. (42), and then carry out the next iteration calculation.

$$Q_{rs}^{t,h+1}=\Delta\tilde{Q}_{rs}^{t,h}\cup Q_{rs}^{t,h},\quad t=1,2,\ldots,T;(r,s)\in RS \quad (42)$$

Further, we denote Ω^h as the feasible region of model M3 at iteration number h, and then we can get the following Proposition 2.

Proposition 2. With the strategies of adding breakpoints, and if the number of initial piecewise intervals is an integer multiple of 2, then for all of the above all four strategies, we have $\Omega^h \supset \Omega^{h+1}$ and the set of optimal function values $\{F_3(\boldsymbol{q}^h, \boldsymbol{f}^h, \boldsymbol{\mathcal{L}}^h)\}$ of model M3 will be a monotonically increasing series.

Proof. The details of this proof are shown in Appendix B.

4.5 SL-ETDDP Global Convergence Algorithm

Based on the above analysis, our initial BL-ETDDP model M1 aligns with the SL-ETDDP model M2, and this indicates that M2's global optimal solution also represents the global optimal solution for our primary problem. As model M3 is relaxed from model M2, the global optimal solution $(\boldsymbol{q}, \boldsymbol{f}, \boldsymbol{\mathcal{L}})$ of model M3 is the lower bound of model M2. Meanwhile, as all the constraints in model M2 are also in M3, this means that $(\boldsymbol{q}, \boldsymbol{f}, \boldsymbol{\mathcal{L}})$ of M3 is also the feasible solution of M2. And we can determine the upper bound of model M2 by using $(\boldsymbol{q}, \boldsymbol{f})$ for the objective function Eq. (6). Therefore, the lower bound and upper bound of model M2 can all be determined by calculating the model M3.

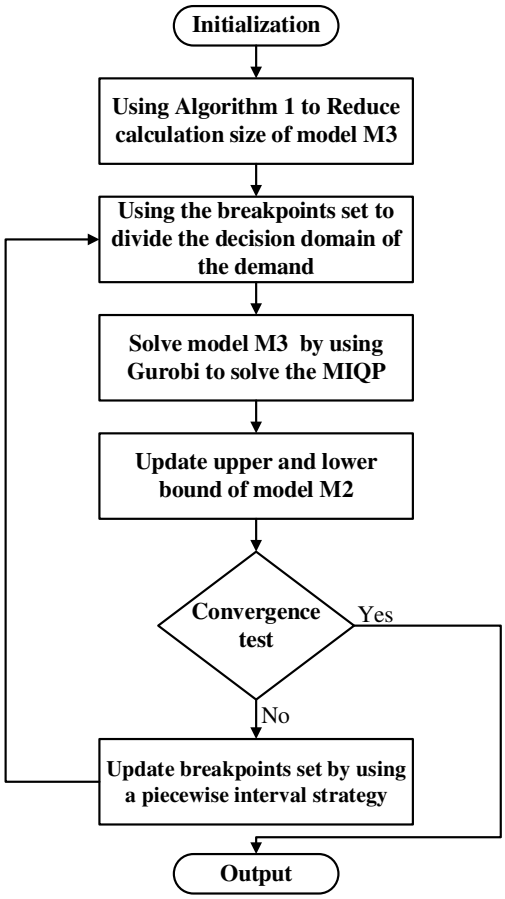

Fig.9. The flowchart of SL-ETDDP global convergence algorithm

As we show in Fig. 9, we can first use the Algorithm 1 to reduce the calculation size of model M3, and then use the breakpoints set to divide the domain $\left[\underline{q}_{rs}^t, \overline{q}_{rs}^t\right]$ into piecewise

intervals by Eq. (26). Then solve model M3 by using the GUROBI to get its global optimal solution $(\boldsymbol{q}, \boldsymbol{f}, \boldsymbol{\mathcal{L}})$, and based on this global optimal solution, we use Eq. (37) to obtain the lower and upper bounds of model M2. Next, we test the convergence. If the criterion is satisfied, we output the results $(\boldsymbol{q}, \boldsymbol{f})$ for model M2; otherwise, using one piecewise interval strategy to update the breakpoints set and go back to the step of using the breakpoints set to divide the decision domain of the demand and do the following steps again.

Based on the above analysis, we propose the **SL-ETDDP** Global Convergence Algorithm as follows.

Algorithm 2: SL-ETDDP Global Convergence Algorithm

Step 0: Initialization.

Using a sufficiently large value and a sufficiently small value as the upper bound $\overline{Z}_2^0$ and lower bound $\underline{Z}_2^0$ of the SL-ETDDP model M2 respectively;

set the iteration number as $h = 1$;

set convergence criterion ε; set the initialize breakpoints N and construct the breakpoints $Q_{rs}^{t,h}$ set by Eq. (26).

Step 1: Using the Algorithm 1 to reduce the calculation size.

Reduce the calculation size of model M3 by using Algorithm 1**.**

Step 2: Solving the MIQP.

Using the GUROBI to solve model M3, then determine its global optimal solution $\left(\boldsymbol{q}^h, \boldsymbol{f}^h, \boldsymbol{\mathcal{L}}^h\right)$ and its objective function value $F_3\left(\boldsymbol{q}^h, \boldsymbol{f}^h, \boldsymbol{\mathcal{L}}^h\right)$.

Step 3: Update the upper bound and lower bound.

Updating the upper bound of SL-ETDDP model M2: $\overline{Z}_2^h = \min\left\{\overline{Z}_2^{h-1}, F_2\left(\boldsymbol{q}^h, \boldsymbol{f}^h\right)\right\}$;

Updating the lower bound of model M2: $\underline{Z}_2^h = \max\left\{\underline{Z}_2^{h-1}, F_3\left(\boldsymbol{q}^h, \boldsymbol{f}^h, \boldsymbol{\mathcal{L}}^h\right)\right\}$.

Step 4: Convergence test.

If the convergence criterion is met, i.e., $\frac{\left|\overline{Z}_2^h - \underline{Z}_2^h\right|}{\overline{Z}_2^h} < \varepsilon$, then stop and output; otherwise, go to Step 5.

Step 5: Updating breakpoints set.

Choose a piecewise interval strategy (Eqs. (38), (39), (40) or (41)) to obtain the added breakpoints set $\Delta\tilde{Q}_{rs}^{t,h}$ and update the breakpoints set $Q_{rs}^{t,h+1}$ by Eq. (42);

set $h = h + 1$ and go to Step 2.

Proposition 3. When the iteration number $h \to \infty$, the above algorithm guarantees the convergence to the globally optimal solution of model M2.

Proof. Appendix C shows the details of this proof.

5. Numerical studies

This section will test our algorithm in two networks. We firstly present a simple network example to illustrate the details process of our algorithm, and then the applicability of our algorithm will test on the real-world networks in China.

All tests are conducted on the computer with Intel Xeon W-2145 3.70 GHz, 64 GB RAM and Windows 10 operating system (64-bit). The MATLAB 2022a together with YALMIP-R20200930 is used to conduct numerical tests. The commercial solver GUROBI optimization studio 10.0.1 is adopted to solve all MILR -ETDDP problems.

5.1 Case study 1: a simple network

We adopt a HSR network with three stations v_1, v_2 and v_3. There are three trains Train 1, Train 2 and Train 3 running in this network. We assume that the operation period is discretized into 10 equal time intervals with $[T^1, T^2] = [1,2,\cdots,10]$. For simplicity, the distances from v_1 to v_2 and v_2 to v_3 are all set as 1. The assumed timetable of those three trains and its schedule are shown in Table 5 and Fig. 10.

Table 5. Timetable of case one

Station	Train 1		Train 2		Train 3	
	Arrival	Depart	Arrival	Depart	Arrival	Depart
v_1		2		5		7
v_2	3	4			8	9
v_3	5		7		10	

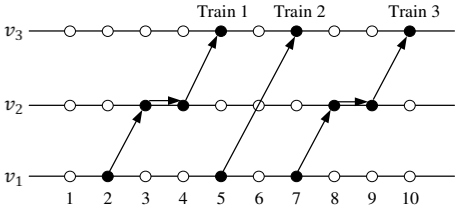

Fig. 10. Scheduling of Case 1

The unit costs for the early and late departure are $\eta' = 0.4$ and $\eta'' = 0.7$ respectively, and the capacity (seats) of all three trains is set as 100. We set the weight parameter value in the objective function as $\alpha_1 = \alpha_2 = 0.5$, the convergence parameter as $\varepsilon = 0.005$ and the initial breakpoints $N = 5$.

With reference to (Wu et al., 2022), other parameters are set as follows: the unit cost of travel time parameter $\omega = 0.5$, the ticket fare rate for all trains are $\gamma(1) = \gamma(3) = 0.4$ and $\gamma(2) = 0.45$, and the transfer cost at each station is $\varphi(v_1) = \varphi(v_2) = \varphi(v_3) = 12$.

From the above information, we can ascertain that there are three OD pairs: (v_1, v_2), (v_2, v_3) and (v_1, v_3). The cost of paths calculated by Eqs. (3) (5) are shown in Table 6.

Table 6. Information about path for each OD pair

OD pair	Path		Cost	Capacity
(v_1, v_2)	Path 1: p^1	Arc ①	0.9	100
	Path 2: p^2	Arc ⑥	0.9	100
(v_2, v_3)	Path 3: p^3	Arc ④	0.9	100
	Path 4: p^4	Arc ⑧	0.9	100
(v_1, v_3)	Path 5: p^5	Arc ①②④	2.3	100
	Path 6: p^6	Arc ⑤	1.9	100
	Path 7: p^7	Arc ⑥⑦⑧	2.3	100
	Path 8: p^8	Arc ①③⑧	16.8	100

i) Different input data

For the purpose of showing the impact from the ticketing volumes (input data), we set two groups of ticket booking volumes for all paths as Case 1.a and Case 1.b (as shown in Table 7). In Case 1.a, the tickets of all arcs are not sold out, but in Case 1.b the ticket booking volumes

of Path 3 for OD pair (v_2, v_3) is 80 (red color in Table 7), which is the only difference between Case 1.a and Case 1.b, and this makes the 100 capacity of Arc ④ fully occupied (80 for Path 3 and 20 for Path 5) in Case 1.b.

Table 7. Two groups of ticket booking volumes for paths

OD pair	Path		Ticket booking volume (input data)	
			Case 1.a	Case 1.b
(v_1, v_2)	Path 1: p^1	Arc ①	50	50
	Path 2: p^2	Arc ⑥	20	20
(v_2, v_3)	Path 3: p^3	Arc ④	70	**80**
	Path 4: p^4	Arc ⑧	45	45
	Path 5: p^5	Arc ①②④	20	20
(v_1, v_3)	Path 6: p^6	Arc ⑤	45	45
	Path 7: p^7	Arc ⑥⑦⑧	20	20
	Path 8: p^8	Arc ①③⑧	0	0

As all arcs have not reached their capacity limits in Case 1.a, each desired departure time node only generates the minimal-cost feasible space-time path, with 10 feasible space-time paths for each OD pair in Case 1.a; while in Case 1.b, because Arc ④ has reached its capacity limit, these feasible space-time paths passed by this Arc ④ may not be insufficient for demand from its corresponding desired departure time points. Consequently, these desired departure time points will use other feasible space-time paths to ensure their demand can be met. Specifically, Case 1.b generates the number of feasible space-time paths for OD pair (v_1, v_2), (v_2, v_3) and (v_1, v_3) are 10, 17 and 13 respectively as shown in Fig. 11.

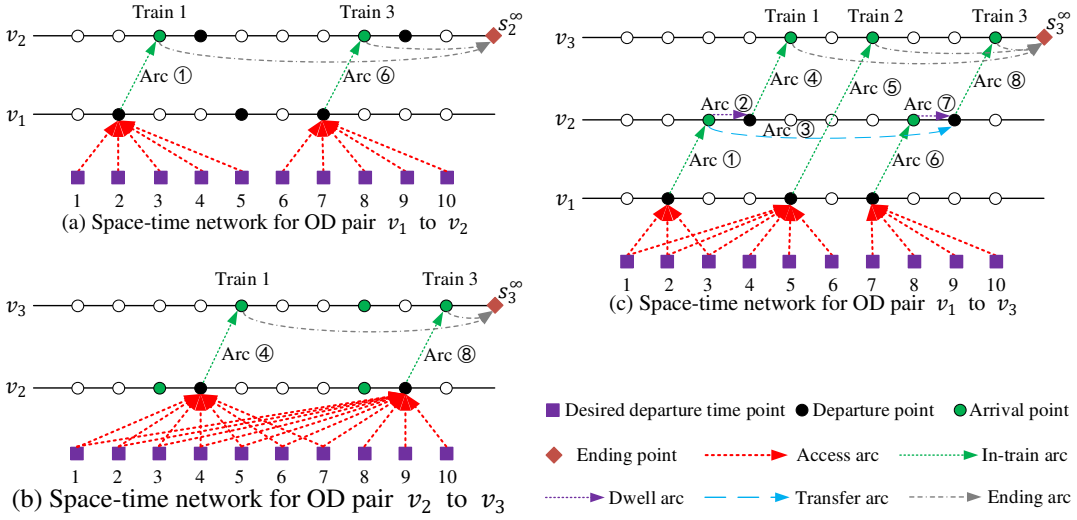

(a) Space-time network for OD pair v_1 to v_2

(b) Space-time network for OD pair v_2 to v_3

(c) Space-time network for OD pair v_1 to v_3

Fig. 11. Space-time network for each OD pair (Case 1.b)

Using the SL-ETDDP global convergence algorithm (all domain divided strategy), we can calculate the results for Case 1.a and Case 1.b. Figs. 12-13, Table 8-9 and Appendix D show the detail of the results.

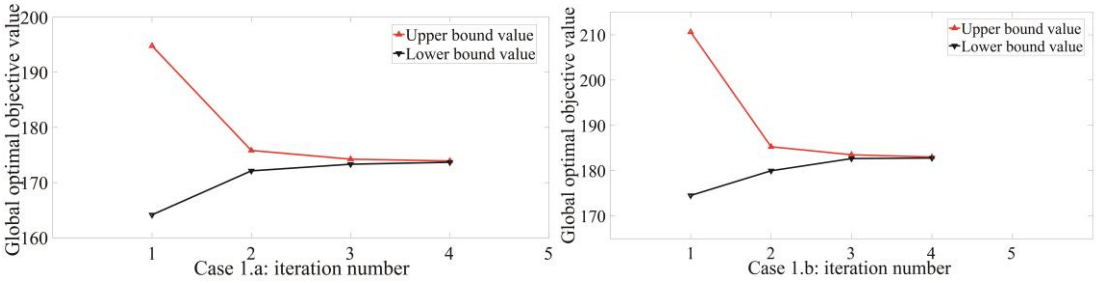

Fig. 12. Objective values with iterations

Table 8. Estimate results for the paths

Path	Case 1.a		Case 1.b	
	Ticket booking volume/input	Estimate results/output	Ticket booking volume/input	Estimate results/output
Path 1: p^1	50	49.80	50	49.80
Path 2: p^2	20	20.20	20	20.20
Path 3: p^3	**70**	70.07	**80**	80.03
Path 4: p^4	45	44.93	45	44.97
Path 5: p^5	20	20.09	**20**	19.97
Path 6: p^6	45	44.70	45	44.84
Path 7: p^7	20	20.21	20	20.19
Path 8: p^8	0	0.00	0	0.0

Table 9. Results for space-time arcs

Arc	Arc type	u_a	Case 1.a			Case 1.b		
			x_a	$u_a - x_a$	π_a	x_a	$u_a - x_a$	π_a
①	In-train arc	100	69.89	30.11	0	69.77	30.23	0
②	Dwell arc	∞	20.09	∞	0	19.97	∞	0
③	Transfer arc	∞	0	∞	0	0	∞	0
④	In-train arc	100	90.17	9.83	0	**100.00**	0	**0.60**
⑤	In-train arc	100	44.70	55.30	0	44.84	55.16	0
⑥	In-train arc	100	40.41	59.59	0	40.39	59.61	0
⑦	Dwell arc	∞	20.21	∞	0	20.19	∞	0
⑧	In-train arc	100	65.13	34.87	0	65.16	34.84	0

For any feasible space-time path $p(t), t = 1,2,\cdots,T; p \in P_{rs}; (r,s) \in RS$, if $f_{p(t)} > 0$, it means that passengers with desired departure time t choose path p for their trips, and this can be seen as path p attracts passengers with desired departure time t, which is abbreviated as path p attracts desired departure time t or desired departure time t is attracted by path p. Then, from the results we can ascertain that:

i) **After a limited number of iterations, our algorithm can obtain global optimal solutions**. Fig. 12 shows that both Case 1.a and Case 1.b obtain the results after only 4 iterations, and Table 8 demonstrates that the quality of the solution is good.

ii) **Our model can effectively reflect the UE statement and the ticket booking competition between different OD pairs in the HSR networks under rigid capacity constraints**. As we can see from Table 9, the results of the space-time arcs (access arc omitted) from both Case 1.a and Case 1.b meet the UE constraints Eqs. (17). In Case 1.a, as no tickets

are sold out for any arc or path, the ticket advance booking fee for all arcs and paths is 0. But in Case 1.b the 100 seat capacity of arc ④ is fully booked and its advance booking fee is 0.6 (red colored in Table 8), which means in the UE statement that passengers who want to choose the path through arc ④ need to compete for the available seat resource by booking tickets in advance, and the advance booking fee is 0.6 (red colored in Appendix D).

iii) **In the situation that the seat capacity of each path providing services for the HSR OD pair is in surplus and passengers do not need to compete for the tickets in advance (advance ticket booking fee is 0), our algorithm results (the TDD estimation results) can approximately be seen as the results of evenly distributing the ticket booking volume of each path to its corresponding attracting desired departure time points (maximal entropy value)**. This leads to a phenomenon that, under the no tickets sold out situation, if the number of desired departure time points attracted by each path for the OD pair is close in quantity, the trend from all paths' ticket booking volumes within the operation period is similar to the trend of TDD estimation results; otherwise, the trends between all paths' ticket booking volumes and TDD estimation results will be inconsistent.

For example, for OD pair (v_1, v_2) in both Case 1.a and Case 1.b, the seat capacities of Path 1 (arc ①) and Path 2 (arc ⑥) are in surplus (30.11 for arc ① and 59.59 for arc ⑥ as shown in Table 9), and as shown in Appendix D, for $t = 1,2,\cdots,5$, $f_{p^1(t)} \in [9.85,10.39]$ and for $t = 6,7,\cdots,10$, $f_{p^2(t)} \in [3.81,4.38]$. This means that Path 1 attracts 5 desired departure time points ($t = 1,2,\cdots,5$) and Path 2 attracts the remaining 5 desired departure time points ($t = 6,7,\cdots,10$). Meanwhile, the estimated results $[9.85,10.39]$ for $t = 1,2,\cdots,5$ can be approximately seen as evenly values of the of ticket booking volume 50 of Path 1 to its attracting 5 departure time points ($50/5 = 10$). And $[3.81,4.38]$ for $t = 6,7,\cdots,10$ can be approximately seen as evenly values of the of ticket booking volume 20 of Path 2 to its attracting 5 departure time points ($20/5 = 4$). Furthermore, as shown in Fig. 13, the trend of ticket booking volumes of these two paths within the operation period is left-peak, which is similar to the trend of TDD estimation results (left-peak). Similarly, for OD pair (v_1, v_3) in Case 1.a, the seat capacities of Path 5, Path 6 and Path 7 are in surplus, and the number of desired departure time points attracted by Path 5, Path 6 and Path 7 are 3, 3 and 4, such that the trend of all three paths' ticket booking volumes is middle-peak, which is similar to the trend of TDD estimation results. By contrast as shown in Table 9 and Appendix D for OD pair (v_2, v_3) in Case 1.a, the seat capacities of Path 3 (arc ④) and Path 4 (arc ⑧) are all in surplus, but the number of desired departure time points attracted by Path 3 is 7 ($t = 1,2,\cdots,7$), which is significantly larger than that of Path 4 (3 points, $t = 8,9,10$). This leads to that Path 3's ticket booking volume (70) is higher than Path 4's ticket booking volume (45), but the TDD estimation results of the desired departure time points attracted by Path 3 ($f_{p^3(t)} \in [9.86,10.79]$) are lower than that by Path 4 ($f_{p^4(t)} \in [14.4,15.26]$). And the trend of ticket booking volumes of Path 3 and 4 (left-peak) is different with the trend of TDD estimation results (right-peak), which is shown in Fig. 13 in Case 1.a for OD pair (v_2, v_3).

iv) **In the situation that the seat capacity of some popular paths for the HSR OD pair is insufficient and passengers need to compete for these popular paths by booking tickets in advance (advance ticket booking fee larger than 0), then some passengers who fail to secure the more popular paths have to choose a less ideal one, and our algorithm can address this situation by reallocating those passengers to alternative departure times**. And

this leads to the phenomenon that under the situation of tickets selling-out for some popular trains, there will be some inconsistency between the trend of our TDD estimation results and the trend of the ticket booking volumes of the paths for the OD pair.

For instance, as we can see in Case 1.b in Fig. 13, as the tickets of Path 3 (arc ④) and Path 5 (arc ①②④) are claimed by passengers from OD pair (v_2, v_3) and (v_1, v_3), the capacity of arc ④ is fully occupied (advance booking fee is 0.6), and some passengers who failed to book tickets for the ideal train have to adjust their departure times on a larger scale and choose less ideal trains (for passengers of OD pair (v_2, v_3) choose Path 4, whilst passengers of OD pair (v_1, v_3) choose Path 6). Compared with Case 1.a, we find that our algorithm reallocates the demand that are forced to choose the less ideal Path 4 and Path 6 due to capacity constraints to the desired departure time points attracted by ideal Path 3 and Path 5 respectively. And this leads to significant inconsistence in the trend of the estimate results for OD pair (v_2, v_3) between Case 1.a and Case 1.b. Furthermore, even both in Case 1.a and Case 1.b the ticket booking volumes of all paths for OD pair (v_1, v_3) are all the same, but in Case 1.b the trend of our TDD estimation results (left-middle-peak) is different from that of the ticket booking volumes of all paths (middle-peak). These adjustments to train/path choices under capacity constraint account for interactions between all OD pairs on the networks – thus highlighting one of the key contributions of our paper.

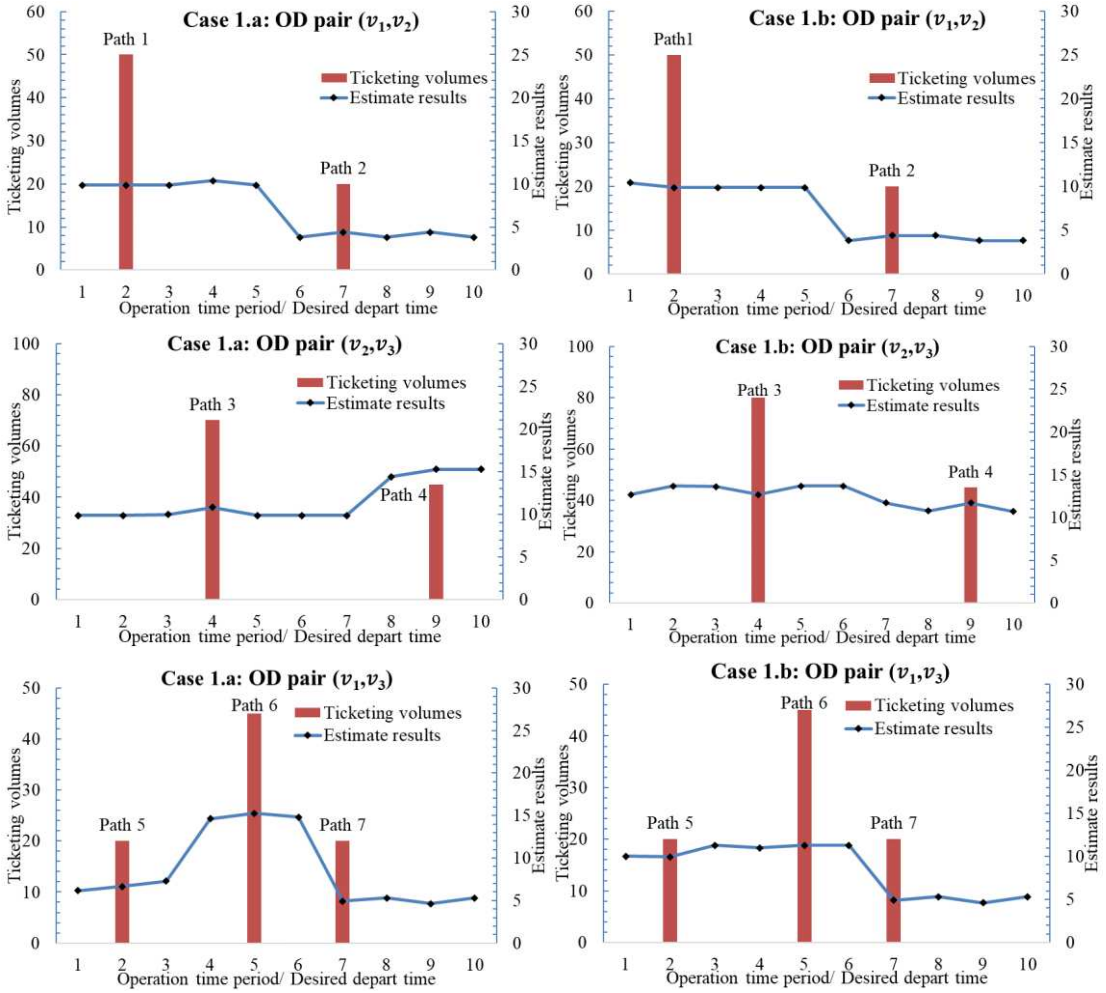

Fig. 13. Estimate results about the time-varying demand distribution

ii) Different Parameter values

As different values of parameters will affect passengers' ticket booking choices and further affect our estimation results, next we will analyze the effect of changes in the early and late departure cost parameters η' and η'' value on our results.

We set the late departure cost parameter η'' as a fixed value 0.7, and change the value of the early departure cost parameter η' from 0.1 to 1.3 in steps of 0.1 (as shown in Table 10). Then, the results of Case 1.a and Case 1.b are shown in Fig. 14.

Table 10. Different values of early and late departure cost parameters

η'	0.1	0.2	0.3	0.4	0.5	0.6	0.7	0.8	0.9	1.0	1.1	1.2	1.3
η''	0.7	0.7	0.7	0.7	0.7	0.7	0.7	0.7	0.7	0.7	0.7	0.7	0.7

From Fig. 14 we can see that:

1) **In the situation with no ticket selling out for the OD pair, the change of parameter values of η' has the same effect on Case 1.a and Case 1.b**. As the η' is the early departure cost parameter, the smaller the value of η', the greater the inclination for passengers to choose the train departure before (rather than after) their desired departure time, this means that the train will attract more passengers whose desired departure time points after the departure time of this train. Conversely, passengers will be more inclined to choose the train departure after their desired departure time as the value of η' larger than η'', and the train will attract more passengers whose desired departure time points before this train's departure time. In Fig. 14 the change of parameter values has the same effect for OD pair (v_1, v_2) in both Case 1.a and Case 1.b: Path 1 with departure time 2 attracts from desired departure time [1,6] at $\frac{\eta'}{\eta''} = \frac{1}{7}$ to [1,3] at $\frac{\eta'}{\eta''} = \frac{13}{7}$. And Path 2 with departure time 7 attracts from desired departure time [7,10] at $\frac{\eta'}{\eta''} = \frac{1}{7}$ to [4,10] at $\frac{\eta'}{\eta''} = \frac{13}{7}$.

2) **In the situation with the tickets selling-out for some paths or arcs of the OD pair, in the range where η' and η'' are relatively close ($\frac{\eta'}{\eta''}$ is close to 1), our model has good consistency in addressing that passengers are force to adjust their departure times due to capacity constraints.** For example, in Fig. 13 the tickets of Path 5 (arc ④) are sold out for the OD pairs (v_1, v_3) in Case 1.b, and the TDD results of OD pairs (v_1, v_3) in Case 1.b of Fig. 14 are almost the same as the parameter values change from $\frac{\eta'}{\eta''} = \frac{3}{7}$ to $\frac{11}{7}$, which are significantly different from that in Case 1.a. Empirical studies (Hess et al., 2017) show that the penalty for early adjustment is slightly lower than that of late in rail, which falls in the range of $\left[\frac{3}{7}, \frac{11}{7}\right]$. And this provides support for the practical application of our model.

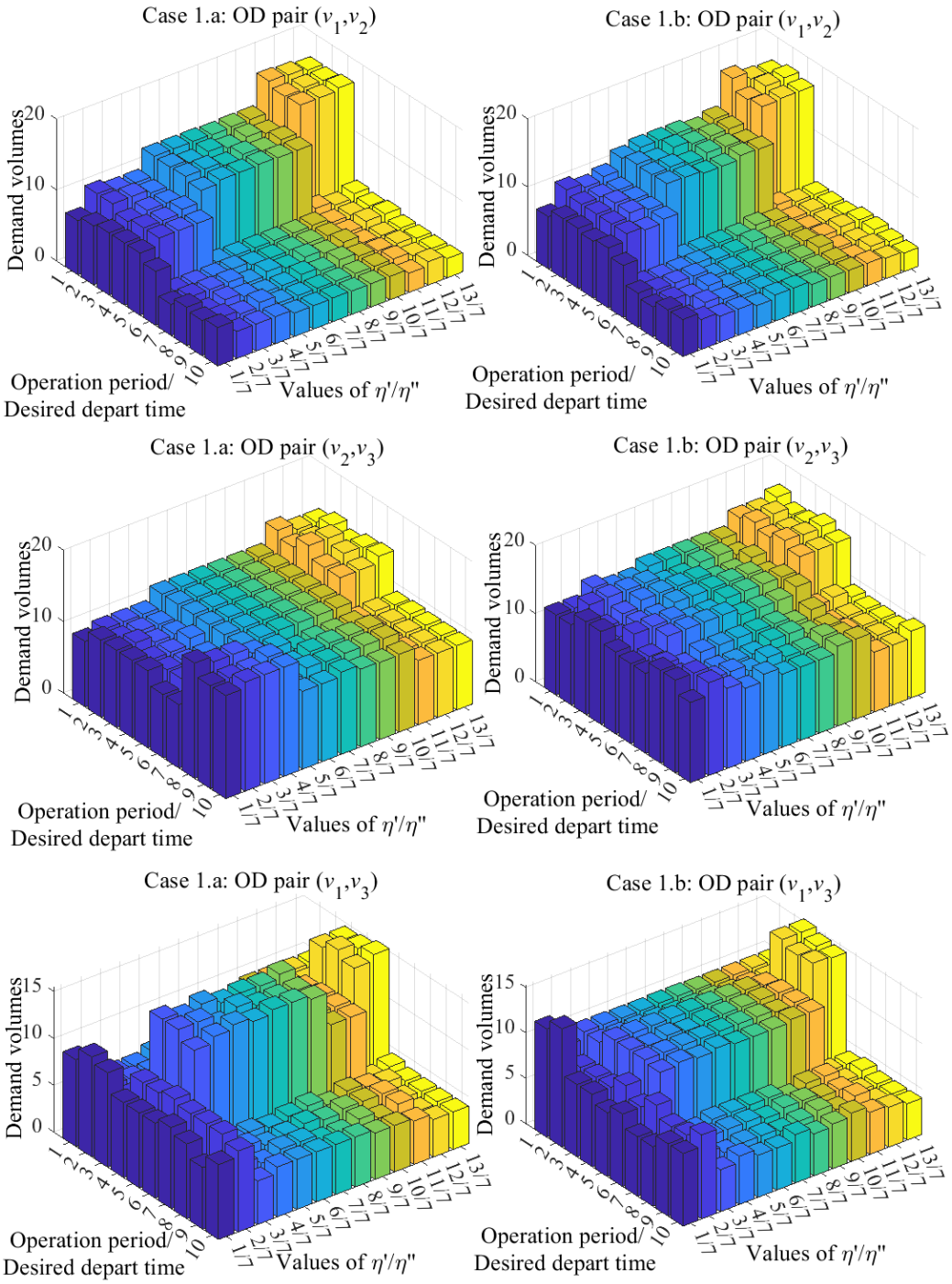

Fig. 14. Estimate results with different parameter values

iii) Different strategies and different calculation sizes

In the above analysis, all the results are calculated by our SL-ETDDP global convergence algorithm with the first piecewise interval strategy (all domain strategy) in the original calculation size. Next, we will test all four strategies in different calculation sizes to compare computational efficiency.

Fig. 15 shows the solution point information after the last iteration for all four piecewise interval strategies. In order to demonstrate the effectiveness of algorithms and strategies proposed in this paper, we test our Algorithm 2 with four strategies in the situation of original calculation size (i.e., not applying Algorithm 1) and the situation of calculation size reduction

(i.e., applying Algorithm 1) respectively. Our problem scale and the corresponding calculation time at each iteration for all four strategies in different situations of calculation size are shown in Table 11.

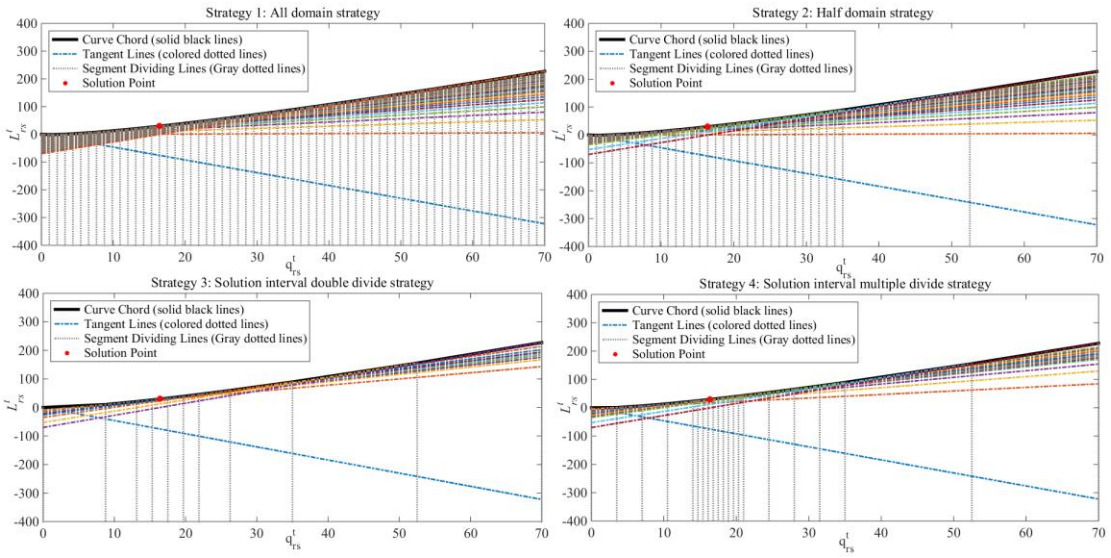

Fig. 15. Solution point information after the last iteration

In Table 11, statistical information about the four strategies in the original calculation size situation and the reduced calculation size situation are shown in black color and red color respectively. From this we can ascertain that:

Firstly, with the increase in iterations, our problem scale (constraints number and variable number) and calculation time are themselves increasing, and all of the strategies in different calculation size situations can obtain the global solution with a limited number of iterations (up to 6 iterations).

Secondly, for all strategies, in terms of constraints number, variables number and total calculation time, the red numbers are smaller than the black numbers, indicating that Algorithm 1 not only reduces the calculation scale but also significantly lowers the total computation time.

Thirdly, for all strategies, the number of iterations in red is less than that in black; this means that tightening the feasible region in Algorithm 1 can make Algorithm 2 converge faster, which further reduces the total calculation time.

Fourthly, under the situation of original calculation size, Strategy 1 performs worst; Strategy 3 has the best performance in computation time but requires more iterations; whilst Strategy 4 has the fewest iterations. In contrast, under the situation of reduced calculation size, the computation time of all strategies is significantly reduced, making the advantage of Strategy 4 over Strategies 1 and 2 less obvious; in particular, due to the relatively high number of iterations, Strategy 3 ends up costing the most time, and this may be due to the relatively small size of the problem, the advantages of Strategy 3 are not well reflected. We can test these effects on larger scale cases.

Table 11. Statistical information for four strategies in different calculation size situations

Iteration number h		1	2	3	4	5	6	total
Strategy 1	Constrains num	1747	2107	2827	4267	7147	/	/
		1117	1477	2197	/	/	/	/

(Original size /Reduction size)	Variables num	842 572	1082 812	1562 1292	2522 /	4442 /	/ /	/ /
	Calculate time(s)	0.11 0.13	0.34 0.34	0.47 0.75	2.4 /	5.45 /	/ /	8.77 1.22
Strategy 2 (Original size /Reduction size)	Constrains num	1747 1117	1927 1297	2287 1837	3007 /	4447 /	/ /	/ /
	Variables num	842 572	962 692	1202 1052	1682 /	2642 /	/ /	/ /
	Calculate time(s)	0.12 0.14	0.17 0.23	0.39 0.47	1.87 /	2.98 /	/ /	5.53 0.84
Strategy 3 (Original size /Reduction size)	Constrains num	1747 1117	1837 1207	1927 1297	2017 1387	2107 1477	2197 /	/ /
	Variables num	842 572	902 632	962 692	1022 752	1082 812	1142 /	/ /
	Calculate time(s)	0.1 0.14	0.11 0.18	0.36 0.21	0.37 0.34	0.6 0.47	0.73 /	2.27 1.34
Strategy 4 (Original size /Reduction size)	Constrains num	1747 1117	2107 1477	2467 1837	2827 /	/ /	/ /	/ /
	Variables num	842 572	1082 812	1322 1052	1562 /	/ /	/ /	/ /
	Calculate time(s)	0.11 0.14	0.36 0.14	1.4 0.49	2.05 /	/ /	/ /	3.92 0.77

In this section, all cases were tested on the small simple network for demonstrating the step details of our algorithms and strategies. Next, we will test our algorithm in the real-world network to verify its effectiveness and computational efficiency.

5.2 Case study 2: a real-world network of Nanchang-Jiujiang Intercity Railway

This section tests our proposed model and algorithm in a real-world network in China, i.e., Nanchang-Jiujiang Intercity Railway, which includes 6 HSR stations and is shown in Fig.16. We adopt the timetable on 15 March 2023 [6] with 54 trains running on the networks, and the timetable of Nanchang-Jiujiang Intercity Railway is shown in Fig. 17 and Appendix E. The operation period $[T^1, T^2] = [6{:}00, 23{:}00]$ is discretized into $[T^1, T^2] = [1, 2, \cdots, 102]$ of 10-minute time intervals.

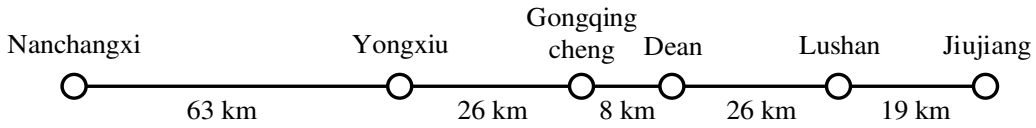

Fig. 16. Nanchang-Jiujiang Intercity Railway

Modelling by the space-time network, there are 180 paths, and in the original calculation situation, there will be $\sum_{(r,s)\in RS} T|P_{rs}| = 180 \times 102 = 18360$ feasible space-time paths, and 18570 space-time arcs (18360 access arcs). While after applying the Algorithm 1 in the situation of reduced the calculation size, there are only 1456 feasible space-time paths, and 1665 space-time arcs (1456 access arcs). The convergence parameter as $\varepsilon = 0.01$ and the initial breakpoints are set as $N = 6$. The ticket fare rate for G trains (300 km/h) is $\gamma(G) = 0.45$ yuan/km and for

[6] China Railway (http:// 12306.cn)

D trains (200 km/h) is $\gamma(D) = 0.4$ yuan/km. The unit cost for the early and late departure $\eta' = 0.4$ and $\eta'' = 0.5$. The values of other parameters are set to be the same as in Section 5.1.

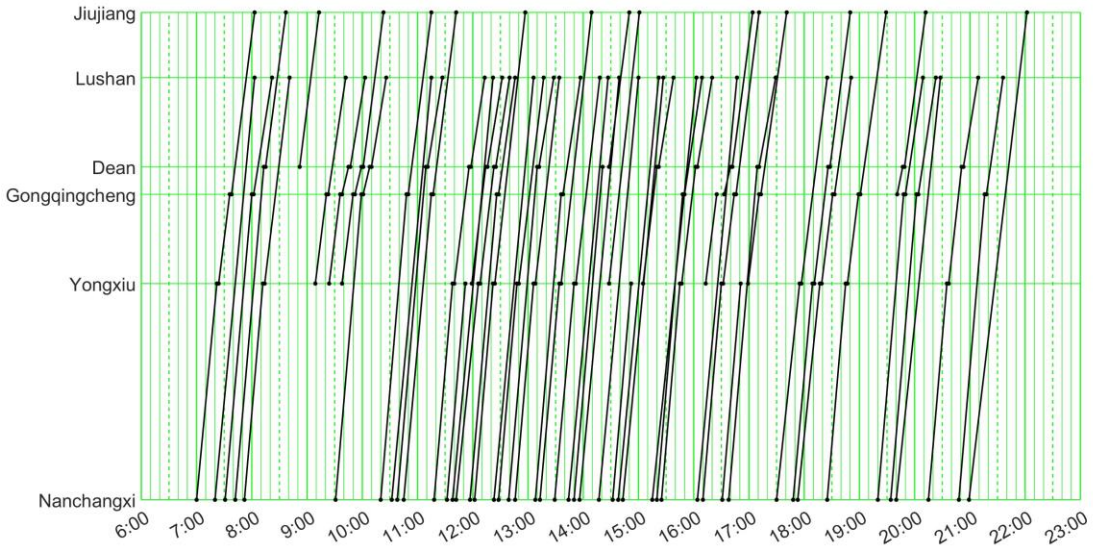

Fig. 17. The Timetable of Nanchang-Jiujiang Intercity Railway

Fig. 18 illustrates the TDD results of each OD pair, from which we can make the following observations:

1) **For the OD pair during the period of high departure frequency of trains or paths, the TDD curve fluctuates significantly; on the contrary, in other periods with low service frequency of trains or paths, the TDD curve fluctuates slightly**. For example, for almost all OD pairs in Fig. 18, the estimated TDD curve naturally fluctuates during the period with peak departure of trains; and most OD pairs have no train service after 21:00, then, their estimated TDD curve after 21:00 remains at a relatively steady altitude. The variation in the estimated TDD curve can be attributed to the availability of information. During peak departure periods, more information or constraints about the ticketing volumes and departure time of the trains or paths can be used. Conversely, during periods with fewer departures, less information can be used, then the estimated TDD curve remains relatively constant reflecting a maximum entropy value.

2) **In the situation with no ticket selling out of the OD pair, if the number of desired departure time points attracted by a train is significantly different from that of others, near the departure time of this train, the trend of ticketing volumes and trend of estimated TDD curve will have some mismatch phenomenon.** For example, the train and its surrounding estimated demand marked by the purple circle in Fig. 18. This is because there are no other trains providing services near the departure time of this train in the purple circle, so the desired departure times nearby are all attracted by this only train. A small number of trains provide services for a relatively long time period, this results in mismatch.

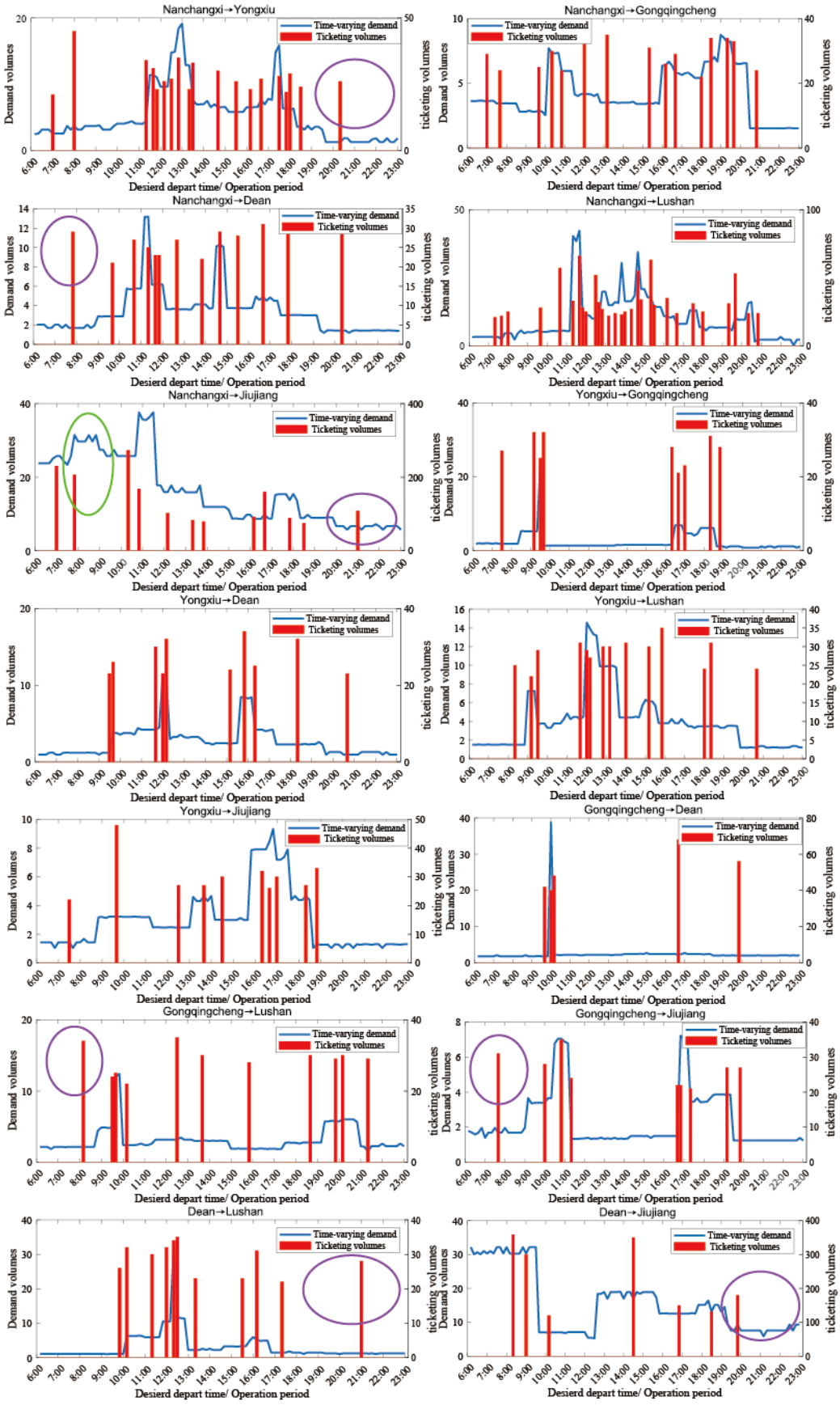

Fig. 18. Results for the Case study 2

3) **In the situation with tickets selling-out for some popular trains of the OD pair, the**

estimated TDD results near the popular train (tickets selling-out) will be relatively higher than the trend of its ticket booking volumes. For example, the train and its surrounding estimated demand results marked by the green circle in Fig. 18. The capacity of train (D6378) in this green circle is fully occupied by the passengers from OD pair Nanchangxi→Jiujiang and Dean→Jiujiang (red colored in Appendix E). Interestingly, the estimated demand results nearby D6378's departure time (7:42) is higher than that of previous departure time (7:00) of another train. However, it's worth noting that the ticket booking volume of train D6378 is lower than that of the preceding departure train. Our estimated results capture these mismatches implying that the model proposed in our paper can effectively applied to the TDD estimation problem.

Table 12 shows the statistical information for four strategies in different calculation size situations of Case 2. The information about the situation of original calculation size and situation of reduce calculation size are shown with black color and red color numbers respectively. From this we can ascertain that:

First, comparing the two situations, reducing the calculation size has brought a significant improvement in the computational efficiency of the algorithm. Specifically, by adding Algorithm 1, on the one hand, the number of constraints and the number of variables are greatly reduced (the red numbers are significantly smaller than the black numbers), which can obviously increase computation speed; on the other hand, the tighter feasible region in Algorithm 1 allows Algorithm 2 to achieve global convergence faster (reducing the number of iterations by 1-2 times for the 4 strategies), thereby significantly reducing the computation time occupied by subsequent iterations. Therefore, using Algorithms 1 to reduce the calculation scale will greatly improve the computational efficiency of Algorithm 2, reducing its total computation time to less than 1% of what it would be without using Algorithm 1.

Second, for the different strategies, Strategy 4 performs the best under the situation of original size without reducing the calculation size (shortest total computation time in black numbers), while Strategy 3 is the fastest when the problem size is reduced (shortest total computation time in red numbers). This may be because, after using Algorithm 1 to reduce the calculation size, the feasible region is greatly tightened, and it is not necessary to have many iteration steps (number of piecewise interval) to obtain the global solution. Therefore, Strategy 3, which adds one piecewise interval at each iteration, appears more flexible, lightweight, and efficient.

Table 12. Statistical information for four strategies in different calculation size situations of Case 2

Iteration number h		1	2	3	4	5	6	total
Strategy 1 (Original size /Reduction size)	Constrains num	357299	442979	614339	957059	1642499	/	/
		56313	77733	120573	/	/	/	/
	Variables num	173829	230949	345189	573669	1030629	/	/
		29535	43815	72375	/	/	/	/
	Calculation time(s)	4601.85	28672.31	16043.58	74417.84	284975	/	408711
		19.28	185.37	618.94	/	/	/	824
Strategy 2 (Original size /Reduction size)	Constrains num	357299	400139	485819	657179	999899	/	/
		56313	77733	120573			/	/
	Variables num	173829	202389	259509	373749	602229	/	/
		29535	43815	72375			/	/
	Calculation time(s)	4418.02	14949.18	33407.99	108383.8	298882.1	/	460041
		19.42	309.87	464.67			/	794

Strategy 3 (Original size /Reduction size)	Constrains num	357299	361583	365867	370151	374435	378719	/
		56313	60579	64881	69165	73449		/
	Variables num	173829	176685	179541	182397	185253	188109	/
		29535	32391	35247	38103	40959		/
	Calculation time(s)	4580.74	17986.53	20099.66	30216.76	51684.11	64332.6	188900
		19.68	19.03	168.12	231.21	261.4		699
Strategy 4 (Original size /Reduction size)	Constrains num	357299	374435	391571	408707	/	/	/
		56313	73449	90585			/	/
	Variables num	173829	185253	196677	208101	/	/	/
		29535	40959	52383			/	/
	Calculation time(s)	4525.55	27260.35	44173.51	67093.6	/	/	143053
		19.27	306.74	423.34			/	749

From the above analysis, it is clear that the use of Algorithm 1 to reduce the calculation size has significantly improved the computational performance of Algorithm 2. This greatly facilitates the application of the model and methods proposed in this paper on larger-scale networks. Meanwhile, it is obvious that the original calculation size situation will not perform well when applied to a larger scale network. So next, we will only test the performance in the situation of reducing the calculation size on the more complex HSR networks.

5.3 Case study 3: a larger real-world network of Guangzhu Intercity Railway

The preceding section evaluated our proposed model and algorithms on a single railway track line to demonstrate its applicability. To further assess its applicability in a more complex context, we apply it to an intersection network scenario in this section.

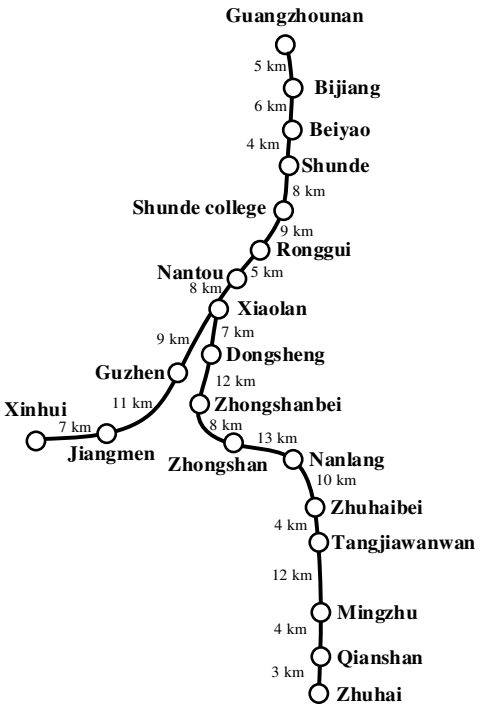

Fig. 19. Guangzhu Intercity Railway

We utilize the timetable on July 1, 2015, of the Guangzhou-Zhuhai Intercity Railway for additional testing. At that time, the railway network, as depicted in Fig. 19, consisted of 20 HSR

stations, encompassing the Guangzhou-Zhuhai main line and the Xiaolan-Xinhui line. The network was serviced by 52 trains, catering to 74 OD pairs, with the corresponding timetable illustrated in Fig. 20. And the values of all parameters are set to be the same as in section 5.2.

We obtained the ticketing volume for each path from the ticketing system[7], and there were 960 paths used by the passengers. The original calculation size of our problem will have $\sum_{(r,s)\in RS} T|P_{rs}| = 102 \times 960 = 97920$ feasible space-time paths and 98478 space-time arcs. After reducing the calculation size by using Algorithm 1, there are 7,703 feasible space-time paths, and 8,261 space-time arcs, of which 7,703 are access arcs and 558 are other types of space-time arcs.

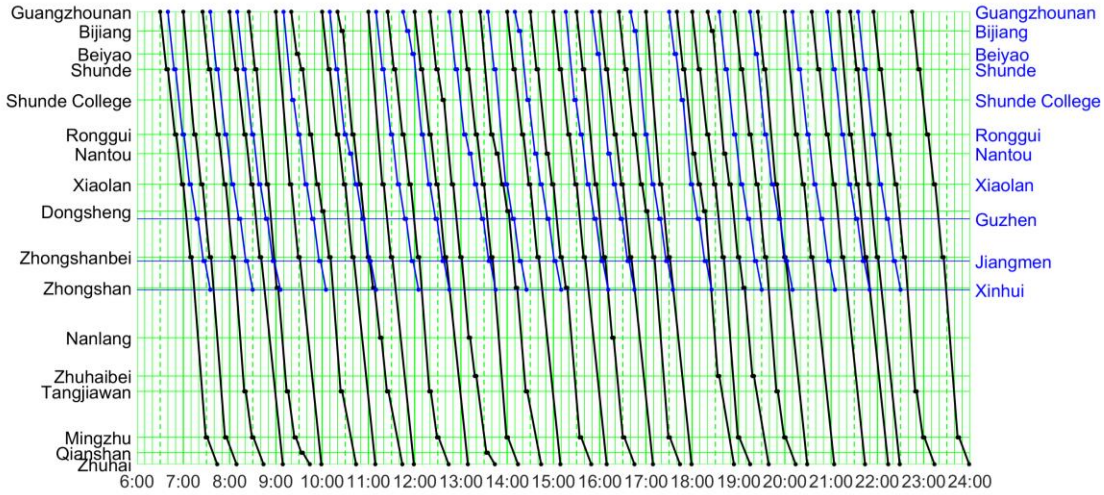

Fig. 20. The Timetable of Guangzhu Intercity Railway

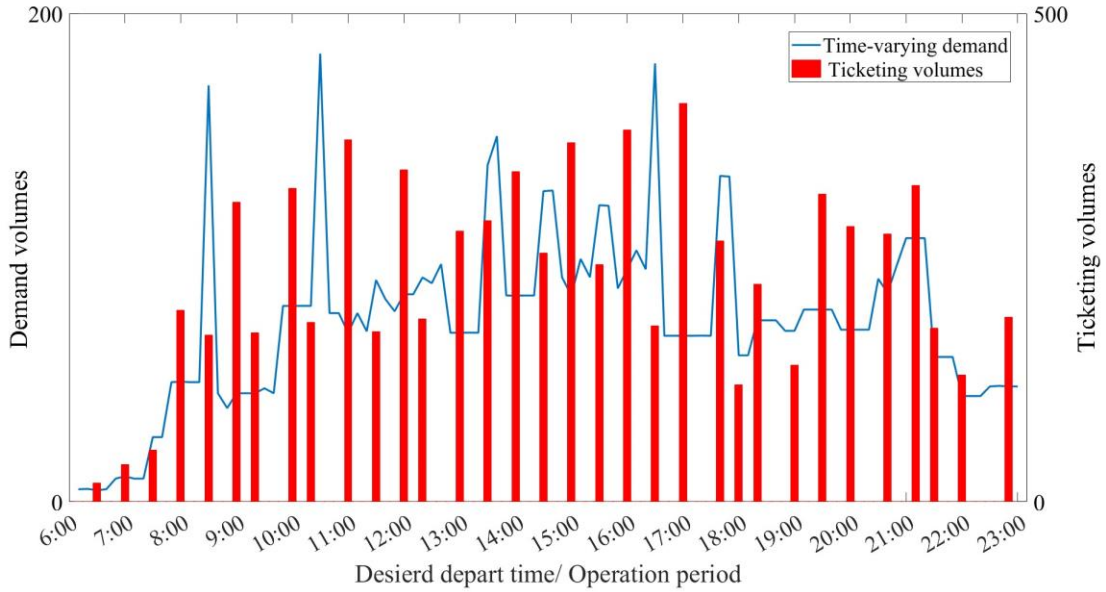

Fig. 21. The TDD results for the OD pair Guangzhounan→zhuhai

Fig. 21 shows the TDD estimation results for one OD pair. And Table 13 shows the statistical information of our Algorithm 2 for case study 3, from which we can obtain the following:

[7] www.12306.cn

First, when applied to large-scale networks with intersecting lines, our SL-ETDDP global convergence algorithm (Algorithm 2) can also obtain the global optimal solution within a limited number of iterations and an acceptable total computation time.

Second, Strategy 1 is the benchmark strategy, which is simple and easy to operate, but requires more computation time than the other strategies; Strategy 3, due to its flexibility and convenience of only adding one piecewise interval per iteration, although requiring a slightly higher number of iterations than other strategies, has a significantly lower total computation time. In combination with the situation of Case study 2, after using Algorithm 1 to reduce the model size, Algorithm 2 achieves the highest computational efficiency when using Strategy 3.

Table 13. Statistical information of algorithm 2 for Case study 3

Iteration number h		1	2	3	4	total
Strategy 1	Constrains num	293934	407154	633594		/
	Variables num	154524	230004	380964		/
	Calculation time(s)	4084.91	6950.66	117701.17		128737
Strategy 2	Constrains num	293934	384510	565662		/
	Variables num	154524	214908	335676		/
	Calculation time(s)	3998.39	9537.06	38661.36		52197
Strategy 3	Constrains num	293934	316578	339222	361866	/
	Variables num	154524	169620	184716	199812	/
	Calculation time(s)	3986.45	1743.86	7217.49	8344.05	21292
Strategy 4	Constrains num	293934	384510	475086		/
	Variables num	154524	214908	275292		/
	Calculation time(s)	4005.27	16075.61	51965.45		72046

5.4 Case study 4: a more complex real-world network of Xi'an region HSR networks

In this section, we will further extend our model and algorithms to more complex railway line networks. The timetable and ticket booking data on June 1, 2015, of the Xi'an region HSR networks are used for this test. At that time, the Zhengxi HSR, Xibao HSR, Daxi HSR, and Baoxi HSR were all connected with Xi'an city and form an 'X' shape intersection, which is shown Fig. 22. The network containing 31 stations was serviced by 73 trains with 145 OD pairs, and the corresponding timetable illustrated in Fig. 23-24. The operation period $[T^1, T^2] = [6{:}00, 24{:}00]$ is discretized into $[T^1, T^2] = [1, 2, \cdots, 108]$ of 10-minute time intervals. The convergence parameter as $\varepsilon = 0.03$ and the values of other parameters are set to be the same as in section 5.3.

We obtained the ticketing volume for each path from the ticketing system, and there were 1091 paths used by the passengers. The original calculation size of our problem will have $\sum_{(r,s)\in RS} T|P_{rs}| = 108 \times 1091 = 117828$ feasible space-time paths and 118487 space-time arcs. After reducing the calculation size by using Algorithm 1, there are 15894 feasible space-time paths, and 16553 space-time arcs.

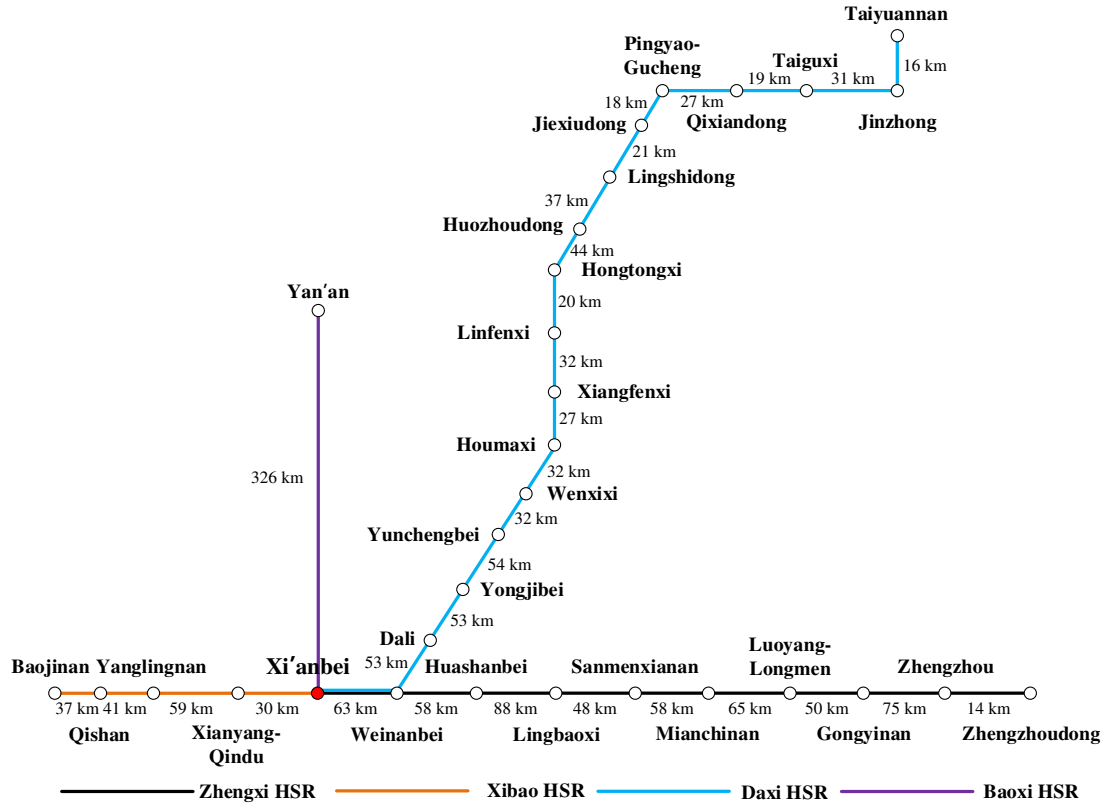

Fig. 22. Xi'an region HSR networks in 2015

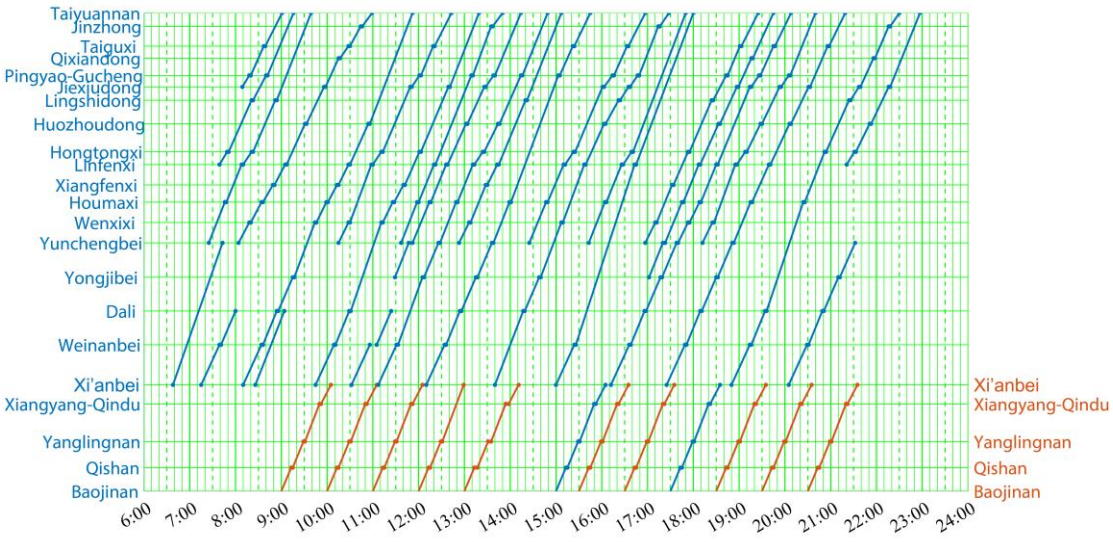

Fig. 23. The Timetables of Xibao HSR and Daxi HSR

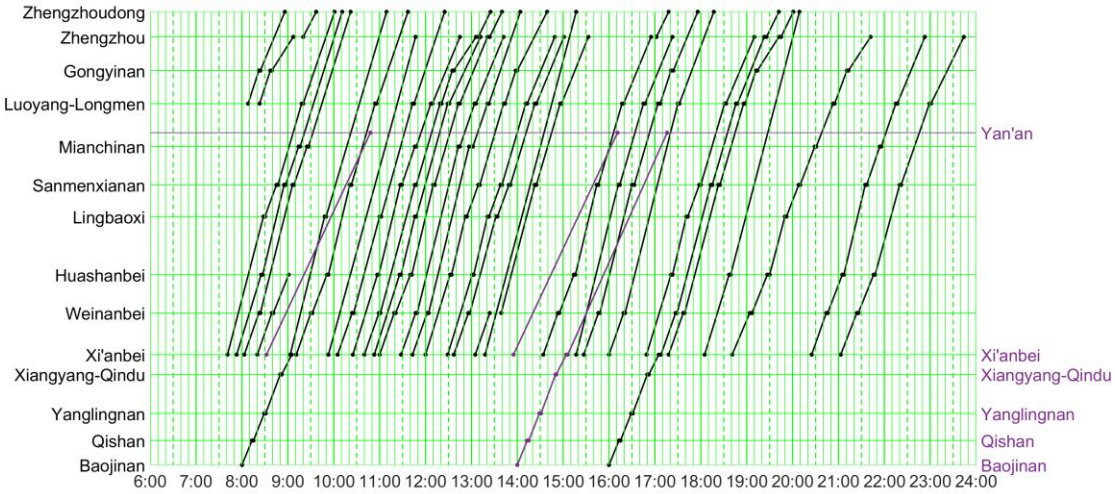

Fig. 24. The Timetables of Zhengxi HSR and Baoxi HSR

Table 14 shows the statistical information of our Algorithm 2 for case study 4. As we can see, all strategies can obtain the results within 3 iterations. Strategy 1, as the foundational strategy, took the most time, followed by Strategy 2. Strategy 4 performed the best this time, consuming the least computation time, with Strategy 3 next in line. Additionally, it is worth noting that although the network in Case Study 4 is more complex than in Case Study 3, and the computation scale is larger than Case Study 3, the time spent by each strategy on computing Case Study 4 is less than that spent on Case Study 3. To more intuitively analyze the effectiveness of our algorithm in different case studies, we further compiled the information from the four case studies into the following Table 14 for comparative analysis.

Table 14. Statistical information of algorithm 2 for Case study 4

Iteration number h		1	2	3	total
Strategy 1	Constrains num	604205	839105	1308905	/
	Variables num	317672	474272	787472	/
	Calculation time(s)	2869.21	19109.28	74928.48	96907
Strategy 2	Constrains num	604205	745145	980045	/
	Variables num	317672	411632	568232	/
	Calculation time(s)	2936.51	6432.11	65498.31	74846
Strategy 3	Constrains num	604205	651185	698165	/
	Variables num	317672	348992	380312	/
	Calculation time(s)	2892.51	3940.85	8935.36	15769
Strategy 4	Constrains num	604205	745145		/
	Variables num	317672	411632		/
	Calculation time(s)	2944.86	2191.62		5136

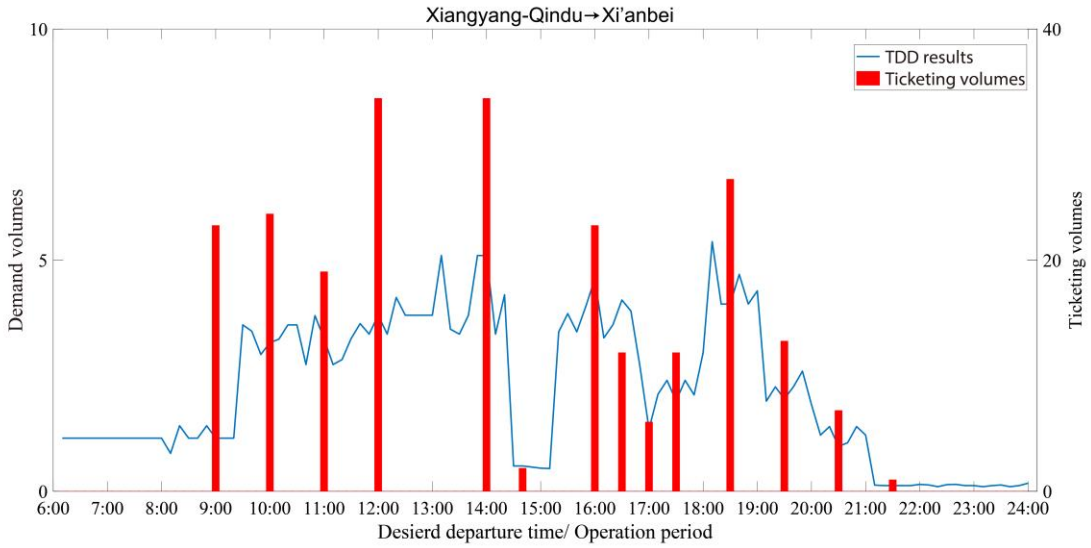

Fig. 25. The TDD results for the OD pair Xiangyang-Qindu→Xi'anbei

From Table 15 we can see that:

First, as the scale of the high-speed rail network increases, the scale of our problems is also increasing. From Case Study 1 to 4, our HSR network evolves from simple line to complex real-world networks, with both the number of feasible space-time paths and space-time arcs continuously growing.

Second, by comparing the original size of feasible space-time paths and space-time arcs with the reduction size, it is clear that our Algorithm 1 significantly reduces the problem scale, which can greatly reduce the consumption of computing resources and computational time.

Third, referring to the performance of different strategies, Strategies 3 and 4 are quite effective in reducing computation time. Strategy 1, as the basic strategy, takes the longest computation time, while Strategy 2 is at a moderate level.

Forth, from Case study 1 to Case study 3, the computation time increases with the scale of the problem; however, from Case study 3 to Case study 4, an increase in problem scale does not lead to an increase in computation time. This is because ticket booking volumes in Case study 4 are relatively lower than that in Case study 3. The Guangzhou-Zhuhai intercity line of the Case study 3 is located in one of the most economically developed regions of China, with relatively high travel demand, leading to more frequent and intense competition among passengers for popular trains. As these popular trains will usually serve more than one OD pair, and each OD pair may carry several train services, the more competition for the ticketing among passengers, the more complex to reach the UE state, which obviously increases the computational time for the TDD problems. This illustrates that the problem of estimating the TDD of HSR networks is not only affected by the scale of the HSR network, but also by the volumes of the demand.

Table 15. Comparison information of Case studies

Case study	Case study 1	Case study 2	Case study 3	Case study 4
Total Station Number	3	6	20	31
Toal OD Number	3	14	74	145

Toal Train Number	3	54	52	73
Toal Feasible Space-time Path Number (Original size/Reduction size)	80/ 40	18360/ 1456	97920/ 7703	117828/ 15894
Total Space-time Arc Number (Original size/ Reduction size)	78/ 48	18570/ 1665	98478/ 8261	118487/ 16553
Calculate time of Strategy 1	1.22	824	128737	96907
Calculate time of Strategy 2	0.84	794	52197	74846
Calculate time of Strategy 3	1.34	699	21292	15769
Calculate time of Strategy 4	0.77	749	72046	5136

6. Conclusions

TDD is a critical input for operation and management in the HSR systems, i.e., it can help to improve the service quality of the HSR systems by informing the appropriate train departure frequency for the peak and off-peak periods within a day to allow passengers to depart at their desired departure times as far as possible. This study is the first in the literature to analytically estimate TDD for HSR networks with the ticket booking data and using the schedule-based UE assignment. A bi-level model is formulated to estimate the TDD problems and the advance booking cost is considered endogenously as a part of passenger choice equilibrium. We convert the bi-level model into a single-level model through equivalent complementary constraints. Furthermore, based on linear relaxation, the single-level model is transformed into a MIQP. By solving the MIQP we get the information about the upper and lower bounds of our original problem, and then a global optimal solution algorithm with four piecewise interval strategies is proposed. And the effectiveness and applicability of the proposed algorithm are illustrated with three case studies. The first simple case illustrates the details of our algorithm result with different input data, different parameter values and different strategies; and the real-world case illustrates the applicability and calculating efficiency of four strategies in a real-world network in China. Further, two more complex real-world networks studies are proposed to test our algorithm in an intersection HSR network. The results of the four case studies show that the proposed model can help operators to elicit the time-varying demand in the HSR systems especially when demand is relatively high and passengers need to book in advance to guarantee their itinerary.

As our study focuses on the demand estimation, we can provide high quality of TDD for HSR operators, especially for the routes experiencing strains on train capacity during the peak hours within a day, where there is a discrepancy between passengers' actually departure time and their desired departure time. By accurately capturing these discrepancies, our proposed solution offers valuable insights for HSR operational management teams. It enables them to make more informed decisions in line planning and timetable scheduling, aiming to align transportation services more closely with passenger demand. This alignment is crucial for enhancing the overall service quality across the HSR network, thereby improving passenger

satisfaction and system efficiency. Meanwhile, implementing our model and algorithm can assist HSR operators in identifying critical bottlenecks and demand patterns, facilitating the development of more responsive and demand-adaptive transportation services. For example, it can guide the allocation of additional train services during identified peak periods or the adjustment of train capacities to better meet passenger demand without significantly overhauling existing schedules.

This study can be further extended along several avenues. Firstly, this study assumes that the ticket price is independent of ticket booking time (this reflects the current practice in China), and future research can extend to variable ticket prices during the pre-sale period (booking time horizon). Secondly, based on the arcs/links capacity constraints, we formulate our current model, and if the seat allocation becomes more popular in the future, we can build the model based on the seat allocation scheme for the TDD estimation problem. Further, the special situation for passengers booking tickets covering more than their desired journey due to the unavailability of direct tickets between their intended OD pair can be considered. Thirdly, this study considers the demand with homogeneity and deterministic choice behaviors (UE principle), while future study can further explore the TDD of heterogeneity passenger demand with Stochastic user equilibrium (SUE) principle, and this problem for multi-class seats (Xu et al., 2018b) can also be considered. Fourth, uncertainty factors, including equipment failures and extreme weather conditions, which can cause train delays and subsequently influence passenger choices, can be incorporated into the TDD estimation problem by utilizing the reliability-based assignment approach (Xu et al., 2018a; Xu et al., 2023b).

CRediT authorship contribution statement

Tangjian Wei: Conceptualization, Investigation, Methodology, Writing-original draft. **Richard Batley**: Conceptualization, Methodology, Writing-original draft. **Ronghui Liu**: Conceptualization, Methodology, Writing-original draft. **Guangming Xu**: Conceptualization, Funding acquisition, Methodology, Visualization, Writing-original draft. **Yili Tang**: Conceptualization, Methodology, Funding acquisition, Writing-original draft.

Declaration of competing Interest

The authors declare that they have no known competing financial interests or personal relationships that could have appeared to influence the work reported in this paper.

Acknowledgment

The authors wish to express their thanks to the editors and anonymous reviewers whose constructive comments have greatly improved this study. Guangming Xu was supported by the National Natural Science Foundation of China (72171236, U1334207). Tangjian Wei and Yili Tang were supported by the Natural Sciences and Engineering Research Council of Canada (NSERC RGPIN-2022-05028 and ALLRP 586566-23).

Appendix A. Estimate the TDD by considering the BRUE

In the theory of Bounded Rationality, individuals are considered to make decisions in a boundedly rational manner, opting for satisfactory rather than optimal solutions. This is attributed to either a lack of precise information or the complexity of scenarios that hinder the

attainment of an optimized decision (Conlisk, 1996; Di and Liu, 2016; Ye and Yang, 2017). Drawing upon the terminology used in Jiang et al. (2022); Liu and Zhou (2016); Lou et al. (2010), we define BRUE as follows:

Definition 2.1: A path is considered "acceptable" if the discrepancy between its cost and that of the least-cost path does not exceed a predetermined threshold value.

Definition 2.2 (BRUE): A path flow distribution achieves BRUE status when it aligns with travel demands, ensuring that each user selects an acceptable path.

We define ε_{rs} as the threshold value of passengers for the OD pair $(r,s) \in RS$. In BRUE, for any feasible space-time path $p(t)$, if its flow $f_{p(t)} > 0$, then we can get the following Eq. (43).

$$c_{p(t)} + \sum_{a\in\mathbb{A}} \pi_a \cdot \delta^a_{p(t)} \le \pi^t_{rs} + \varepsilon_{rs}, \qquad t = 1,2,\cdots T; p \in P_{rs}; (r,s) \in RS \quad (43)$$

The left of Eq. (43) means the actual cost of path $p(t)$, and right of Eq. (43) means minimal cost between OD pair (r,s) for demand $q_{rs}(t)$ plus the threshold value ε_{rs}.

Then, the Eq. (20) of UE conditions can be rewritten as Eq. (44) with BRUE conditions.

$$\begin{cases} f_{p(t)} \ge 0 \\ c_{p(t)} + \sum_{a\in\mathbb{A}} \pi_a \cdot \delta^a_{p(t)} - \pi^t_{rs} \ge 0 \\ f_{p(t)} \cdot \left(\varepsilon_{rs} - c_{p(t)} - \sum_{a\in\mathbb{A}} \pi_a \cdot \delta^a_{p(t)} + \pi^t_{rs} \right) \ge 0 \\ \varepsilon_{rs} \ge 0 \end{cases}, \quad t = 1,2,\cdots T; p \in P_{rs}; (r,s) \in RS \quad (44)$$

In the above Eq. (44), when $\varepsilon_{rs} = 0$, the BRUE (Eq. (44)) is equivalent with UE (Eq. (20)); and when $\varepsilon_{rs} > 0$, if $f_{p(t)} > 0$, then we can obtain Eq. (43). And similarly with subsection 4.1, Eq. (44) can be replaced by the following linear constrains Eqs. (45).

$$\begin{cases} U \cdot h_{p(t)} + \vartheta \le f_{p(t)} \le M \cdot (1 - h_{p(t)}) \\ U \cdot h_{p(t)} \le \varepsilon_{rs} - c_{p(t)} - \sum_{a\in\mathbb{A}} \pi_a \cdot \delta^a_{p(t)} + \pi^t_{rs} \\ f_{p(t)} \ge 0 \\ c_{p(t)} + \sum_{a\in\mathbb{A}} \pi_a \cdot \delta^a_{p(t)} - \pi^t_{rs} \ge 0 \\ \varepsilon_{rs} \ge 0 \\ h_{p(t)} \in \{0,1\} \end{cases}, \quad t = 1,2,\cdots T; p \in P_{rs}; (r,s) \in RS \quad (45)$$

Thus, our estimation problem for TDD by considering the BRUE can be formulated as the following model M4.

M4:

$$\min Z_3 = \alpha_1 \sum_{(r,s)\in RS} \sum_{t=1}^{T} \mathcal{L}^t_{rs} + \alpha_2 \sum_{(r,s)\in RS} \sum_{p\in P_{rs}} \left(\sum_{t=1}^{T} f_{p(t)} - \hat{f}_p \right)^2 \quad (24)$$

subject to

Eqs. (7)-(8), (10), (13)-(14), (22), (45)

Constraints in Eqs. (27)-(34), $t = 1,2,\ldots,T; (r,s) \in RS$

As the only difference between model $M4$ and $M3$ is the use of $Eqs.\ (45)$ instead of $Eqs.\ (43)$, and $Eqs.\ (45)$ are also the linear constraints, we still can use the algorithm proposed in Subsection 4.4 to calculate the model M4.

Appendix B. Proof of proposition 2

From Eqs. (38) - (41) we know that each strategy does not move existing breakpoints when adding the new breakpoints if the number of initial piecewise intervals is an integer multiple of 2. And we use the following Fig. B1 to provide some intuition. The existing breakpoints are shown as green points and the additional breakpoints are shown as red ones. We know that the region defined by the red solid curve chords and the curve of $\mathcal{L}_{rs}^{t}(q_{rs}^{t})$ is a subset of that defined by the green solid curve chords and the curve of $\mathcal{L}_{rs}^{t}(q_{rs}^{t})$. Similarly, the region defined by red dotted tangent lines, green dotted tangent lines and the cure of $\mathcal{L}_{rs}^{t}(q_{rs}^{t})$ is the subset of that defined by the green dotted tangent lines and the cure of $\mathcal{L}_{rs}^{t}(q_{rs}^{t})$. Furthermore, with the strategy of adding breakpoints, $\Omega^{h} \supset \Omega^{h+1}$. As $\Omega^{h} \supset \Omega^{h+1}$, then we have $\{F_3(\boldsymbol{q}^{h}, \boldsymbol{f}^{h}, \boldsymbol{\mathcal{L}}^{h})\} \leq \{F_3(\boldsymbol{q}^{h+1}, \boldsymbol{f}^{h+1}, \boldsymbol{\mathcal{L}}^{h+1})\}$. Thus, proposition 2 is true. □

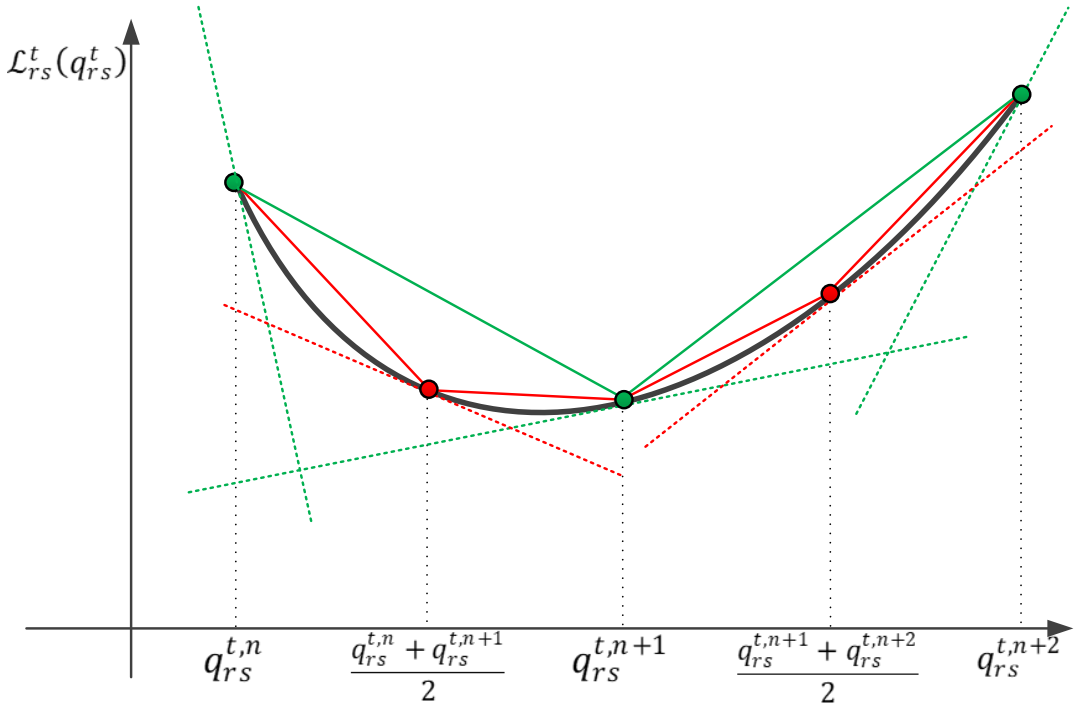

Fig. B1. The updated breakpoints

Appendix C. Proof of proposition 3

This proof follows a similar logic to that in Wang et al. (2015) and Xu et al. (2022) .Let Z_2^* be the optimal objective function value of the SL-EDTTP model M2. As the model M3 is relaxed from model M2, then model M3 has a larger solution space than M2, and the objective function value $F_3(\boldsymbol{q}, \boldsymbol{f}, \boldsymbol{\mathcal{L}})$ of model M3 is always the lower bound of model M2 , i.e., $F_3(\boldsymbol{q}, \boldsymbol{f}, \boldsymbol{\mathcal{L}}) \leq Z_2^*$. Meanwhile, from proposition 2 we know that the set of optimal objective function values $\{F_3(\boldsymbol{q}^{h}, \boldsymbol{f}^{h}, \boldsymbol{\mathcal{L}}^{h})\}$ is a monotonically increasing series with respect to the

iteration number h. From our SL-ETDDP Global Convergence Algorithm, we have $\underline{Z}_2^h = \max\{\underline{Z}_2^{h-1}, F_3(\boldsymbol{q}^h, \boldsymbol{f}^h, \boldsymbol{\mathcal{L}}^h)\} \leq Z_2^*$, then we can know that $\{\underline{Z}_2^h\}$ is also a monotonically increasing series and can obtain the following equation.

$$\underline{Z}_2^1 \leq \underline{Z}_2^2 \leq \cdots \leq \underline{Z}_2^h \leq \cdots \leq Z_2^*$$

Furthermore, with an increasing number of iterations h, Eqs. (27)-(34) will make $\mathcal{L}_{rs}^t(q_{rs}^t)$ closer to approach the curve of $q_{rs}^t \ln q_{rs}^t - q_{rs}^t$, and then, the solution of model M3 will approach the solution of model M2. If the optimal solution of model M2 is still not achieved, then the solution $(\boldsymbol{q}^h, \boldsymbol{f}^h, \boldsymbol{\mathcal{L}}^h)$ in model M3 will be updated with the set of additional breakpoints and its corresponding reduction region by step 4, and then the lower bounds $\underline{Z}_2^h$ will be updated by $\underline{Z}_2^h = \max\{\underline{Z}_2^{h-1}, F_3(\boldsymbol{q}^h, \boldsymbol{f}^h, \boldsymbol{\mathcal{L}}^h)\}$. Therefore, with the number of iterations approaches infinity, we have $\lim_{h\to\infty} \underline{Z}_2^h = Z_2^*$ and $(\boldsymbol{q}^h, \boldsymbol{f}^h)$ will approach the optimal solution $(\boldsymbol{q}^*, \boldsymbol{f}^*)$.

Moreover, as all the constraints in model M3 are also in model M2, the optimal solution $(\boldsymbol{q}^h, \boldsymbol{f}^h, \boldsymbol{\mathcal{L}}^h)$ of model M3 at iteration number h is also the feasible solution of model M2. Then the objective function value $F_2(\boldsymbol{q}^h, \boldsymbol{f}^h)$ can be calculated by given $(\boldsymbol{q}^h, \boldsymbol{f}^h)$, and $F_2(\boldsymbol{q}^h, \boldsymbol{f}^h)$ are the upper bounds of model M2, i.e., $F_2(\boldsymbol{q}^h, \boldsymbol{f}^h) \geq Z_2^*$. And from our algorithm in section 4.4, we have $\overline{Z}_2^h = \min\{\overline{Z}_2^{h-1}, F_2(\boldsymbol{q}^h, \boldsymbol{f}^h)\} \geq Z_2^*$, which means that $\{\overline{Z}_2^h\}$ is a monotonically decreasing series and it can be expressed as

$$\overline{Z}_2^1 \geq \overline{Z}_2^2 \geq \cdots \overline{Z}_2^h \geq \cdots \geq Z_2^*$$

Furthermore, with iteration number h approach infinity, we have $\lim_{h\to\infty} \overline{Z}_2^h = Z_2^*$. The above means that by using the upper and lower bounds, our proposed algorithm will converge to the global optimal solution of the model M2. □

Appendix D. Path flow results of Case 1

Table D. Path flow results of Case 1

OD pair	t	$p(t)$	$c_{p(t)}$	Case 1.a			Case 1.b		
				$\sum_{a\in\mathbb{A}} \pi_a \cdot \delta^a_{p(t)}$	$c_{p(t)} + \sum_{a\in\mathbb{A}} \pi_a \cdot \delta^a_{p(t)} - \pi^t_{rs}$	$f_{p(t)}$	$\sum_{a\in\mathbb{A}} \pi_a \cdot \delta^a_{p(t)}$	$c_{p(t)} + \sum_{a\in\mathbb{A}} \pi_a \cdot \delta^a_{p(t)} - \pi^t_{rs}$	$f_{p(t)}$
$v_1 \to v_2$	1	$p^1(1)$	1.6	0	0	9.85	0	0	10.39
	2	$p^1(2)$	0.9	0	0	9.85	0	0	9.85
	3	$p^1(3)$	1.3	0	0	9.85	0	0	9.85
	4	$p^1(4)$	1.7	0	0	10.39	0	0	9.85
	5	$p^1(5)$	2.1	0	0	9.85	0	0	9.85
	6	$p^2(6)$	1.6	0	0	3.81	0	0	3.81
	7	$p^2(7)$	0.9	0	0	4.38	0	0	4.38
	8	$p^2(8)$	1.3	0	0	3.81	0	0	4.38
	9	$p^2(9)$	1.7	0	0	4.38	0	0	3.81
	10	$p^2(10)$	2.1	0	0	3.81	0	0	3.81
$v_2 \to v_3$	1	$p^3(1)$	3	0	0	9.86	**0.6** 0	0 2.9	12.68 0
	2	$p^3(2)$	2.3	0	0	9.86	**0.6** 0	0 2.9	13.68 0
	3	$p^3(3)$	1.6	0	0	9.96	**0.6** 0	0 2.9	13.63 0
	4	$p^3(4)$	0.9	0	0	10.79	**0.6** 0	0 2.9	12.68 0
	5	$p^3(5)$	1.3	0	0	9.86	**0.6** 0	0 1.8	13.68 0

	6	$p^3(6)$	1.7	0	0	9.86	**0.6** 0	0 0.7	13.68 0
	7	$p^3(7)$	2.1	0	0	9.86	**0.6** 0	0.4 0	0 11.73
	8	$p^4(8)$	1.6	0	0	14.4	0	0	10.8
	9	$p^4(9)$	0.9	0	0	15.26	0	0	11.73
	10	$p^4(10)$	1.3	0	0	15.26	0	0	10.72
	1	$p^5(1)$	3	0	0	6.15	**0.6** 0	0 1.1	10.02 0
	2	$p^5(2)$	2.3	0	0	6.65	**0.6** 0	0 1.1	9.96 0
	3	$p^5(3)$	2.7	0	0	7.29	**0.6** 0	0 0	0 11.28
$v_1 \rightarrow v_3$	4	$p^6(4)$	2.6	0	0	14.62	0	0	10.99
	5	$p^6(5)$	1.9	0	0	15.27	0	0	11.28
	6	$p^6(6)$	2.3	0	0	14.81	0	0	11.28
	7	$p^7(7)$	2.3	0	0	4.94	0	0	4.92
	8	$p^7(8)$	2.7	0	0	5.32	0	0	5.32
	9	$p^7(9)$	3.1	0	0	4.63	0	0	4.63
	10	$p^7(10)$	3.5	0	0	5.32	0	0	5.32

Appendix E. Timetable of Nanchang-Jiujiang Intercity Railway

Table E. Timetable of Nanchang-Jiujiang Intercity Railway

Train No	Station Name	Arrival Time	Depart Time	Capacity	Train No	Station Name	Arrival Time	Depart Time	Capacity
D6258	Nanchangxi	----	7:00		D3274	Yongxiu	13:50	13:52	565
D6258	Yongxiu	7:22	7:24	565	D3274	Lushan	14:18	14:20	
D6258	Gongqingcheng	7:36	7:38		G2712	Nanchangxi	13:41	13:44	518
D6258	Jiujiang	8:03	8:05		G2712	Lushan	14:27	14:29	
G892	Nanchangxi	----	7:20	518	G1480	Nanchangxi	13:33	13:50	
G892	Lushan	8:03	8:05		G1480	Dean	14:21	14:28	518
G1466	Nanchangxi	----	7:31		G1480	Jiujiang	14:50	14:50	
G1466	Gongqingcheng	8:00	8:02	518	G2296	Nanchangxi	13:49	13:56	518
G1466	Lushan	8:22	8:24		G2296	Lushan	14:39	14:41	
D6378	Nanchangxi	----	7:42		D6264	Yongxiu	14:26	14:28	565
D6378	Dean	8:13	8:15	565	D6264	Jiujiang	15:01	15:05	
D6378	Jiujiang	8:37	8:37		G3156	Nanchangxi	14:13	14:17	518
D3252	Nanchangxi	----	7:52		G3156	Lushan	15:00	15:02	
D3252	Yongxiu	8:12	8:14	565	G648	Nanchangxi	14:29	14:32	
D3252	Lushan	8:41	8:43		G648	Yongxiu	14:52	15:05	518
D6344	Dean	8:50	8:52	565	G648	Dean	15:20	15:22	
D6344	Jiujiang	9:13	9:13		G648	Lushan	15:38	15:40	
D2236	Yongxiu	9:07	9:09		G1470	Nanchangxi	----	14:38	518
D2236	Gongqingcheng	9:21	9:23	565	G1470	Lushan	15:22	15:24	
D2236	Lushan	9:42	9:44		G896	Nanchangxi	----	14:43	518
D3190	Nanchangxi	----	9:02		G896	Lushan	15:27	15:29	
D3190	Yongxiu	9:22	9:24		D3198	Nanchangxi	----	15:15	565
D3190	Gongqingcheng	9:36	9:38	565	D3198	Lushan	16:03	16:05	
D3190	Dean	9:45	9:47		D3256	Nanchangxi	----	15:20	
D3190	Lushan	10:03	10:05		D3256	Gongqingcheng	15:48	15:50	565
D6266	Yongxiu	9:36	9:38		D3256	Lushan	16:09	16:11	
D6266	Gongqingcheng	9:50	9:52	565	D3288	Nanchangxi	15:15	15:25	
D6266	Dean	9:59	10:01		D3288	Yongxiu	15:45	15:47	565
D6266	Jiujiang	10:23	10:26		D3288	Dean	16:02	16:04	
D3194	Nanchangxi	----	9:31		D3288	Lushan	16:20	16:22	
D3194	Gongqingcheng	9:59	10:01	565	D6352	Yongxiu	16:11	16:13	
D3194	Dean	10:08	10:10		D6352	Gongqingcheng	16:25	16:33	565
D3194	Lushan	10:26	10:28		D6352	Dean	16:40	16:42	
D6254	Nanchangxi	----	10:20		D6352	Jiujiang	17:04	17:04	
D6254	Gongqingcheng	10:48	10:50	565	G2694	Nanchangxi	16:01	16:04	565
D6254	Jiujiang	11:15	11:19		G2694	Lushan	16:47	16:49	
D2242	Nanchangxi	10:27	10:32	565	D2202	Nanchangxi	16:10	16:10	
D2242	Lushan	11:15	11:17		D2202	Yongxiu	16:30	16:32	565
G2790	Nanchangxi	10:33	10:38		D2202	Gongqingcheng	16:44	16:46	
G2790	Dean	11:09	11:11	518	D2202	Jiujiang	17:11	17:15	
G2790	Lushan	11:27	11:29		G2766	Nanchangxi	16:24	16:31	
G2382	Nanchangxi	----	10:45	518	G2766	Yongxiu	16:51	16:59	518
G2382	Gongqingcheng	11:15	11:17		G2766	Gongqingcheng	17:11	17:13	

G2382	Jiujiang	11:42	11:45		G2766	Jiujiang	17:41	17:41	
G636	Nanchangxi	11:14	11:18		G2698	Nanchangxi	16:35	16:38	
G636	Yongxiu	11:38	11:40	518	G2698	Dean	17:09	17:11	518
G636	Dean	11:56	11:58		G2698	Lushan	17:29	17:31	
G636	Lushan	12:13	12:15		G2786	Nanchangxi	17:22	17:30	
D376	Nanchangxi	11:23	11:32		G2786	Yongxiu	17:55	17:57	518
D376	Yongxiu	11:52	11:59	565	G2786	Lushan	18:25	18:27	
D376	Dean	12:14	12:16		D6252	Nanchangxi	17:48	17:48	
D376	Lushan	12:32	12:34		D6252	Yongxiu	18:09	18:11	565
G894	Nanchangxi	----	11:38	518	D6252	Dean	18:26	18:28	
G894	Lushan	12:22	12:24		D6252	Jiujiang	18:50	18:54	
G2046	Nanchangxi	11:39	11:42		G2036	Nanchangxi	17:45	17:53	
G2046	Yongxiu	12:06	12:08	518	G2036	Yongxiu	18:17	18:19	518
G2046	Dean	12:23	12:25		G2036	Gongqingcheng	18:31	18:33	
G2046	Lushan	12:40	12:42		G2036	Lushan	18:51	18:53	
D3266	Nanchangxi	11:53	11:57		D6508	Nanchangxi	18:21	18:25	
D3266	Gongqingcheng	12:26	12:28	565	D6508	Yongxiu	18:45	18:47	565
D3266	Lushan	12:46	12:48		D6508	Gongqingcheng	18:59	19:01	
G2762	Nanchangxi	11:59	12:02		D6508	Jiujiang	19:29	19:29	
G2762	Yongxiu	12:22	12:24	518	D6260	Gongqingcheng	19:39	19:41	
G2762	Jiujiang	12:57	12:57		D6260	Dean	19:47	19:49	565
D2232	Nanchangxi	12:19	12:23	565	D6260	Jiujiang	20:12	20:14	
D2232	Lushan	13:06	13:08		D3264	Nanchangxi	19:14	19:20	
G2294	Nanchangxi	12:24	12:28		D3264	Gongqingcheng	19:48	19:50	565
G2294	Yongxiu	12:48	12:50	518	D3264	Lushan	20:09	20:11	
G2294	Lushan	13:17	13:19		D3278	Nanchangxi	19:24	19:34	
D2226	Nanchangxi	12:35	12:39		D3278	Gongqingcheng	20:02	20:04	565
D2226	Dean	13:10	13:12	565	D3278	Lushan	20:23	20:25	
D2226	Lushan	13:28	13:30		G2782	Nanchangxi	19:32	19:40	518
G2794	Nanchangxi	12:42	12:46		G2782	Lushan	20:28	20:30	
G2794	Yongxiu	13:06	13:08	518	G2796	Nanchangxi	20:11	20:15	
G2794	Lushan	13:34	13:36		G2796	Yongxiu	20:35	20:37	518
D2376	Nanchangxi	13:02	13:08		G2796	Dean	20:51	20:53	
D2376	Gongqingcheng	13:36	13:38	565	G2796	Lushan	21:09	21:11	
D2376	Lushan	13:57	13:59		G2706	Nanchangxi	20:42	20:48	
G2764	Nanchangxi	13:09	13:13		G2706	Gongqingcheng	21:16	21:18	518
G2764	Yongxiu	13:34	13:36	518	G2706	Lushan	21:36	21:38	
G2764	Jiujiang	14:09	14:13		D734	Nanchangxi	20:51	20:59	565
D3274	Nanchangxi	13:25	13:29	565	D734	Jiujiang	22:02	22:05	

Reference

Abegaz, D., Hjorth, K., Rich, J., 2017. Testing the slope model of scheduling preferences on stated preference data. *Transportation Research Part B: Methodological* 104, 409-436.

Bierlaire, M., Crittin, F., 2004. An Efficient Algorithm for Real-Time Estimation and Prediction of Dynamic OD Tables. *Operations Research* 52, 116-127.

Börjesson, M., Eliasson, J., 2014. Experiences from the Swedish Value of Time study. *Transportation*

Research Part A: Policy and Practice 59, 144-158.

Caicedo, A., Estrada, M., Medina-Tapia, M., Mayorga, M., 2023. Optimizing bike network design: A cost-effective methodology for heterogeneous travel demands using continuous approximation techniques. *Transportation Research Part A: Policy and Practice* 176, 103826.

Carrese, S., Cipriani, E., Mannini, L., Nigro, M., 2017. Dynamic demand estimation and prediction for traffic urban networks adopting new data sources. *Transportation Research Part C: Emerging Technologies* 81, 83-98.

Cheng, Z., Trépanier, M., Sun, L.J.T.s., 2022. Real-time forecasting of metro origin-destination matrices with high-order weighted dynamic mode decomposition. *Transportation Science* 56, 904-918.

Conlisk, J., 1996. Why Bounded Rationality? *Journal of Economic Literature* 34, 669-700.

Di, X., Liu, H.X., 2016. Boundedly rational route choice behavior: A review of models and methodologies. *Transportation Research Part B: Methodological* 85, 142-179.

Ekström, J., Sumalee, A., Lo, H.K., 2012. Optimizing toll locations and levels using a mixed integer linear approximation approach. *Transportation Research Part B: Methodological* 46, 834-854.

Emami Javanmard, M., Tang, Y., Wang, Z., Tontiwachwuthikul, P., 2023. Forecast energy demand, CO2 emissions and energy resource impacts for the transportation sector. *Applied Energy* 338, 120830.

Froger, A., Mendoza, J.E., Jabali, O., Laporte, G., 2019. Improved formulations and algorithmic components for the electric vehicle routing problem with nonlinear charging functions. *Computers & Operations Research* 104, 256-294.

Hamdouch, Y., Ho, H.W., Sumalee, A., Wang, G., 2011. Schedule-based transit assignment model with vehicle capacity and seat availability. *Transportation Research Part B: Methodological* 45, 1805-1830.

Hess, S., Daly, A., Dekker, T., Cabral, M.O., Batley, R., 2017. A framework for capturing heterogeneity, heteroskedasticity, non-linearity, reference dependence and design artefacts in value of time research. *Transportation Research Part B: Methodological* 96, 126-149.

Huang, Z., Zhang, Y., Zhang, Z., Yang, L., 2023. Optimization of train timetables in high-speed railway corridors considering passenger departure time and seat-class preferences. *Transportation Letters* 15, 111-128.

Jiang, Y., Rasmussen, T.K., Nielsen, O.A., 2022. Integrated Optimization of Transit Networks with Schedule- and Frequency-Based Services Subject to the Bounded Stochastic User Equilibrium. *Transportation Science* 56, 1452-1468.

Kaspi, M., Raviv, T., 2013. Service-Oriented Line Planning and Timetabling for Passenger Trains. *Transportation Science* 47, 295-311.

Krishnakumari, P., van Lint, H., Djukic, T., Cats, O., 2020. A data driven method for OD matrix estimation. *Transportation Research Part C: Emerging Technologies* 113, 38-56.

Liang, Z., Tang, Y., Yu, J., Wang, Y., 2024. A Collective Incentive Strategy to Manage Ridership Rebound and Consumer Surplus in Mass Transit Systems. *Transportation Research Part A: Policy and Practice* In presee.

Liu, H., Szeto, W.Y., Long, J., 2019. Bike network design problem with a path-size logit-based equilibrium constraint: Formulation, global optimization, and matheuristic. *Transportation research part E: logistics and transportation review* 127, 284-307.

Liu, H., Wang, D.Z.W., 2015. Global optimization method for network design problem with stochastic user equilibrium. *Transportation Research Part B: Methodological* 72, 20-39.

Liu, J., Zhou, X., 2016. Capacitated transit service network design with boundedly rational agents.

Transportation Research Part B: Methodological 93, 225-250.

Liu, W., Zhang, F., Wang, X., Tang, Y., 2023. *A review of selected transport pricing, funding and financing issues in Asia*. Edward Elgar Publishing.

López-Ospina, H., Cortés, C.E., Pérez, J., Peña, R., Figueroa-García, J.C., Urrutia-Mosquera, J., 2022. A maximum entropy optimization model for origin-destination trip matrix estimation with fuzzy entropic parameters. *Transportmetrica A Transport Science* 18, 963-1000.

Lou, Y., Yin, Y., Lawphongpanich, S., 2010. Robust congestion pricing under boundedly rational user equilibrium. *Transportation Research Part B: Methodological* 44, 15-28.

Luathep, P., Sumalee, A., Lam, W.H.K., Li, Z.-C., Lo, H.K., 2011. Global optimization method for mixed transportation network design problem: A mixed-integer linear programming approach. *Transportation Research Part B: Methodological* 45, 808-827.

Mo, B., Li, R., Dai, J., 2020. Estimating dynamic origin–destination demand: A hybrid framework using license plate recognition data. *Computer-Aided Civil and Infrastructure Engineering* 35, 734-752.

Montoya, A., Guéret, C., Mendoza, J.E., Villegas, J.G., 2017. The electric vehicle routing problem with nonlinear charging function. *Transportation Research Part B: Methodological* 103, 87-110.

Nakanishi, Y.J., Western, J., 2005. Ensuring the security of transportation facilities: evaluation of advanced vehicle identification technologies. *Transportation research record* 1938, 9-16.

Niu, H., Zhou, X., Gao, R., 2015. Train scheduling for minimizing passenger waiting time with time-dependent demand and skip-stop patterns: Nonlinear integer programming models with linear constraints. *Transportation Research Part B: Methodological* 76, 117-135.

Osorio, C., 2019. High-dimensional offline origin-destination (OD) demand calibration for stochastic traffic simulators of large-scale road networks. *Transportation Research Part B: Methodological* 124, 18-43.

Qin, L., Li, W., Li, S., 2019. Effective passenger flow forecasting using STL and ESN based on two improvement strategies. *Neurocomputing* 356, 244-256.

Qin, X., Ke, J., Wang, X., Tang, Y., Yang, H., 2022. Demand management for smart transportation: A review. *Multimodal Transportation* 1, 100038.

Ros-Roca, X., Montero, L., Barceló, J., Nökel, K., Gentile, G., 2022. A practical approach to assignment-free Dynamic Origin–Destination Matrix Estimation problem. *Transportation Research Part C: Emerging Technologies* 134, 103477.

Shang, P., Li, R., Guo, J., Xian, K., Zhou, X., 2019. Integrating Lagrangian and Eulerian observations for passenger flow state estimation in an urban rail transit network: a space-time-state hyper network-based assignment approach. *Transportation Research Part B: Methodological* 121, 135-167.

Shannon, C.E., 1948. A mathematical theory of communication. *The Bell System Technical Journal* 27, 379-423.

Shi, F., Zhao, S., Zhou, Z., Wang, P., Bell, M.G.H., 2017. Optimizing train operational plan in an urban rail corridor based on the maximum headway function. *Transportation Research Part C: Emerging Technologies* 74, 51-80.

Szeto, W.Y., Jiang, Y., 2014. Transit route and frequency design: Bi-level modeling and hybrid artificial bee colony algorithm approach. *Transportation Research Part B: Methodological* 67, 235-263.

Tang, K., Cao, Y., Chen, C., Yao, J., Tan, C., Sun, J., 2021. Dynamic origin-destination flow estimation using automatic vehicle identification data: A 3D convolutional neural network approach. *Computer-Aided Civil and Infrastructure Engineering* 36, 30-46.

Tang, Y., Jiang, Y., Yang, H., Nielsen, O.A., 2020a. Modeling and optimizing a fare incentive strategy to manage queuing and crowding in mass transit systems. *Transportation Research Part B: Methodological* 138, 247-267.

Tang, Y., Yang, H., Wang, B., Huang, J., Bai, Y., 2019. A Pareto-improving and revenue-neutral scheme to manage mass transit congestion with heterogeneous commuters. *Transportation Research Procedia* 38, 586-605.

Tang, Y., Yang, H., Wang, B., Huang, J., Bai, Y., 2020b. A Pareto-improving and revenue-neutral scheme to manage mass transit congestion with heterogeneous commuters. *Transportation Research Part C: Emerging Technologies* 113, 245-259.

Teye, C., Bell, M.G.H., Bliemer, M.C.J., 2017. Urban intermodal terminals: The entropy maximising facility location problem. *Transportation Research Part B: Methodological* 100, 64-81.

Tsai, T.-H., Lee, C.-K., Wei, C.-H., 2009. Neural network based temporal feature models for short-term railway passenger demand forecasting. *Expert Systems with Applications* 36, 3728-3736.

Van Zuylen, H.J., Willumsen, L.G., 1980. The most likely trip matrix estimated from traffic counts. *Transportation Research Part B: Methodological* 14, 281-293.

Vielma, J.P., Ahmed, S., Nemhauser, G., 2010. Mixed-integer models for nonseparable piecewise-linear optimization: Unifying framework and extensions. *Operations research* 58, 303-315.

Wang, D.Z.W., Liu, H., Szeto, W.Y., 2015. A novel discrete network design problem formulation and its global optimization solution algorithm. *Transportation Research Part E: Logistics and Transportation Review* 79, 213-230.

Wang, D.Z.W., Lo, H.K., 2010. Global optimum of the linearized network design problem with equilibrium flows. *Transportation Research Part B: Methodological* 44, 482-492.

Wang, W., Attanucci, J.P., Wilson, N.H., 2011. Bus passenger origin-destination estimation and related analyses using automated data collection systems. *Journal of Public Transportation* 14, 20.

Wardman, M., 1997. Inter-urban rail demand, elasticities and competition in Great Britain: Evidence from direct demand models. *Transportation Research Part E: Logistics and Transportation Review* 33, 15-28.

Wardman, M., 2006. Demand for rail travel and the effects of external factors. *Transportation Research Part E: Logistics and Transportation Review* 42, 129-148.

Wardman, M., Lythgoe, W., Whelan, G., 2007. Rail Passenger Demand Forecasting: Cross-Sectional Models Revisited. *Research in Transportation Economics* 20, 119-152.

Wei, T., Shi, F., Xu, G., 2019. Estimation of Time-Varying Passenger Demand for High Speed Rail System. *Complexity* 2019, 1-24.

Wei, T., Yang, X., Xu, G., Shi, F., 2023. Medium-Term Forecast Method for Daily Passenger Flow of High-Speed Railway Based on DLP-WNN. *China Railway Science* 2, 121-139.

Wen, K., Zhao, G., He, B., Ma, J., Zhang, H., 2022. A decomposition-based forecasting method with transfer learning for railway short-term passenger flow in holidays. *Expert Systems with Applications* 189, 116102.

Wijeweera, A., To, H., Charles, M.B., Sloan, K., 2014. A time series analysis of passenger rail demand in major Australian cities. *Economic Analysis and Policy* 44, 301-309.

Wong, S.C., Tong, C.O., 1998. Estimation of time-dependent origin–destination matrices for transit networks. *Transportation Research Part B: Methodological* 32, 35-48.

Wu, R., Shi, F., Zhao, S., Xu, G., Yang, H., 2022. A Dantzig-Wolfe decomposition-based algorithm for capacitated passenger assignment problem with time-varying demand in high-speed railway

networks. *Transportation Research Part C: Emerging Technologies* 145, 103909.

Xi, H., Tang, Y., Waller, S.T., Shalaby, A., 2023. Modeling, equilibrium, and demand management for mobility and delivery services in Mobility-as-a-Service ecosystems. *Computer-Aided Civil and Infrastructure Engineering* 38, 21.

Xie, C., Kockelman, K.M., Waller, S.T., 2011. A maximum entropy-least squares estimator for elastic origin–destination trip matrix estimation. *Transportation Research Part B: Methodological* 45, 1465-1482.

Xu, G., Gao, Y., Liu, W., 2023a. Pareto-improving seat allocation for high-speed railway networks with equilibrium flows. *Transportation Research Part C: Emerging Technologies* 154, 104261.

Xu, G., Liu, W., Wu, R., Yang, H., 2021. A double time-scale passenger assignment model for high-speed railway networks with continuum capacity approximation. *Transportation Research Part E: Logistics and Transportation Review* 150.

Xu, G., Liu, W., Yang, H., 2018a. A reliability-based assignment method for railway networks with heterogeneous passengers. *Transportation Research Part C: Emerging Technologies* 93, 501-524.

Xu, G., Xiao, Y., Song, Y., Li, Z., Chen, A., 2023b. Capacity-constrained mean-excess equilibrium assignment method for railway networks. *Transportation Research Part C: Emerging Technologies* 156, 104350.

Xu, G., Yang, H., Liu, W., Shi, F., 2018b. Itinerary choice and advance ticket booking for high-speed-railway network services. *Transportation Research Part C: Emerging Technologies* 95, 82-104.

Xu, G., Zhong, L., Hu, X., Liu, W., 2022. Optimal pricing and seat allocation schemes in passenger railway systems. *Transportation Research Part E: Logistics and Transportation Review* 157.

Yang, H., Bell, M.G.H., 2001. Transport bilevel programming problems: recent methodological advances. *Transportation Research Part B: Methodological* 35, 1-4.

Yang, H., Tang, Y., 2018. Managing rail transit peak-hour congestion with a fare-reward scheme. *Transportation Research Part B: Methodological* 110, 122-136.

Yao, X.-m., Zhao, P., Yu, D.-d., 2015. Real-time origin-destination matrices estimation for urban rail transit network based on structural state-space model. *Journal of Central South University* 22, 4498-4506.

Ye, H., Yang, H., 2017. Rational Behavior Adjustment Process with Boundedly Rational User Equilibrium. *Transportation Science* 51, 968-980.

Zhang, C., Qi, J., Gao, Y., Yang, L., Gao, Z., Meng, F., 2021. Integrated optimization of line planning and train timetabling in railway corridors with passengers' expected departure time interval. *Computers & Industrial Engineering* 162, 107680.

Zhang, X., van Wee, B., 2012. Enhancing transportation network capacity by congestion pricing with simultaneous toll location and toll level optimization. *Engineering Optimization* 44, 477-488.

Zhang, Z., Wang, C., Gao, Y., Chen, Y., Chen, J., 2020. Passenger Flow Forecast of Rail Station Based on Multi-Source Data and Long Short Term Memory Network. *IEEE Access* 8, 28475-28483.

Zhao, B., Tang, Y., Wang, C., Zhang, S., Soga, K., 2022. Evaluating the flooding level impacts on urban metro networks and travel demand: behavioral analyses, agent-based simulation, and large-scale case study. *Resilient Cities and Structures* 1, 12-23.

Zhao, S., Wu, R., Shi, F., 2021. A line planning approach for high-speed railway network with time-varying demand. *Computers & Industrial Engineering* 160, 107547.

Zhou, X., Mahmassani, H.S., 2006. Dynamic Origin–Destination Demand Estimation Using Automatic Vehicle Identification Data. *IEEE Transactions on Intelligent Transportation Systems* 7, 105-114.

Zhou, Y., Meng, Q., Ong, G.P., 2022. Electric Bus Charging Scheduling for a Single Public Transport Route Considering Nonlinear Charging Profile and Battery Degradation Effect. *Transportation Research Part B: Methodological* 159, 49-75.